ACELLULAR MATRICES DERIVED FROM DIFFERENTIATING EMBRYONIC STEM CELLS

A Dissertation
Presented to
The Academic Faculty

by

Rekha Nair

In Partial Fulfillment
of the Requirements for the Degree
Doctor of Philosophy in Biomedical Engineering
Wallace H. Coulter Department of Biomedical Engineering

Georgia Institute of Technology
December 2009

ACELLULAR MATRICES DERIVED FROM DIFFERENTIATING EMBRYONIC STEM CELLS

Approved by:

Dr. Todd C. McDevitt, Advisor
School of Biomedical Engineering
Georgia Institute of Technology

Dr. Andrés García
School of Mechanical Engineering
Georgia Institute of Technology

Dr. Barbara Boyan
School of Biomedical Engineering
Georgia Institute of Technology

Dr. Themis Kyriakides
Department of Pathology
Yale University

Dr. Tamara Caspary
Department of Human Genetics
Emory University

Date Approved: November 3, 2009

To my family – Acha, Amma, Chechi, and Deepa Chechi – for teaching me perseverence, courage, ambition, and compassion. Thank you for your constant support and encouragement.

ACKNOWLEDGEMENTS

The Biomedical Engineering Ph.D. program at Georgia Tech and Emory has provided me with countless opportunities to expand my scientific knowledge and improve my analytical thinking skills. Throughout the past five years in graduate school, the unwavering support of a number of faculty, staff, friends, and family has been essential not only for the completion of my work, but for my personal growth and education, and I'm happy to have an opportunity here to express my sincere gratitude.

I would like to first start off by thanking my committee, each of whom has given me invaluable support over the years: my advisor Dr. Todd McDevitt, Dr. Barbara Boyan, Dr. Tamara Caspary at Emory University, Dr. Andrés García, and Dr. Themis Kyriakides at Yale University. First, I must express my profound gratitude to my advisor, Todd, who was willing to give a naïve, fresh-out-of-undergrad materials engineering student a chance in a stem cell lab. I joined the BME department having taking one semester of biology and not having retained much of that information. It was an extremely steep learning curve for me, and I am so grateful for the open, patient, and encouraging environment under Todd's guidance that allowed me to constantly learn and thrive. There was never a time when I needed to talk to him that he didn't make himself available to talk about science, experimental challenges, or more personal battles. To be able to help set up his lab with him has been a tremendous experience that has benefited me both professionally and personally. Todd was very candid about his plans for the lab and projections for the future, and in return, he asked us to be as open with him (although at times I imagine he may regret having encouraged me to be so vocal!). I have learned

so much about the joys and pains of setting up a lab and consider that an irreplaceable experience. So thank you, Todd, for all your support, patience, and mentoring that has not only helped me grow as a person and scientist the past five years, but that will undoubtedly serve me in the future as well.

The other members of my committee also played important roles in my professional and personal development. Dr. Boyan's direct no-nonsense questions always kept me on my toes and made me strive to accomplish the best science possible in my studies. With her expertise in developmental biology, Tamara offered a unique perspective that was essential to the development of my thesis (and I most certainly appreciate her numerous treks to Georgia Tech's campus for our meetings!). Andrés's rigorous approach to science had a significant impact on my work, and it was clear from my first interaction with him that he had a sincere interest in guiding the growth and development of my research. The analysis of the *in vivo* studies benefitted greatly from Themis's insight and familiarity with the dermal wound healing model, and I'm extremely grateful for the generous amount of time he invested into its development. Each of these faculty members has both pushed and encouraged me along the way and has subsequently fundamentally improved the quality of work presented in this dissertation.

There are also a number of faculty and staff in IBB, Whitaker, and at other institutions who have been instrumental in the progression of this work. Dr. Melissa Kemp's bioinformatics background has significantly influenced the analytical development of our global matrix synthesis that, along with Dr. Brani Vidakovic's statistical knowledge, has shaped the progress of that manuscript. The proteoglycan

expertise of Dr. Tom Wight (Benaroya Research Institute) and Dr. Marsha Rolle (now at WPI) was essential to analysis of hyaluronan and versican in our system, as was the technical help of Kathleen Braun, Christina Chan, and Pamela Johnson (Benaroya Research Institute). In addition, I would like to acknowledge the contributions of Dr. Taby Ahsan (now at Tulane) who, during her years here at Tech, was extremely helpful in the development not only of this project, but of my scientific growth. I would also like to thank Dr. Laura O'Farrell, the veterinary consultant for the *in vivo* studies. Dr. O'Farrell, along with Kim Benjamin, helped ensure that all the appropriate tools were in place and that the surgeries ran as smoothly as possible. I also appreciated the friendliness and helpfulness of the rest of the PRL staff (Odel, Autumn, and Andrea), who helped keep things running very efficiently. Also in IBB, the histologist Aqua Asberry and the previous histologist Tracey Couse were extremely helpful in offering their histology expertise and teaching me useful techniques. I would also like to express my sincere gratitude towards the BME administrative department as well as the faculty instrumental in developing the program. Sally Gerrish, Beth Bullock Spencer, and Shannon Sullivan have kept all of us on task with the necessities of registration and paperwork, and I am certain that without their guidance, I would not be in the position to graduate! I appreciate the interest that Dr. Steve DeWeerth, and now Dr. Gilda Barabino, have taken as heads of the graduate program. Steve, as well as his colleague Dr. Bob Lee, took a sincere interest in my class when we first joined Georgia Tech and helped each of us get accustomed to life as a graduate student, and for that, I am extremely grateful. Also, having thanked my advisor Todd, I would be remiss not to give my heartfelt thanks to his wife, Megan McDevitt. Her concern for the McDevitt lab's

welfare and well-being has not gone unnoticed. I particularly remember one Saturday, when Todd called the lab in for a meeting, that he bought us lunch because "Meg said that if I want to have a Saturday meeting, I have to feed you". So thank you, Meg, for having our best interests at heart and for keeping your husband in check on our behalf!

I would also like to express deep gratitude to all of my labmates who made the McDevitt lab environment challenging, fun, and supportive. I have to first especially acknowledge Ima Ebong, Rich Carpenedo, and Carolyn Sargent, who were the other members of the original "founding four". Ima was the first to graduate from the lab with her Masters, but before she left, she made a lasting mark with her fun spirit and encouragement. Rich is that guy during lab meeting who you know will ask the tough questions, but who is always willing to offer his advice and help you think through difficulties. For a while, he was the only male in the lab, and thinking back, I'm not sure how he managed! But I'm grateful that he stuck it through with us because his intermittent Craig's list explorations for tandem bikes, crossword puzzle challenges, and instigation of Friday lab happy hours has made sporadic breaks from experiments very memorable. Carolyn has shared the post doc office space with me for the past few years, and I am so lucky to have found such a generous and sincere friend. Carolyn and I have both struggled at points through the up-and-down roller coaster of graduate school, and I am grateful that there was always someone who could empathize with me and was willing to listen. In moments of self-doubt, she is always the first person to reassure me. I also want to thank Carolyn for introducing me to biking and swimming! She has been a patient and encouraging coach, and I'm looking forward to moving ahead with both

sports after the completion of this dissertation. So thank you, Carolyn, for your support and constant encouragement when times were tough.

Alyssa Ngangan joined the lab one year after us, and the lab has truly benefited from her molecular biology knowledge and experience. Alyssa is always willing to help troubleshoot experiments or take care of things when you're in a pinch. In addition to her scientific contributions to the lab, Alyssa has been become a great friend over the past few years. I have really enjoyed exploring Atlanta's variety of quality restaurants with her and Brandon while sharing food, wine, stories, and a good laugh. I love that Alyssa is always willing to try new things and inspires me to do the same. She, along with Amanda Bridges, made a wonderful travel partner on our tour of Amsterdam and Barcelona (next time we'll throw our napkins on the floor, too!). Our continued travels to Madrid and Lisbon were experiences I will not soon forget – especially our "incident" at the flamenco show in Madrid. After Alyssa, Andrés Bratt-Leal joined the lab, followed shortly by a transfer MD/PhD student from another lab, Ken Sutha, and Barbara Nsiah, who is co-advised by Dr. Bob Nerem. Each of these individuals has added warmth, fun, knowledge, and support that make it more enjoyable to come to lab every day. I am grateful to Andrés for his sense of humor, but also for his readiness to help out in lab. Ken is one of the most laid-back people I think I will ever meet, and he has unknowingly taught me a lot about how to approach life with a smile on my face (and preferably with free food in my stomach!). I have also learned from Barbara, who is more resistant to peer pressure than anyone else I know – and when she's not bugging Alyssa by calling her the Clermont or Libation Queen, she's showing us that life is too short to be filled with anything but what you alone want to do with it. Melissa Kinney is

the newest student to join our lab and has not ceased to amaze me with her dedication to the lab and her willingness to help out. I am certain that she has an outstanding graduate career ahead of her. So a big thank you to these amazing and talented group of students – not only for their intellectual support, but also for all the memories of eating challenges (the olive-eating one and El Gigante being my personal favorites), group cycling classes (especially 80's day), lab happy hours, and more.

Apart from my fellow graduate students, there have been a number of labmates who have contributed not only intellectually, but also on a more personal level. Dr. Priya Baraniak joined our lab as a post doc last year and has made immense contributions to the development of my project. She has selflessly offered her time on numerous occasions to help me wrap up my studies, and I don't think I could thank her enough for her generosity. Being academically one stage ahead of me, she is able to empathize with the pains of finishing a dissertation and is also able to offer perspectives that, being the first student in the lab to defend, I would not otherwise have received. I would also like to thank Beth Krauth and Marissa Cooke for their help in the animal surgeries. Beth was hired in the summer right after my first year and had the not-so-enviable task of instilling some sense of organization to the brand new lab. Always willing to offer her support, Beth helped me set up the animal model in our lab and was a friendly companion during the otherwise tiring hours of animal surgeries. I wish Beth all the success in her new job and am sure that her kind and generous nature will serve her well. Marissa joined the lab towards the end of last year and immediately impressed me with her work ethic, her attention to detail, and, most of all, her humor. She makes a great office mate, always making me laugh and reminding me of the joys of appreciating the little things in life.

More recently, she has been a tremendous help with my *in vivo* surgeries, an experience which I hope will benefit her as much as it did me. And while I'm on the subject of surgeries, at the risk of sounding facetious, I would also like to thank the many mice who gave their lives for my studies. I'm sure that sounds silly to many people, but a significant portion of my work would literally not have been possible without them.

Significant contributions to the work presented in this dissertation came from some spectacular undergrads with whom I have had the pleasure of working. Mentoring these students has been one of the most rewarding experiences of the past five years, and I am excited to watch them grow into phenomenal scientists and professionals. First, I want to thank the first undergrad I mentored, Shreya Shukla. She joined our lab in the beginning of my second year, so she had to bear with me as I struggled through the learning process as well. Shreya worked tirelessly on her projects and remained an extremely dedicated researcher even after her graduation. As she enters her second year in graduate school, I am confident that she will continue to encourage and challenge her peers. Shortly after Shreya joined the lab, two other undergraduates, Geoff Buergig (mentored by Carolyn) and Ross Marklein (mentored by Rich), followed. These three phenomenal researchers formed the first group of undergraduates in our lab and helped make lab a fun and stimulating environment. It has been rewarding to see each of them move on to their own graduate careers – Geoff to University of Washington, Ross to University of Pennsylvania, and Shreya to University of Toronto. I would also like to acknowledge Luke Hiatt, who was exceptionally dedicated during his time in our lab and worked tirelessly. With his efforts, he will undoubtedly be extremely successful in medical school, and I look forward to witnessing all his accomplishments. In addition, I

appreciate the efforts of Ginger Tsai, Julia Lundrigan, and Megan Coale, each of whom contributed to this thesis.

On a more personal note, there are a number of people not directly affiliated with my project who were instrumental in getting me to where I am today. First, I'd like to acknowledge the close group of girlfriends I met during my first year here in Atlanta: Abbey Wojtowicz, Priya Santhanam, Laveeta Joseph, and Swathi Ravi. Abbey, Priya, Swathi and I met through our BME classes, and Laveeta was Abbey and Swathi's roommate first year. The five of us hit it off instantly – we all had similar goals and tastes and simply enjoyed each other's company. We have had some great times going out together – around Atlanta, Charleston, even India! I will always remember our Hindi movie nights, girls' nights, birthday celebrations, proposal celebrations, engagement parties, shopping trips, Halloweens…the list goes on and on. Each of these girls is very special to me. .Abbey and I became running buddies as we trained for the Rock n' Roll Half Marathon at Virginia Beach that was in the beginning of our second year. More important than our actual weekly runs, though, was the time we spent together during those workouts. We would catch up on life, commiserate about graduate school, complain about our experiments, and share any other joys and pains occurring in our lives. Despite the injuries, aches, and bruises (yes, I fell down on multiple occasions), I will always look back very fondly on those runs together. Priya and I have shared so many laughs together – she always knows how to make me smile, and I've gotten through many a tough time with her humor and care. I will miss our Priya-Rekha nights and our Schlotszky's dinners and will always remember the birthday that never was (too soon, Priya?). Laveeta is a great friend, and I thank her for all her support over the years.

She and her husband Ryan have such great spirits and kind hearts, and I am so glad that I was able to attend their wedding in Hyderabad, India earlier this year. I know that we'll be lifelong friends, and I look forward to seeing all the successes that they are going to achieve together. What I appreciate most about Laveeta is that she always has kind words when I'm feeling down and can make me smile just by her giggling. Swathi and I are the "twins" – when we first started grad school, no one could tell us apart. When we rotated in Dr. Chaikof's lab together, it was a while before people could distinguish us – we even drove the exact same car. We have had some great times together, and she makes a fantastic tennis buddy. She's the only person I know who matches my "talents" precisely and is perfectly willing to just hit around and not play competitively. Thanks, Swathi, for waking up earlier than you normally would on a weekend to come and play with me. And to all these girls, I want to sincerely thank them for the memories and support network they've created that helped me immensely at many points throughout my graduate school career.

I would also like to thank other fellow BME students Victoria Stahl and Adele Doyle. The three of us along with Abbey have consistently been doing at least one community service project a month for the past couple of years. I really enjoyed these times together. As our work allowed us fewer and fewer opportunities to socialize with our classmates, this fun and rewarding commitment gave us the chance to catch up (and think of something other than experiments!). I enjoyed our weeknight evenings at the Food Bank, our weekend mornings at the Nature Center, and all things in between. I'd also like to acknowledge all the other members of our class. We spent a lot of time together during our first two years of graduate school, and we quickly grew to respect

each other and have fun together. I am eager to see how all of these talented people will contribute to science, medicine, policy, and any other project they tackle. In addition, I'd like to send a shout-out to my roommate for my first couple of years here, Dr. Jennifer Phillips. Jenn was an amazing roommate and friend. Without any students ahead of me in my lab, I was fortunate to have Jenn as a role model, and her dedication to science and love for her work has influenced me considerably. She was always willing to lend an ear or offer advice and perspective on a number of issues, especially women in science and work/life balance. So thank you, Jenn, for being someone I could look up to and for setting such a great example for me.

I would also like to acknowledge my roommate during the last three years of graduate school, Dr. Krystle Chavez. Krystle and I were roommates in college at the University of Florida, and we have remained close friends ever since. I don't think I could have asked for a better roommate – she was extremely laid back and supportive of everything I did. She's the queen of bad television, and many a night I would return home exhausted from work and loved nothing more than to sit on the couch with her and watch whatever terrible show she happened to be tuned into. Krystle, along with our other college roommates Alicia Smith and Dr. Seema Qaiyumi, has been a constant source of friendship, inspiration, and a reminder to not take myself too seriously. Thank you, Krystle, Alicia, and Seema, for always reminding me that you will be here to support me and love me, no matter how my experiments turn out, when I defend, or whether I graduate at all!

Next, I must acknowledge someone I met during my first year in graduate school and who has had more impact on me than anyone else I have encountered along the way.

Kartik (excuse me, Dr. Kartik Sundar) was my T.A. for Dr. DeWeerth's class my first semester at Tech, and following that we became good friends. What struck me about Kartik was his laid-back, easy-going personality that was somehow intertwined with strong ambition and intelligence. He is the most sincere person I know and will bend over backwards to help a friend or family member in need. Kartik has taught me so many things over the past few years – most significantly, how to not take things so seriously and how to better balance work and life. As I learn and stumble through those tricky concepts, I am so grateful that he has stuck by me through all my self-doubt with more confidence in my abilities and strengths than I thought possible. Through all the trials of finishing up a dissertation, one thing that keeps me going is looking forward to our wedding in late October. So thank you, Kartik, for all your support and encouragement over the years. It has meant more to me than you could possibly imagine.

Finally, I would like to express my most profound gratitude towards my family: my parents, Drs. P.K. and Vimala Nair, my sisters, Dr. Bindu Nair (Chechi) and Deepa Nair (Deepa Chechi), my brothers-in-law, Dr. Raj Suri (Chettan) and Sunil Kutty (Sunil Chettan), my niece Vidya, and my nephew Vivek. I couldn't possibly say enough about these people, who have collectively made me the person that I am today. I must thank my father for the lessons he has instilled in me since I was young – if you're going to do something, do it right, he always says. His words, which have sounded harsh in the past, have inspired me to give everything I have to each aspect of my life. From my dad I have learned to fight for what I believe in and to not let people tell me that I'm not good enough – to paraphrase him: "they will always say that your ideas aren't good when they're afraid that you're challenging the concepts they've always held as true". My

father is also one of the most generous people I know, which has taught me a lot about selflessness and sincerity. My mother is the strongest woman I know. I am still amazed at the number of things she has been able to accomplish – not only in a lifetime, but even in a single day. She somehow had the energy to put in a full day of work as a respected graduate advisor and researcher, come home to three hungry children and a husband, and create a delicious full-spread home-made Indian meal every single night. And, of course, the house would be spotless before she went to bed at night. I still don't know how she did it, but I have so much respect and appreciation for her efforts. Part of what has enabled me to get through the trials and tribulations of graduate school is her voice always reminding me: be grateful for what you have and try to not let life's little upsets get you down, knowing how much you truly have to appreciate. To my older sisters, I owe so much. Being four and eight years older to me, I have respected them and trusted their opinions for as long as I can remember. They have always taken care of me and even as I hit my late twenties, they are continuing to do so. Chechi has instilled a love for education and learning in me, starting at a very young age. I was 8 years old when I first remember her reading *Hamlet* to me and explaining each verse. It wasn't too many years later that she would draw polymer structures on our white board to show me what polyester looked like. She has been like a second mother to me, and I know that she will always have my best interest in heart. Although only four years older to me, Deepa Chechi has also always taken care of me and does everything in her power to make sure I am happy and well. Whether it's cooking food for me or ensuring me that she'll "beat up" anyone who bothers me, she has provided incredible support over the years. The support of these two phenomenal women has had a tremendous impact in my life, and I

am certain that I am a better person for it. And to Vidya and Vivek, I would like to express my gratitude for serving as a constant reminder that life holds many joys. If I am ever feeling down about lab, research, or anything else, all I need to do is look at the two of you to remind me of the important things in life. And finally, I would like to thank my extended family, specifically my grandparents in India, for their constant love and support. I owe everything I am to my family – their sincerity, strength, encouragement, dedication, and ambition have instilled values in me that have not only carried me through graduate school, but that will undoubtedly show their worth throughout my life.

TABLE OF CONTENTS

LIST OF TABLES

LIST OF FIGURES

LIST OF ABBREVIATIONS

BMP	Bone morphogenetic protein
EBs	Embryoid bodies
ECM	Extracellular matrix
EMT	Epithelial-mesenchymal transition
ESCs	Embryonic stem cells
FGF	Fibroblast growth factor
GAG	Glycosaminoglycan
HA	Hyaluronan
HAS	Hyaluronan synthase
IL	Interleukin
IPA	Ingenuity Pathway Analysis
MMP	Matrix metalloproteinase
LIF	Leukemia inhibitory factor
PAA	Peracetic acid
RT-PCR	Real-time polymerase chain reaction
SDS	Sodium dodecyl sulfate
SPARC	Secreted protein acidic and rich in cysteine
VEGF	Vascular endothelial growth factor

SUMMARY

Regenerative medicine strategies restore function to damaged tissues by delivering factors that stimulate endogenous cells to undergo repair processes, by providing exogenous cells that will themselves facilitate repair, or by a combination of these two methods. Embryonic stem cells (ESCs) are able to differentiate into all somatic cells, and as such, are a promising cell source for therapeutic applications. *In vitro*, ESCs can be cultured to spontaneously differentiate via the aggregation of cells into clusters termed embryoid bodies (EBs). EBs recapitulate various aspects of early development, including expression of morphogenic cues necessary for tissue growth, as well as differentiation processes, such as the epithelial to mesenchymal transition. The embryonic environment harbors a unique reservoir of cues critical for tissue formation and morphogenesis. Importantly, embryonic healing responses to external insults appear to employ the same intrinsic machinery used for tissue development, and these morphogenic cues may be captured within the EB microenvironment. Recent studies have shown that when injected into injury or defect models *in vivo*, ESCs synthesize and secrete extracellular factors that ultimately contribute to wound repair, suggesting that these molecules may be as important for regenerative therapies as functional differentiation of the cells. Despite such recognition of the potential of endogenous matrix molecules synthesized by differentiating ESCs, however, surprisingly little is known about its composition. The *overall objective* of this project was to develop novel acellular matrices derived from differentiating ESCs undergoing morphogenesis. The *central hypothesis* was that embryonic matrices contain complex mixtures of extracellular

factors that, when isolated, retain bioactivity and enhance wound healing in an adult environment.

To further elucidate the expression profile of endogenous ECM synthesized by differentiating ESCs, we analyzed the temporal gene profile of matrix molecules and growth factors expressed in ESCs and EBs using Extracellular Matrix (84 adhesion molecules, basement membrane constituents, structural components, and proteases) and Growth Factor (84 angiogenic growth factors, apoptosis regulators, development controllers, and morphogenic factors) PCR arrays. During early EB differentiation, approximately 30% of the molecules examined retained expression values similar to ESC levels, but increased significantly by later time points, while a smaller subset (~12%) exhibited a significant increase earlier in differentiation and continued increasing. Interestingly, by the end of the differentiation time course examined, almost no molecules decreased significantly compared to earlier time points, all together suggesting that an onset of specification events later in EB differentiation is coincident with a surge of matrix synthesis. Importantly, gene ontology analysis of ECM and growth factor expression values highlighted that matrix synthesis alone is a reliable indicator of differentiation events occurring within the EBs, further emphasizing the underlying role of ECM in ESC differentiation.

While gene array studies provided global insight into ESC matrix synthesis, additional in-depth investigation of versican, which appeared in network analyses, was performed to more specifically examine its different isoforms. Of the four splice variants, gene expression of V0 and V1 dominated over the course of differentiation and increased significantly with time. Interestingly, the glycosaminoglycan hyaluronan (HA)

was found to co-localize with versican, and the HA/versican spatial localization patterns in EBs strengthened the notion that ECM molecules play a role in cell differentiation events. Importantly, the cell morphology in areas rich in HA and versican appeared to be distinctly different from those excluded from the region, and when examined more closely, those cells were found to be N-cadherin-positive, indicative of mesenchymal cells. Cells excluded from the versican-rich region stained positive for the epithelial marker E-cadherin. These results suggested that HA and versican are associated with an epithelial-mesenchymal transition within the EBs, which more broadly implies that the temporal expression of ECM molecules is linked to cell differentiation events.

In order to isolate the complex matrices synthesized by differentiating ESCs, a variety of reagents were tested to assess their efficacy in decellularizing EBs. Based on established protocols developed for decellularizataion of other tissue types, Triton X-100, peracetic acid (PAA), and sodium dodecyl sulfate (SDS) were tested alone and in combination with DNase. A combination of Triton X-100 and DNase significantly reduced cell viability and DNA content while maintaining a greater protein:mass ratio than either PAA or SDS treatments. More in-depth studies indicated that longer Triton durations significantly reduced protein content, and lower DNase concentrations were less efficient at DNA removal. In addition, greater solvent volumes were effective for decellularizing a range of EBs, up to ~6000 EBs. The combination of lower concentrations of Triton X-100 (0.1 -1 %) and higher concentrations of DNase (1 - 2 mg/mL) applied for relatively short durations (15 – 30 minutes) was found to be sufficient for decellularizing thousands of EBs simultaneously. The effect of Triton X-100 and DNase were further examined on EBs harvested at different differentiation time

points. In all cases, the decellularization protocol efficiently inhibited cell viability, reduced DNA content, and retained a substantial portion of the initial EB mass and corresponding protein content. Histological and ultrastructural analysis clearly indicated a lack of cellularity within acellular matrices compared to native EBs, and immunostaining results confirmed the retention of extracellular matrix components, such as collagen IV, laminin, fibronectin, and hyaluronan in the EB-derived acellular matrices.

The matrix resulting from the decellularization of EBs was then examined in an *in vivo* dermal wound healing model. Acellular EBs were applied to wounds either alone or using fibrin as a delivery vehicle and were compared to wounds left untreated or treated with fibrin alone. Matrix-treated wounds (delivered with fibrin) exhibited significantly greater percent wound closure during the 2-week post-wounding examination period than untreated wounds. In addition, compared to both fibrin-treated and untreated groups, wounds treated with matrix alone had significantly greater blood vessels per area that extravasated towards the epithelial layer. Similar observations in other studies have been linked to improved healing, which, along with the wound closure data, demonstrates that matrix derived from differentiating ESCs significantly improve dermal wound healing compared to untreated wounds. These promising results suggest that acellular EB-derived matrices can be a clinically relevant therapy for a variety of wound healing applications.

In summary, this work has examined the previously unexplored dynamic nature of ECM synthesized by ESCs and its relevance to differentiation events. Studies investigating the development of novel techniques to obtain matrices from EBs have resulted in an acellular ESC-derived matrix that significantly enhances wound healing *in*

vivo. While other work has alluded to the importance of the extracellular factors synthesized by differentiating ESCs, no other studies have derived matrices that harness the potency of these molecules for therapeutic applications. These studies lay the foundation for future work that can further examine the direct role of endogenous matrix on ESC differentiation and investigate the utility of a stem cell-derived matrix for a variety of regenerative medicine applications.

CHAPTER 1

INTRODUCTION

Embryonic stem cells (ESCs) are a pluripotent cell source derived from the inner cell mass of the pre-implantation blastocyst [1-4]. ESCs are able to differentiate into all three germ layers (endoderm, ectoderm, and mesoderm), giving rise to all somatic cells of the body, as well as germ cells. This remarkable capacity for specialization renders them an invaluable and unique cell source for regenerative medicine and tissue engineering applications where researchers are continually seeking to replace endogenous cells that have been lost due to injury or disease. *In vitro*, the differentiation of ESCs typically progresses via the spontaneous aggregation of cells into three-dimensional clusters termed embryoid bodies (EBs). EBs recapitulate the dynamic molecular machinery that elicits tissue organization and morphogenic responses during early embryonic development. Insults to embryonic tissues during this period of early development are met with intrinsic regenerative mechanisms and potent molecular factors that return the injured site to its original condition. Since EBs mimic aspects of embryogenesis, these inherent cues may be captured within the EB microenvironment.

Due to the difficulties of accessing and studying mammalian embryo systems, manipulations of ESCs and EBs have often been used to provide insight into early development processes [5-7]. More recently, tissue engineers and scientists seeking to exploit the pluripotential of ESCs for the design of cell-based therapeutics have used existing knowledge of early embryonic events to identify key regulators for directing the differentiation of the heterogeneous stem cell populations [8, 9]. As this work has

progressed, the importance of extracellular matrix (ECM) molecules in both differentiation and embryology studies has emerged. Knockdown studies of specific molecules demonstrate the resulting direct impact on ESC differentiation *in vitro* [10, 11], while others have investigated the often embryonic lethal consequences of inhibiting production of certain ECM components *in vivo* [12-19]. Despite these findings, however, there is surprisingly little information available about the complex mixture of matrix molecules (growth factors, glycosaminoglycans, proteoglycans, etc.) synthesized by differentiating ESCs.

A significant portion of ESC research has thus far focused on directing differentiation of the cells into specific cell types relevant for the disease or injury of interest, partly due to the belief that ESCs can contribute to and stimulate injured tissues via functional differentiation. In recent years, however, this notion has been challenged with a significant paradigm shift that has focused more attention on the beneficial effects of stem cell-derived molecules. In a landmark study, ESCs were injected into *Id* knockout blastocysts (a cardiac defect mouse model), and subsequent rescue of the otherwise embryonic lethal phenotype was observed [20]. Upon further investigation, the mechanism of repair was reported as the synthesis and release of extracellular factors by the injected ESCs, suggesting that stem cell-produced biomolecules could be as important, if not more so, than the functional differentiation of the cells themselves for therapeutic applications. Subsequent studies have provided supporting evidence of the potency of ESC trophic effects, ranging from anti-apoptotic cues [21, 22] to the release of anti-inflammatory molecules [23].

All together, recent studies suggest that the matrix factors naturally synthesized by differentiating ESCs and captured within the EB microenvironment may be rich in morphogenic cues that could be applied to regenerative medicine therapies. Therefore, the *objective* of this project was to develop novel acellular matrices derived from differentiating ESCs undergoing morphogenesis. The *central hypothesis* was that embryonic matrices contain complex mixtures of extracellular factors that, when isolated, retain bioactivity and enhance wound healing in an adult environment. The overall objective was accomplished by testing the hypothesis through the following specific aims:

Specific Aim 1. Investigate the production of extracellular matrix by differentiating embryonic stem cells as a function of differentiation time. The *working hypothesis* was that ESCs would produce extracellular matrix (ECM) components whose expression profiles shift with the progression of differentiation. This hypothesis was examined by using a PCR SuperArray to assess the expression profiles of 168 ECM components, adhesion molecules, and growth factors in ESCs differentiating for 4, 7, 10, and 14 days in culture. Temporal gene expression profiles were analyzed using hierarchical clustering, k-means analysis, statistical evaluation, and gene ontology software (Ingenuity Pathway Analysis) to assess the dynamic global expression of matrix synthesized by differentiating ESCs. In order to more thoroughly investigate the relationship between ECM and differentiation, two matrix molecules, hyaluronan and versican, were further analyzed via quantitative PCR, immunostaining, enzyme-based quantification, and

Western blot. The relationship between these molecules and cell differentiation was investigated by co-immunostaining with E-cadherin and N-cadherin antibodies.

Specific Aim 2. Assess the ability of solvents to efficiently decellularize embryoid bodies. The *working hypothesis* was that a combination of detergents and enzymes would allow for cellular permeabilization and extraction/digestion of cellular material, while retaining ECM protein content. This hypothesis was examined by evaluating combinations of Triton X-100, peracetic acid, sodium dodecyl sulfate, and DNase for their ability to remove cellular material in EBs while maintaining protein content. The degree of decellularization was assessed quantitatively based on cell viability, mass retention, DNA retention, and total protein content, and qualitatively based on histology. A combination of Triton X-100 and DNase was subsequently evaluated for optimal volume and concentration values using on the same multi-parametric measures as before. The ability of the Triton X-100/DNase combination to decellularize EBs cultured for different amounts of time was also investigated. Retention of structural and adhesive proteins was examined using immunostaining.

Specific Aim 3. Evaluate the healing response elicited by acellular matrices derived from embryoid bodies in an *in vivo* dermal wound healing model. The *working hypothesis* was that the ESC-derived acellular matrix would elicit improved healing responses *in vivo* as compared to untreated controls. Two bi-lateral 6-mm excisional wounds were placed on the dorsum of mice and were treated with decellularized day 10 EBs delivered alone or using fibrin as a delivery vehicle. Matrix-treated wounds were

compared to wounds treated with fibrin alone (vehicle control) or those left untreated. Wounds were analyzed quantitatively for rate of wound closure over a two week period and were excised at 7 and 14 days post-wounding to assess re-epithelialization and tissue structure (via hematoxylin and eosin staining), as well as vascularization (PECAM-1 immunostaining).

This work is *significant* because it developed a novel means of isolating extracellular factors naturally synthesized by differentiating ESCs. First, it evaluated an array of matrix molecules produced by ESCs in EBs and highlighted the possible relationship between ECM components and cellular differentiation patterns. Second, it established a protocol for removing cellular components from EBs and retaining the naturally produced ECM. Third, it evaluated the ability of stem cell-derived matrices to elicit improved wound healing responses *in vivo*. This work is *innovative* because it established a novel means of harnessing the therapeutic potential of ESCs. The combination of stem cell therapy and decellularization techniques could lead to a unique method of presenting the potency of stem cell factors in a cell-free manner. Due to the inherent pluripotency of the starting cell source, this robust new technology could be broadly applicable to the treatment of a variety of chronic diseases and traumatic injuries in need of regenerative technologies.

CHAPTER 2

BACKGROUND

Embryonic Stem Cells

Embryonic stem (ES) cells are a pluripotent cell source derived from the inner cell mass of a pre-implantation blastocyst [1-4]. The ability of ESCs to differentiate into all somatic cells of the body, as well as germ cells, renders them an ideal cell source for applications where endogenous cells are lost due to injury or disease. As such, tissue engineering strategies have used ESCs in technologies targeted towards cardiac [24], neural [25], and diabetes [26] therapies, among others. In addition, ESCs have been explored for their uses in studying developmental biology events. Thus far, ESCs have been used to improve our understanding of broad developmental events such as the epithelial-mesenchymal transition [27], early pancreatic differentiation [28], and mechanisms of early embryonic blood vessel development [29]. ESCs have also been exploited to probe more specific questions, including epigenetic mechanisms of human disorders and birth defects [30, 31], the effect of nicotine exposure to embryos [32, 33], and the role of phosphoinositide 3-kinase signaling in early development [34]. This wide range in which ESCs have been used to engineer therapies for regenerative medicine as well as to probe early developmental events has taken advantage primarily of the cells' differentiation potential, but has also in recent years considered the internal intricacies of cell-cell and cell-matrix signaling within differentiating ESCs. Conventional methods of initiating ESC differentiation *in vitro* rely on suspension culture systems in which the cells spontaneously aggregate to form clusters of differentiating cells typically referred to

as embryoid bodies (EBs) [35, 36]. Individual EBs recapitulate the temporal sequence of molecular signaling and cell differentiation events of embryonic pre-gastrulation tissues, culminating in the differentiation of the cells into the three germ lineages (ectoderm, endoderm, and mesoderm) from which all other somatic cells are subsequently formed [6, 37-40].

In early mammalian embryonic development, the pluripotent inner cell mass cells from which ESCs are derived reside in the blastocyst (Figure 2.1). The cells lining the cavity differentiate into the primitive endoderm, while the internal cells (termed the primitive ectoderm) remain pluripotent [41]. Subsequent to the appearance of a proamniotic cavity, the remaining primitive ectoderm cells differentiate into a pseudostratified columnar epithelium with distinct differentiation potential [42-44], typically called the epiblast [7]. Finally, the primitive endoderm cells differentiate into either visceral or parietal endoderm [45], while the epiblast serves as the substrate for gastrulation from which all three germ layers will form. ESCs and their EB differentiation model recapitulate these early embryonic events (Figure 2.1), from the formation of an epithelial layer to the mechanism of cavity formation [46]. As such, researchers have used ESCs as a model system of development to gain further mechanistic insight into the signaling cues and environmental necessities relevant to the morphogenic embryo.

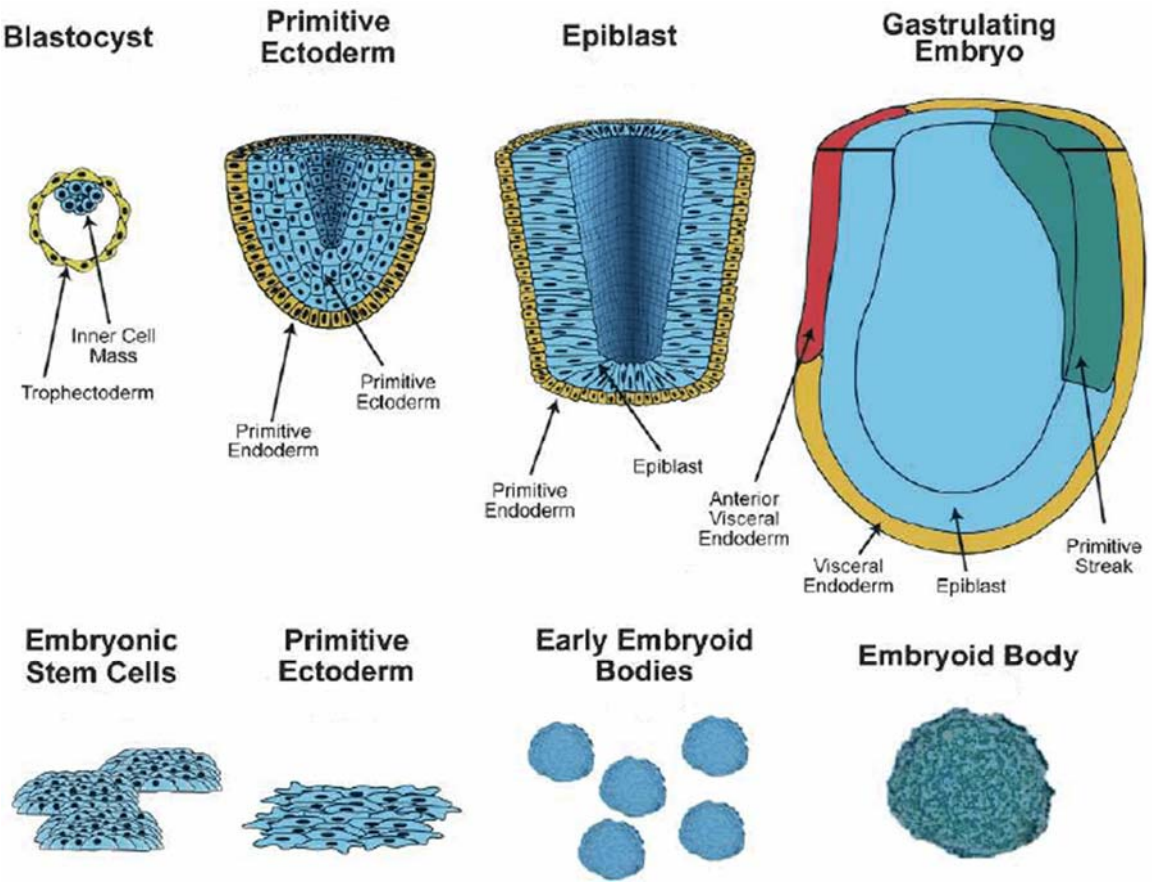

Figure 2.1. Early embryonic events and ESC differentiation. ESC differentiation via EB formation recapitulates the early events of embryonic development (modified from [7]).

Paracine actions of ESC populations

Since the derivation of ESCs, a significant portion of stem cell research has been focused on directing the differentiation of the cells into a phenotype of therapeutic interest. However, a recent paradigm shift has drawn attention to the synthesis of endogenous factors and subsequent secretions by ESCs *in vivo* that may directly contribute to the observed output in the absence of functional differentiation. In a landmark study, ESCs injected into *Id*-knockout embryos were able to rescue the otherwise lethal cardiac defect through the secretion of molecular factors [47]. Importantly, there was also a partial rescue of the cardiac phenotype when ESCs were injected into female mice bearing Id mutants, demonstrating the presence of long-range factors secreted by the ESCs, as the cells themselves would not have been able to cross the placenta barrier. In separate studies, ESCs were found to suppress seizures through a paracrine mode of action [48] and were also shown to release extracellular factors into their medium that significantly decreased apoptosis in a cardiomyocyte-derived cell line [21, 22]. In addition, hearts subjected to ischemic conditions recovered significantly when treated with ESCs, due in part to protection conferred by stem cell release of anti-inflammatory molecules (e.g. interleukin (IL)-10) [23]. Importantly, mesenchymal stem cells derived from ESCs deposited fetal-like tendon matrix as well as a host of growth factors that likely contributed to improved healing responses in an *in vivo* tendon repair model [49]. All together, these significant observations suggest that biomolecules produced by stem cells may be at least as important as differentiation of the cells to achieve cell restoration and functional tissue repair. Curiously, little is known about the actual molecular composition of the extracellular factors synthesized within EBs during

the course of *in vitro* differentiation. Since EBs provide a snapshot into the earliest stages of morphogenesis, analysis of the proteins, glycosaminoglycans, and proteoglycans they produce would lend insight into the potential regenerative nature of embryonic extracellular matrices (ECMs).

Extracellular Matrix

Tissue engineering and regenerative medicine have long relied on the use of extracellular molecules to aid in the culture or delivery of cells for therapeutic purposes. Extracellular matrix (ECM) is a mixture of structural and adhesive proteins, growth factors, glycosaminoglycans (GAGs), proteoglycans, and matricellular proteins that is secreted by the local cell population and organized in a network associated with those cells. Collagens constitute 25% of total protein mass in mammals and are a primary component of both skin and bone. Collagen molecules contain three polypeptide α chains rich in proline and glycine that are folded into a helical conformation. Of the 20 distinct collagens that have been identified, collagen I is the most abundant [50]. Collagens I, II, and III assemble into fibrillar structures, whereas collagen IV molecules form a mesh-like network that comprise a significant portion of the basment membrane in tissues. Along with collagen IV, laminin-1 is one of the key components constituting the basal lamina and is composed of three polypeptide (α1, β1, and γ1) chains. There are seven individual laminin molecules (laminins-1 to -7), each containing different combinations of eight genetically separate laminin chains, although laminin-1 is perhaps the most well-characterized [51]. Fibronectin, another well studied multidomain adhesive glycoprotein, is found in blood plasma and can also be synthesized by local

cells [52]. Matricellular proteins, which regulate interactions between cells and matrix, include secreted protein acidic and rich in cysteine (SPARC), thrombospondin 1 and 2, and osteopontin [52].

GAGs are negatively charged polysaccharide chains whose anionic and hydrophilic properties cause them to swell and occupy large volumes, thereby allowing the GAGs to withstand high compressive forces [50]. They are composed of repeating disaccharide units: an amino sugar (N-acetylglucosamine or N-acetylgalactosamine) and typically a uronic acid (glucuronic or iduronic). GAGs are generally categorized into four groups, based on the sugars, sugar linkages, and sulfate groups: hyaluronan, chondroitin sulfate and dermatan sulfate, heparan sulfate, and keratan sulfate. Of the different GAG classifications, hyaluronan (HA) is particularly abundant in embryonic tissues. Unlike the other GAGs, it contains no sulfated sugars and is typically not linked to a core protein. Several of HA's functions, however, rely on the interactions between HA and proteoglycans, which are GAG chains linked to a core protein.

GAGs also serve as reservoirs for growth factors that play important roles in cell signaling as well as ECM synthesis. Growth factors can regulate matrix production by stimulating resident cells to synthesize matrix molecules or augment production of matrix metalloproteinases (MMPs) that degrade the ECM. In turn, growth factor activity can be directly controlled by the ECM, which can either sequester the growth factors and hinder their activity, or can harbor molecules such that they are protected from degradation and their activity is concentrated [52].

Primarily, exogenous ECM has been used in studies as substrates for cell culture as well as for scaffolds for *in vivo* implantation, but little emphasis has been placed on the

endogenous matrix being supplied by more primitive cell sources. As mentioned above, in the case of ESCs, matrix synthesis may be particularly important to characterize due to its potential to actively participate in and contribute to regenerative or healing processes.

Extracellular molecules in tissue engineering

For stem cell-based tissue engineering strategies, matrix proteins have been widely used for substrate coatings to influence the progression of cell differentiation. In some key studies, an array platform was used in which mixtures of fibronectin, laminin, collagen I, collagen III, and collagen IV were spotted onto wells and subsequently seeded with ESCs to allow for an extensive examination of the combinatorial effect of multiple ECM proteins on stem cell fate [53, 54]. While previous studies tended to focus primarily on one particular molecule, the results of these studies demonstrated the effects that a complex mixture of matrix molecules can have on differentiation.

In an effort to take advantage of the potency of ECM molecules and growth factors, researchers have employed tissue engineering strategies to mimic matrix function. For example, growth factor delivery systems have been engineered for the local release of heparin-binding growth factors coincident with enzymatic activity in wound healing applications [55]. Inkjet printing methods have also been developed in order to present growth factors in a biologically relevant manner, with examinations of growth factor concentration gradients as well as combinations of different growth factors contributing to identification of cell fate influences [56]. Biomimetic adhesive peptides have also been engineered to promote cell surface interactions [57] and influence matrix mineralization [57, 58], while exogenous additions of growth factors and cytokines to

culture media or the use of conditioned media have been shown to promote cell proliferation [59], survival [60], and differentiation [61, 62].

Extracellular matrix in ESC populations

As discussed above, several studies have investigated the effects of culturing cells on different ECM substrates or subjecting cells to exogenously added growth factors and cytokines; however, less emphasis has been placed on examining the role of the endogenous matrix on stem cell maintenance and differentiation. In recent years, however, the stem cell niche has received increasing attention from researchers seeking to understand the interplay of the cells and ECM within the microenvironment of differentiating cell clusters. As research has progressed, the presence of endogenous matrix molecules has been found to have a significant influence on subsequent differentiation patterns.

As interest has grown in this area, researchers have largely focused on individual molecules of specific interest to them. Reports on specific molecules synthesized by differentiating ESCs have recently surfaced, gradually developing the story of ESC endogenous matrix production. Laminin in particular has been the focus of several studies and in EBs has been found to correlate with the induction of epiblast differentiation and cavitation, possibly with some of the cell-cell and cell-matrix interactions mimicking those *in vivo* [63]. Specifically, laminin-γ1 (LAMC1) was found to be necessary for laminin assembly, which was essential for basement membrane formation in both EBs and *in vivo* [12]. The addition of exogenous laminin-1 to cultures was able to rescue LAMC1-/- knockouts [64] that otherwise could not cavitate or form an

epiblast layer or basement membrane [11]. In addition, a recent study demonstrated that matrix proteins synthesized by ESCs, specifically collagen I, are essential for ESC survival and differentiation and cannot necessarily be rescued by exogenous addition of the protein [65]. These results are perhaps not surprising, as studies from developmental biology have shown the appearance of laminin-1 at the 2-cell stage [66] and fibronectin and collagen IV in the inner cell mass of 3-4 day-old blastocysts [67], suggesting a role for matrix proteins in the earliest embryo stages. Other studies have also looked specifically at the role of certain molecules in differentiating ESCs [10, 68], while some have focused on conditioned media studies wherein ESCs were found to release specific growth factors and cytokines [60]. As discussed previously, such studies that examine the release of ESC-derived factors have elucidated paracrine mechanisms by which ESCs or EBs contribute to the repair of wounded tissue. The majority of studies investigating endogenous ECM in ESCs have examined specific molecules of interest, but importantly, a few researchers have now begun to examine endogenous ECM production at a more global level [69, 70], thereby identifying possible candidates for future studies.

Acellular Biomaterials

Decellularization methodologies have been developed as a means of separating cells from tissues. This technology arose as researchers investigated the potential of the complex mixture of matrix molecules found naturally in tissues. Before the use of such tissues would be clinically applicable, however, it was necessary to eliminate or significantly reduce elements in the tissue that would elicit immune reactions in the host. Consequently, decellularization technologies arose as a means to remove cells from

tissues without disrupting the native composition of its matrix. Examples of tissues that have been decellularized include small intestinal submucosa (SIS), peripheral nerve, arteries, pericardium, skin, tendon, placenta, and bladder [71-78]. Some of these acellular scaffolds have been applied to aid in the repair of the same tissue from which it was derived, whereas others have been used in different sites, such as SIS for tendon/ligament repair, myocardial healing, or as a reparative wound dressing [79-82]. In addition, acellular tissues are not only capable of stimulating neovascularization and eliciting a minimal host immune response, but can also promote tissue repair *in vivo* [83-85]. These benefits could perhaps be amplified if the original tissue contained morphogenic cues naturally embedded within its matrix.

Decellularization methods

Given the wide variety of tissues in the body, different decellularization methods must be optimized to account for the range in matrix composition and tissue density [86]. Common protocols typically involve both physical and chemical means of disrupting membranes and removing cellular components. Physical methods can involve freeze-thaw, pressure, and sonication techniques [87, 88]. General mechanical agitation has also been used, though optimal cellular removal combines physical disruption with chemical extraction treatments [73]. A variety of chemicals have been used to decellularize tissues, including alkaline or acid treatments, non-ionic or ionic detergents, and enzymatic treatments. Acid/alkaline treatments, such as peracetic acid (PAA), and ammonium hydroxide are used to solubilize cellular cytoplasmic components and disrupt nucleic acids. PAA in particular has been found to be effective as a disinfectant and at

removing cellular material while maintaining matrix proteins, GAGs, and growth factors of thin tissues [80, 89, 90]. Ionic detergents, such as sodium dodecyl sulfate (SDS), have been used for solubilization of nuclear and cytoplasmic membranes, although they tend to significantly disrupt ECM components [91]. In contrast, non-ionic detergents can lyse cellular membranes in a gentler manner without significantly disrupting lipid-lipid and lipid-protein interactions. Triton X-100 is a common non-ionic detergent used for decellularization, although some studies have reported variable success in its ability to remove cellular material and retain ECM components after treatment [91-93]. Finally, enzymatic treatments such as trypsin and DNase have been used to extract cellular proteins and nucleotides [85, 92]. The conflicting evidence on the varying successes of similar decellularization treatments on diverse tissues indicates that different reagents and combinations of reagents must be optimized for each tissue by controlling the concentrations, durations, and sequences of treatments to effectively yield bioactive decellularized products.

Wound Healing

In recent years, developmental biology and regenerative medicine have reached a crossroads as tissue engineers have realized the importance of examining early morphogenic processes to gain insight into potential treatment strategies [94]. The regenerative potential of humans is highest in the earliest embryonic stages, where ECM composition and signaling molecules provide a forgiving template for developing tissues. For example, adults who are subjected to external wounding will not regenerate the damaged skin; they will instead repair the injured area imperfectly, leaving a scar. On

the contrary, when embryos are wounded, the morphogenic cues present within their structures are able to completely regenerate the injured tissue. As such, wound healing is one area where clear differences between embryonic and adult responses to injury are leading to a greater mechanistic understanding of possible approaches to developing regenerative therapeutics.

Wound healing and animal models

Wound healing responses in adult animals involve a cascade of events beginning with an inflammatory response, re-epithelialization of the wound, formation of granulation tissue, and final healing with scar. After injury, a fibrin clot is formed and platelets aggregate and release various inflammatory mediators, such as platelet-derived growth factor (PDGF), transforming growth factor (TGF-α and –β), fibroblast growth factor (FGF), epidermal growth factor (EGF), and insulin-like growth factor (IGF) [95]. These factors, as well as chemokines, recruit inflammatory cells (e.g. neutrophils and monocytes) to the site of injury, with macrophage infiltration peaking 3-5 days post-wounding. During the reparative phase of wound healing, fibroblasts lay down a provisional matrix consisting mainly of collagen and fibronectin, leading to scar formation, and further differentiate into myofibroblasts, which aid in wound contraction during the secondary phase of healing. These events are also accompanied by the migration of keratinocytes from the wound edge, re-epithelialization, and vascularization [96].

The two main injury models typically used to examine treatments for dermal wound healing are the incisional and excisional models, which can be performed on large

(e.g. lamb) or small (rat, mouse, rabbit) animals. In the incisional model, 1-cm cuts penetrating the epidermis, dermis, and panniculus carnosus are made along the dorsum of the back. Similarly, excisional cuts penetrate through the three layers, but are performed using a dermal biopsy punch. Comparable analyses can be performed on the two models, although incisional wounds are more amenable to tensile testing, while wound closure data is easier to obtain with excisional wounds. These models offer several methods of parameter quantification, including a combination of staining and image analysis to quantify re-epithelialization and vascularization.

Embryonic versus adult wound healing

The primary and well-studied difference between embryonic and adult wound healing is the ability of early fetal skin injuries to heal scarlessly. This remarkable capability does not translate to all tissues of the fetus, as full thickness incisional wounds in the stomach, intestine, and diaphragm heal with a scar [97]. Differences between embryonic and adult dermal injury healing have been widely studied, and several key differential features have emerged. In the ECM deposition of embryonic wounds, hyaluronic acid (HA) increases more rapidly and is more sustained [98], and collagen is characterized by a fine reticular pattern and has a higher ratio of type III to type I [99]. Embryonic wounds also heal with fewer inflammatory cells, decreased expression of PDGF, FGF, TGF-β1, TGF-β2, interleukin-6 (IL-6), and IL-8, and increased expression of TGF-β3 and VEGF [100-104]. Finally, fetal and adult fibroblasts behave differently, with fibroblasts in the adult environment differentiating into myofibroblasts, which have an essential role in wound contraction [105]. Importantly, addition of specific molecules,

such as IL-10 [106], TGFβ3 [107], and hyaluronan [108], to an adult wound results in an improved healing response, suggesting that exogenous effector molecules can alter the typical course of healing and more closely mimic fetal regeneration. The myriad of differences between the embryonic and adult environments, which are independent of the *in utero* extra-embryonic milieu [109], help elucidate the mechanisms by which an embryonic dermal wound can heal scarlessly, and may therefore also provide insight into potential methods to elicit tissue regeneration in the adult.

Studies that compare mechanisms of tissue movements in embryonic development and adult wound healing processes have uncovered many parallels, such as dorsal closure in *Drosophila* and ventral enclosure in *C. elegans*, that involve the re-epithelialization of tissue gaps [110]. Embryonic healing and subsequent regeneration may be the result of a response that essentially recapitulates developmental dynamics wherein the tissue insult triggers typical morphogenic mechanisms in the embryo [110]. Therefore, therapies that provide cues present in an embryonic environment may similarly be able to stimulate a morphogenic response in an adult.

CHAPTER 3

DYNAMIC PATTERNS OF EXTRACELLULAR MATRIX AND GROWTH FACTOR EXPRESSION BY PLURIPOTENT EMBRYONIC STEM CELLS UNDERGOING EMBRYOID BODY DIFFERENTIATION*

Introduction

Embryonic stem cells (ESCs) have been widely used as a model of embryonic morphogenesis to examine the differentiation of pluripotent cells into mature differentiated phenotypes. Typically, ESC research focused on the differentiation potential of the cells as a source of therapy where endogenous cells have been lost due to injury or disease. More recently, however, the molecules synthesized and secreted by ESCs have been investigated for their potent paracrine morphogenic effects [21, 47, 111]. *In vitro*, ESCs can be cultured to differentiate via the spontaneous aggregation of cells into clusters termed embryoid bodies (EBs). The inherent and spontaneous differentiation that occurs by ESCs within EBs recapitulates aspects of embryogenesis, including ESC differentiation towards all three germ lineages – ectoderm, endoderm, and mesoderm [5, 36]. Typically, ESC differentiation studies have focused on the phenotypic outcomes towards a more restricted cell fate through characterization of the resulting cell types, such as endothelial cells [112, 113], hepatocytes [113, 114], and neurons [115,

---

* Modified from:
R Nair†, A Ngangan†, ML Kemp, and TC McDevitt. *Dynamic patterns of extracellular matrix and growth factor expression by pluripotent embryonic stem cells undergoing embryoid body differentiation*, in preparation. † Both authors contributed equally to this work.

116]. The molecular composition of the extracellular microenvironment associated with the differentiation process can influence these phenotypic outcomes, yet is generally overlooked.

The dynamic expression of extracellular matrix (ECM) molecules and growth factors during differentiation can provide feedback to the cells that in turn can modulate cell phenotype, thereby affecting the outcome of cell specification events. The addition of exogenous ECM and growth factor molecules has also been shown to affect cell phenotype during directed differentiation schemes. For example, exogenous vascular endothelial factor (VEGF) or bone morphogenetic protein (BMP)-4 [117] encourage cells towards a vascular phenotype, while the addition of laminin to culture media can enhance neural progenitor differentiation from human ESCs [118]. Despite these and other successes relating to the promotion of differentiated phenotypes via exogenous matrix additions, curiously little is known about the inherent ECM and growth factors produced during early spontaneous differentiation of ESCs within developing EBs. Some studies have begun to examine the gene expression profile of early EBs using microarrays [119-121], while others have investigated aspects of the EB transcription factor [122] and glycomics [123] profiles. These studies typically analyzed hundreds or thousands of genes, including a subset of ECM genes, yet little work has specifically extracted and analyzed that matrix data or examined the endogenous expression of the ECM and growth factors in differentiating ESCs. The molecules produced within EBs can provide direct feedback to the ESCs as they differentiate; thus, the profile of extracellular factors could offer further insight into the self-regulation of ESC differentiation via extracellular cues.

The focus of this study was to globally assess the dynamics of ECM and growth factor expression associated with the differentiation of ESCs within the EB microenvironment using gene expression and pathway analysis. Gene expression was examined using low density RT-PCR arrays specific for ECM components, including cell adhesion molecules, matricellular proteins, integrins, and proteases, as well as growth factors, including members of the BMP, fibroblast growth factor (FGF), transforming growth factor β (TGFβ), and interleukin (IL) families. Gene expression analyses included hierarchical clustering, k-means clustering, and significance testing that contrasted different patterns of expression and determined similarities among specific molecules. Subsequent pathway analyses highlighted signaling pathways reconstructed solely from ECM and growth factor content information. This study investigates the dynamic relationship between ECM/growth factor expression and differentiation time using novel analytical approaches and provides insights into the extracellular microenvironment of pluripotent stem cell matrix biology.

Methods

Embryoid Body Culture

Mouse embryonic stem cells (ESCs; D3 cell line) were cultured on 0.1% gelatin-coated 150 mm polystyrene cell culture dishes (Corning) with Dulbecco's modified eagle medium (Mediatech), supplemented with 15% fetal bovine serum (HyClone), 2 mM L-glutamine (Mediatech), 1x MEM non-essential amino acid solution (Mediatech), antibiotic/antimycotics (Mediatech), and 0.1 mM β-mercaptoethanol (MP Biomedicals, LLC). Undifferentiated cells were expanded prior to EB formation in the presence of 10^3

U/mL leukemia inhibitory factor (LIF) (ESGRO), which was added to the culture media upon each re-feeding. Cells were passaged every two to three days before reaching ~70% confluence. To initiate EB culture, ESCs were trypsinized from the gelatin-coated dishes using 0.05% Trypsin/0.53 mM EDTA (Mediatech). A density of 400,000 cells/mL was used to inoculate 10 mL EB cultures in 100 mm bacteriological grade polystyrene Petri dishes (Corning) using differentiation media (media without LIF). Cultures were placed on rotary orbital shakers (Barnstead Lab-Line, Model 2314) at 40 rpm at 37^{o}C in 5% CO_2 for the entire duration of suspension culture. Previous work from our lab has demonstrated that rotary orbital suspension culture methods result in greater yields of homogeneous populations of EBs [124]. EBs were cultured in suspension for up to 14 days and re-fed every other day after collecting the EBs via gravity-induced sedimentation in 15 mL conical tubes. Spent media was aspirated, and the cultures were replenished with 10 mL of fresh differentiation media before being placed back in the Petri dishes and returned onto the rotary orbital shakers.

Microscopy and histological analysis

Phase images of the EBs were taken at each day of EB differentiation (up to 14 days) using a TE2000 microscope and a Spot Flex camera (Diagnostic Instruments, Inc.). For histological analysis, EBs collected at different stages of differentiation (4, 7, 10, or 14 days) were fixed with 10% formalin for 30 minutes and embedded in Histogel® (Richard-Allan Scientific). Each Histogel® block was processed for histological sectioning through a series of xylene and alcohol rinses prior to paraffin embedding. Sections of EB samples (5 μm each) were obtained using a Microm HM 355S rotary

microtome and stained with hematoxylin and eosin (H&E) using a Leica AutoStainer XL. Each slide was coverslipped using low viscosity mounting medium (Cytoseal™ 60) and imaged on a Nikon 80i microscope.

Quantitative reverse-transcription polymerase chain reaction (qRT-PCR)

RNA was extracted from undifferentiated ESCs and EBs at days 4, 7, 10, and 14 of differentiation (n = 3 for each sample) using the RNeasy Mini Kit (Qiagen). Complimentary DNA was reverse transcribed from 1 μg of total RNA using the iScript cDNA synthesis kit (Bio-Rad), and real-time RT-PCR was performed using SYBR Green technology on the MyiQ cycler (Bio-Rad). Beacon Designer software was used to design forward and reverse primers for pluripotency marker *Oct-4*, endoderm differentiation marker α-fetoprotein (*Afp*), and housekeeping gene glyceraldehyde-3-phosphate dehydrogenase (*Gapdh*), which were validated with appropriate positive controls. Relative levels of *Oct-4* gene expression were calculated compared to undifferentiated ESC samples using the Pfaffl method [125], whereas *Afp* concentrations were calculated based upon standard curves and normalized to *Gapdh* expression levels.

For SuperArray RT^2 Profiler™ PCR array analysis, cDNA synthesis was performed using the SuperArray RT^2 First Strand kit (SABiosciences). A genomic DNA elimination mixture was prepared by first mixing 0.5 μg RNA with 5x gDNA Elimination Buffer and RNase-free water and then incubating at 42°C for 5 minutes. The RT cocktail (4 μL 5x RT Buffer 3, 1 μL Primer & External Control Mix, 2 μL RT Enzyme Mix 3, and 3 μL RNase-free water) was prepared and added to the elimination buffer mixture. Each sample was synthesized in an iCycler Thermal Cycler (Bio-Rad)

(15 minutes at 42°C, 5 minutes at 95°C) and diluted with RNase-free water after synthesis was complete. RT-PCR was performed by first preparing the experimental cocktail (1275 μL 2x SuperArray RT^2 qPCR Master Mix, 102 μL diluted first strand cDNA synthesis reaction, 1173 μL RNase-free water) and equally distributed into all of the individual wells of the PCR 96-well array (Mouse Extracellular Matrix and Adhesion Molecules array or Mouse Growth Factors array). Each array was tightly sealed with optical thin-wall 8-cap strips and run in a MyiQ cycler (Bio-Rad) with a two-step cycling program (1 cycle, 10 minutes, 95°C; 40 cycles, 15 seconds, 95°C; 40 cycles, 1 minute, 60°C). Fold changes in gene expression were analyzed using the $\Delta\Delta C_t$ method of quantitation, whereby samples of EBs from different time points (days 4, 7, 10, and 14) were compared relative to undifferentiated ESC values after individual sample values were normalized to internal GAPDH levels.

Gene clustering analysis: hierarchical clustering and k-means

Differences in gene expression over time in differentiating EBs were calculated as fold change increases or decreases compared to ESCs, calculated as described above. Triplicate fold change values obtained from the ECM and Growth Factor arrays were separately input into the array analysis software Genesis (Release 1.7.5). Hierarchical clustering was then performed across both genes and time points on log2-transformed data using average linkage clustering. The clustering was visualized via a heat map and dendrogram, with green indicating decreased expression compared to ESCs and red indicating increased expression. The color intensity corresponds to the magnitude of decreases or increases.

The average fold change values of ESCs (fold change = 1) and EBs from both array sets were merged and input into Genesis for k-means clustering analysis. Based on a trial-and-error process in which different cluster numbers were qualitatively evaluated for the optimal number that captured the different profile possibilities, parameters were set as 12 clusters and a maximum of 300 iterations. Expression profiles of each gene across the 14 day time course were generated in gray for each of the 12 clusters, with the centroid for each cluster depicted in pink.

Ingenuity Pathway Analysis (IPA)

Pathway analysis was performed using Ingenuity Pathway Analysis (Version 7.5, Ingenuity® Systems) to examine the biological functions and signaling pathways that were implicated in EB development over time. For each time point (days 4, 7, 10, and 14), fold change ratios (values: 0 to +513.58) were inputted into IPA and converted to fold changes (-46.25 to -1 and 1 to +513.58). Genes with a minimum of 3-fold change were input into IPA software analysis to filter the dataset and obtain "focus" genes. The results of the "core analysis" consisted of top "biological functions" and "networks" for each time point using the eligible "focus" genes. The association of a specific gene to other genes, either by interaction or in a functional annotation within IPA's knowledge base, determined a gene's eligibility. Biological functions were tested for significance ($p < 0.01$) using the Benjamini-Hochberg (B-H) multiple testing correction to account for false-positives and ranked most to least significant (–log B-H p-value). The networks for each observation were generated based on the interaction of "focus" genes found in IPA's knowledge base. Each resulting networks included up to 35 genes, to maintain a

manageable size, and was scored based on the probability of finding a "focus" gene in that network, with higher scores indicating a lower chance of finding a "focus" gene within that network.

Statistics

Significance testing was conducted using SYSTAT (Version 12) software. For each gene, expression fold change comparisons across time points were conducted using a one-way analysis of variance (ANOVA) with subsequent post-hoc Tukey analysis to determine significance ($p < 0.05$).

Results

EB differentiation

Prior to performing the PCR array analysis for ECM and growth factor expression, the time course of EB differentiation was evaluated by histological analysis and phenotypic gene expression. The size and morphology of the population of EBs remained relatively uniform over the time course examined (Figure 3.1A-D) using rotary orbital suspension culture, similar to previously published results [124]. Evidence of progressive differentiation was indicated by changes in the organization and morphology of the cells within EBs (indicated by black arrows), as well as the increasing appearance of cystic cavities (red arrows) (Figure 3.1E-H). The eosinophilic (pink) staining apparent by day 10 and accumulating by day 14 was visible primarily in regions of EBs with a lower cell density and was suggestive of increasing matrix deposition by the cells. Over time, the ESCs expressed significantly less *Oct-4*, a pluripotent transcription factor

(Figure 3.1I), and conversely, expressed significantly increasing levels of the endoderm differentiation marker α-fetoprotein (*Afp)* (Figure 3.1J), as well as several genes indicative of ectoderm (Nestin) and mesoderm differentiation (*Gata4*, *Nkx2.5*, myocyte enhancer factor-2c, alpha myosin heavy chain, myosin light chain-2 ventricle) (data not shown) [124, 126], thus further confirming the expected time course of differentiation. By day 10 of differentiation, *Oct-4* decreased significantly compared to day 4 EBs ($p = 0.03$) and by day 14 exhibited significantly lower expression than both day 4 and day 7 EBs ($p = 0.002$, 0.005, respectively). *Afp* was significantly greater in day 14 EBs compared to all other time points examined ($p = 0.001$). The coincident series of morphological and phenotypic changes over the course of EB differentiation are consistent with previous studies from our laboratory [124, 126, 127], as well as others.

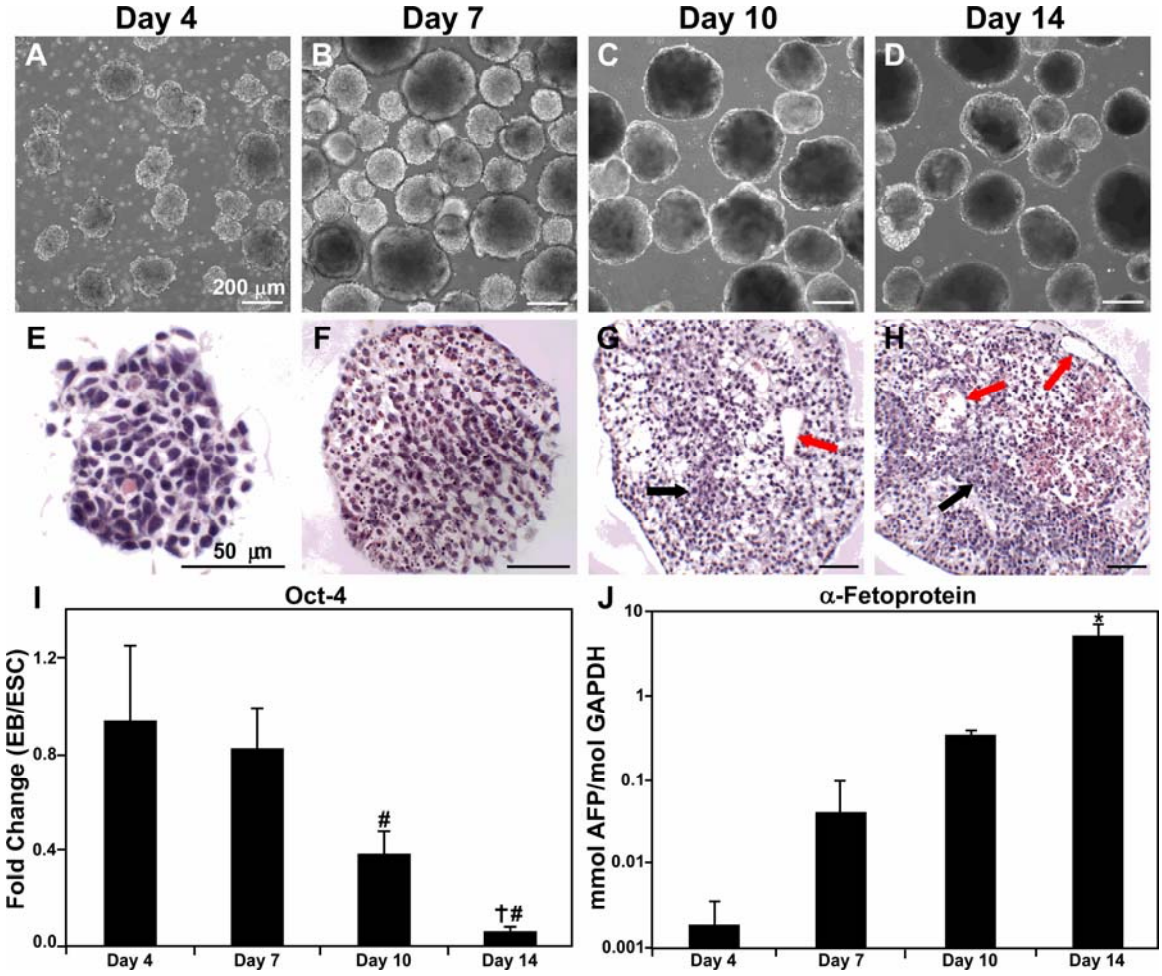

Figure 3.1. EB morphological and gene expression analyses over the course of differentiation. EBs cultured on a rotary orbital shaker remain relatively homogeneous in size and shape throughout differentiation (A-D). Noticeable differences in cell morphology (black arrows) and the onset of cavitation (red arrows) indicate the progressive differentiation of cells within EBs through H&E histological analysis (E-H). The significant decrease of the pluripotent marker *Oct-4* (I) and steady increase of the endoderm differentiation marker *a-fetoprotein* (J) assessed through RT-PCR demonstrates the gradual progression of differentiation with time. # Significantly different from day 4 EBs, $p \leq 0.03$; Significantly different from day 7 EBs, $p = 0.005$; * Significantly different all other time points, $p = 0.001$.

Gene clustering based on expression profiles

Two-dimensional hierarchical clustering of the individual experimental replicates as a function of time was initially performed independently for both the Extracellular Matrix and Adhesion Molecules array (referred to subsequently as the ECM array; Figure 3.2A) and the Growth Factors array (Figure 3.2B). Importantly, independent samples for each of the individual time points clustered together, and both the earlier (4 and 7 days) and later (10 and 14 days) time points clustered more closely together, demonstrating the reproducibility of experimental samples and distinct shifts in gene expression occurring over time with differentiation. For each array, two patterns of increased (red signal) or decreased (green) gene expression over time were evident, whereas most of the remaining genes were relatively unchanged compared to undifferentiated ESCs. In the ECM array, 16 molecules clustered together that tended to decrease in expression relative to ESC levels, while 14 molecules that consistently increased over the course of differentiation clustered together. The remaining 59 molecules, which included housekeeping genes such as heat shock protein 90kDa alpha (cytosolic) class B member 1 (*Hsp90ab1*), *Gapdh*, glucuronidase beta (*Gusb*), and β-actin (*Actb*), exhibited baseline values that increased or decreased only slightly compared to ESCs. The housekeeping genes were similarly clustered in the Growth Factors array, indicating the consistency of analysis across the separate, independent arrays. In contrast to the ECM array, more of the genes from the Growth Factor array clustered together in both the increasing (26 molecules) and decreasing groups (28 molecules). Within these relatively broad classifications, a few visibly distinct clusters emerged from both arrays, including five sharply increasing molecules in the ECM array that exhibited 46- to 513-fold increases

compared to ESCs by day 14 (catenin alpha 2 (*Ctnna2*), periostin (*Postn*), hyaluronan proteoglycan link protein 1 (*Hapln1*), collagen III alpha 1 (*Col3a1*), vitronectin (*Vtn*)). In the growth factor array, 13 molecules (including bone morphogenetic protein 8a/8b (*Bmp8a/8b*) and fibroblast growth factor (*Fgf17*)) clustered together that exhibited as much as a 25-fold decrease compared to ESCs, while 7 molecules increased (including *Bmp5* and insulin-like growth factor (*Igf2*)) up to 240-fold over ESCs. Hierarchical clustering provided a visual depiction of general patterns of gene expression by differentiating EBs and identified specific genes that were highly increased or decreased in expression.

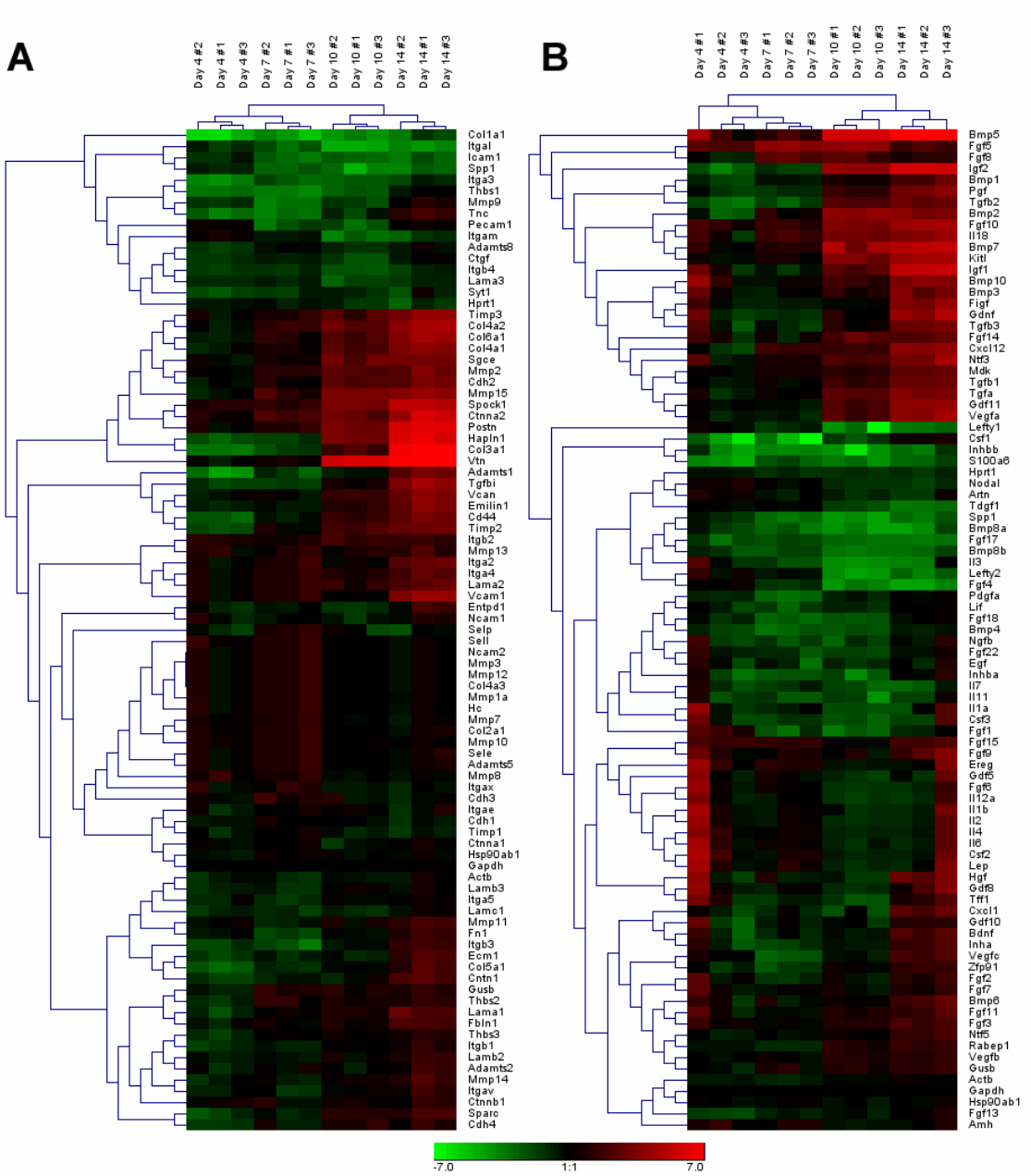

Figure 3.2. Hierarchical clusters and dendrograms of ECM and growth factor arrays. Two-dimensional hierarchical clustering was performed on ECM (A) and Growth Factor (B) arrays. Genes were clustered as either increasing (red) or decreasing (green) compared to undifferentiated ESCs.

Table 3.1. Genes in each cluster represented in Figure 3.3A.

Cluster I	Cluster II	Cluster III		Cluster IV	Cluster V
Fgf5	Col1a1	Fgf15	Vegfb	Adamts1	Csf1
Fgf8	S100a6	Fgf9	Ctnnb1	Col5a1	Thbs1
Igf1	Itga3	Gdf8	Fbln1	Cntn1	Tnc
Bmp10	Inhbb	Hgf	Adamts2	Ecm1	Pdgfa
Fgf14	Itgal	Ereg	Itgav	Itgb3	Mmp9
Ntf3	Bmp8b	Gdf5	Lamb2	Tgfb2	Bmp4
Gdnf	Fgf17	Il2	Ntf5	Tgfbi	Il11
Figf	Icam1	Il4	Mmp14	Gdf11	Fgf18
Bmp3	Bmp8a	Il1b	Cdh4	Vegfa	Inhba
Tgfb3	Spp1	Csf2	Thbs3	Tgfb1	Pecam1
Bmp2	Fgf4	Il6	Thbs2	Vcan	Adamts8
Kitl	Lefty1	Lep	Gusb	Pgf	Ctgf
Mmp15	Lefty2	Fgf6	Artn	Emilin1	Syt1
Ctnna2	Tdgf1	Il12a	Nodal	Lama1	Itgb4
Postn	Fgf1	Csf3	Selp	Bmp1	Lama3
Bmp7	Il3	Il1a	Cdh1	Sparc	Il7
Il18	Itgam	Tff1	Timp1	Cd44	Hprt1
Fgf10		Fgf2	Cdh3	Timp2	Egf
Spock1		Fgf7	Hc		Fgf22
Cxcl12		Gdf10	Mmp10		Ngfb
Mmp2		Bdnf	Mmp7		Lif
Cdh2		Cxcl1	Mmp1a		Lamc1
Tgfa		Entpd1	Col4a3		Fgf13
Col4a1		Inha	Mmp12		Itgb1
Sgce		Vegfc	Mmp3		Lamb3
Col4a2		Zfp91	Ncam2		Itga5
Col6a1		Fn1	Adamts5		Actb
Timp3		Itga2	Col2a1		
Vcam1		Mdk	Sele		
Col3a1		Itga4	Itgax		
Igf2		Lama2	Amh		
Hapln1		Bmp6	Mmp8		
Bmp5		Fgf11	Sell		
Vtn		Fgf3	Ctnna1		
		Itgb2	Ncam1		
		Mmp13	Itgae		
		Rabep1	Hsp90ab1		
		Mmp11	Gapdh		

The average fold change values of the individual replicates from the independent arrays were also combined to generate a heat map of the entire set of experimental data (Figure 3.3A). Based on hierarchical clustering, five groups of genes were identified whose expression pattern increased or decreased to varying degrees compared to ESCs (Table 3.1). Similar to the hierarchical clustering in Figure 3.2, Groups I and IV contained genes whose expression increased over the course of differentiation, while genes in groups II and V decreased, and those in group III remained relatively unchanged compared to the ESCs. In order to more clearly define the temporal expression patterns embedded within the data, k-means analysis of the average log2-transformed fold changes was performed (Figure 3.3B-M). Groups identified in the heat map were represented in the k-means plots by the corresponding colors, clearly showing the ability of k-means analysis to further parse out groups identified by hierarchical clustering. K-means analysis was performed using 12 clusters; analysis with fewer clusters (4-8) did not distinguish different patterns of expression as clearly, whereas larger numbers of clusters yielded independent groups with as a few as 1-2 genes. Thus, 12 clusters captured an array of different patterns of expression with a range of 6-29 genes (Table 3.2).

In the k-means graphs, the x-axis at zero represents the undifferentiated ESC baseline, and the centroid of each cluster is indicated by the black line. Overall, genes that fell into groups II and V in the hierarchical cluster were represented below the baseline in the k-means plots (Figure 3.3B-E). In addition, all but eight of the genes that clustered with other molecules around the baseline in the k-means plots (Figure 3.3F-I) also fell into group III. Genes that were separated into groups I and IV from the

hierarchical clustering tended to cluster together in multiple k-means plots (Figure 3.3J-M). In general, k-means clustering further divided the groups generated by hierarchical analysis by accounting for differences in the slope magnitudes between time points. For example, genes that appeared to change nominally over time by hierarchical clustering analysis (group III) were split into four different k-means plots, depending on whether the gene profile (or the centroid of the gene cluster) increased or decreased by day 7 and the corresponding specific expression pattern between days 7 and 14. Overall, k-means cluster analysis more clearly highlighted temporal expression patterns not readily identified by hierarchical clustering.

A total of 43 genes (~25% of the total genes examined) were clustered in the first four k-means plots (Figure 3.3B-E), with their expression patterns generally falling below the ESC baseline, while ~41% (71 genes) remained around the baseline (Figure 3.3F-I) and ~34% (58 genes) tended to increase over the course of differentiation (Figure 3.3J-M). Clusters B, H, and M all contained genes solely from groups II, III, and I, respectively, whereas clusters E, G, and K contained a mixture of genes from three hierarchical cluster groups. Clusters F, I, and J each contained one "outlier" molecule from a different group (*Fgf8*, *Figf*, and *Tnc*, respectively). Importantly, a subset of genes that fell into cluster B (genes that exhibit a gradual decrease in expression with differentiation) is known to be associated with pluripotent phenotypes, specifically *Fgf4*, *Lefty1*, *Lefty 2*, and teratoma-derived growth factor 1 (*Tdgf1*). These markers have all been shown in other studies to decrease gradually with differentiation [128-130], thereby independently confirming the expression of this gene subset. Similarly, although some interleukins were dispersed between clusters, six of them were concentrated in H,

indicating a coordinated temporally-regulated role for the subclass. Other groups of molecules, however, were distributed among a variety of clusters. The 11 Bmp genes, for example, fell into five clusters, while the eight collagens were dispersed among six clusters. This variety of temporal gene expression profiles within classes of molecules suggests that each of them may play different roles in the stem cell differentiation process. Interestingly, with the exception of colony stimulating factor 1 (*Csf1*) and S100 calcium binding protein A6 (*S100a6*), all the genes in clusters C and J (initially decreased compared to ESCs, but steadily increasing after day 4) were from the ECM array, raising the possibility that matrix molecules, as opposed to growth factors, play stronger roles particularly at later differentiation time points. By visualizing gene profiles via k-means analysis, sets of genes with similar trends in specific temporal expression patterns emerge, highlighting, for example, genes that increase between days 7 and 10, regardless of their expression trend prior to that time point. Therefore, k-means analysis is able to identify groups of genes whose expression trends follow similar (or diverging) patterns at each time point, which could importantly allow for subsequent analysis of these specific sub-classes and their contributions to coincident cell behavior patterns.

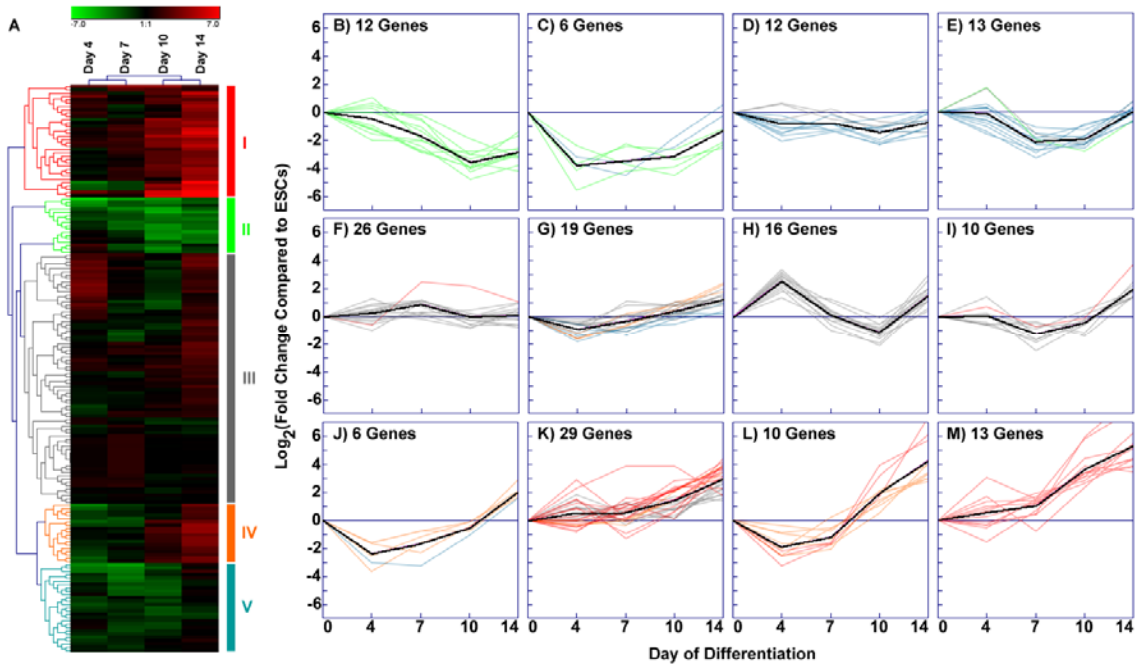

Figure 3.3. Hierarchical and k-means clustering analyses. Heat maps were generated for combined ECM and Growth Factor arrays using hierarchical clustering (A), and the resulting clusters were further grouped qualitatively into five groups, marked I – V. K-means analysis was performed on the same group of data (B-M), with the colors of the genes in each k-means plot corresponding to the hierarchical cluster group of the same color. K-means analyses parsed out temporal similarities and differences between genes that remained grouped together in the hierarchical clusters.

Table 3.2. Genes in each k-means plot represented in Figure 3.3B.

Cluster B	Cluster C	Cluster D	Cluster E	Cluster F		Cluster G
Bmp8a	Csf1	Adamts8	Egf	Fgf8	Mmp7	Rabep1
Bmp8b	Col1a1	Timp1	Fgf22	Amh	Mmp8	Lamb3
Fgf17	Itga3	Hprt1	Ngfb	Adamts5	Ncam2	Sparc
Fgf4	Thbs1	Nodal	Fgf1	Ctnnb1	Sele	Vegfb
Lefty1	S100a6	Lama3	Lif	Cdh3	Sell	Cdh4
Lefty2	Inhbb	Ctgf	Pecam1	Col2a1	Itgax	Itgb1
Tdgf1		Syt1	Csf3	Col4a3	Hsp90ab1	Lama1
Icam1		Il7	Il11	Hc	Gapdh	Lamb2
Itgal		Itgb4	Inhba	Itgae	Ctnna1	Mmp14
Itgam		Lamc1	Pdgfa	Mmp10	Selp	Thbs3
Spp1		Actb	Fgf18	Mmp12	Cdh1	Bmp1
Il3		Artn	Mmp9	Mmp1a	Ncam1	Fgf13
			Bmp4	Mmp3	Fgf7	Ntf5
						Adamts2
						Fbln1
						Itgav
						Thbs2
						Gusb
						Itga5

Cluster H	Cluster I	Cluster J	Cluster K		Cluster L	Cluster M
Gdf5	Entpd1	Adamts1	Mdk	Ntf3	Col3a1	Bmp7
Il1b	Vegfc	Col5a1	Itga2	Tgfb3	Emilin1	Ctnna2
Il2	Fn1	Ecm1	Itga4	Cdh2	Pgf	Spock1
Csf2	Mmp11	Cntn1	Itgb2	Mmp2	Tgfb2	Bmp2
Ereg	Bdnf	Itgb3	Lama2	Cxcl12	Cd44	Bmp5
Fgf15	Cxcl1	Tnc	Mmp13	Gdnf	Tgfbi	Fgf10
Fgf6	Inha		Vcam1	Tgfa	Timp2	Igf1
Gdf10	Figf		Bmp10	Tgfb1	Vegfa	Il18
Gdf8	Fgf2		Bmp3	Col4a1	Hapln1	Kitl
Hgf	Zfp91		Bmp6	Vcan	Igf2	Col4a2
Il12a			Fgf11	Sgce		Mmp15
Il1a			Fgf14	Timp3		Postn
Il4			Fgf3	Gdf11		Vtn
Il6			Fgf5	Col6a1		
Lep			Fgf9			
Tff1						

Parallel analysis of variance (ANOVA) significance testing

In order to determine statistically significant changes ($p < 0.05$) in gene expression over the course of differentiation for individual genes, parallel one-way ANOVA analyses were performed. Significant changes in gene expression between each time point were depicted with a branch schematic, with increasing or decreasing slopes representing positive or negative fold changes, respectively, while non-significant changes were illustrated as horizontal lines (Figure 3.4A). As EB differentiation time progressed, the number of genes with significant changes increased with time. Between ESCs and day 7 EBs, approximately 16% of the genes examined significantly change at day 4 and 10% at day 7; whereas, at day 10 approximately 22% genes significantly change in expression, and by day 14 about 44% of all the genes examined change significantly. Initially, molecules that changed significantly primarily decreased compared to ESCs by day 4, with the majority of genes remaining unchanged. Of these 141 molecules that were initially not significant, only 9 genes (5 increasing and 4 decreasing) significantly changed between days 4 and 7. Interestingly, over the course of differentiation no gene continually increased significantly past day 7. By days 10 and 14, however, larger numbers of genes (30 and 47 genes, respectively) significantly changed that previously were not significant, with one small subset (10 genes) significantly decreasing at day 10. In contrast, at day 14 all the significant changes, except one gene (*Fgf5*), increased in expression. A list of genes grouped according to significant expression profiles by day 14 (Figures 3.4B-F) are listed in Table 3.3.

Approximately a third of the genes examined did not change significantly throughout the entire 14-day EB culture period (Figure 3.4B), including the housekeeping

gene *Hsp90ab1*, *Fgf2*, and matrix metalloproteinase 2 (*Mmp2*). Significant decreases in fold change were observed in 24 genes between ESCs and day 4 EBs (Figure 3.4C), including platelet-derived growth factor A (*PdgfA,* ~2-fold difference), inter-cellular adhesion molecule 1 (*Icam1*, ~2-fold difference), and *S100a6* (~18-fold difference). Genes with the most significant change in decreased gene expression were *Col1a1* (~46-fold difference), *S100a6* (~18-fold difference), and *Csf1* (~13-fold difference) between ESCs and day 4 EBs. Within this subset of 24 genes that significantly decreased in expression by day 4, 7 genes did not changed significantly in the remaining time period examined (Figure 3.4C), and 10 genes significantly increased between days 10 and 14 (Figure 3.4D). Genes with the largest significant increase between 10 and 14 days of EB differentiation were *Csf1,* thrombospondin 1 (*Thbs1*; both ~5-fold difference), connective tissue growth factor (*Ctgf*), and integrin β3 (*Igb3*; both ~4-fold difference).

Another third of all the genes in the arrays only increased significantly in fold change between days 10 and 14 (Figures 3.4E, F). The group of genes with the expression profile depicted in Figure 3.4E significantly increased from days 7 through 14, ranging from ~2-fold to ~50-fold between days 7 and 10 (20 genes) and from ~1.5-fold to ~4-fold between days 10 and 14 (12 genes). The genes with the largest fold difference between days 7 and 10 include *Igf2* (~50-fold difference), *Bmp5* (~20-fold difference), and transforming growth factor β2 (*Tgfb2*) (~18-fold difference); the genes with the largest fold differences between days 10 and 14 were *Bmp5*, *Gdf11* (both ~4-fold difference), *Igf2,* and *Spock1* (both ~3-fold difference). The expression profile of molecules illustrated in Figure 3.4F exhibited significant increases in expression at later stages of EB differentiation, with 47 genes that did not significantly change until day 14

with fold differences of ~2-fold to ~50-fold. The genes with the largest significant increases were *Col3a1* (~50-fold difference), *Vcam1* (~16-fold difference), *Gdnf*, and *Figf* (both ~14-fold difference).

Of the subsets of molecules identified through statistical analysis (Table 3.3), several genes from certain families of molecules appeared in the same groups. Within the 58 genes not changing significantly over 14 days of EB culture (Figure 3.4B), several gene families are present, including the cadherins (4/4 genes analyzed in the array), fibroblast growth factors (6/17 genes), interleukins (10/10 genes), and matrix metalloproteinases (4/12 genes). Gene families that increased significantly between days 10 and 14 (Figure 3.4E and 3.4F) included transforming growth factors (5/5 genes), laminins (3/6 genes), and collagens (5/8 genes). Overall, analyzing the significant changes in decreased or increased gene expression clearly identifies groups of genes with similar expression profiles. By including significant changes between consecutive time points in the analysis of the arrays, the progression of certain genes involved in EB development can be easily examined.

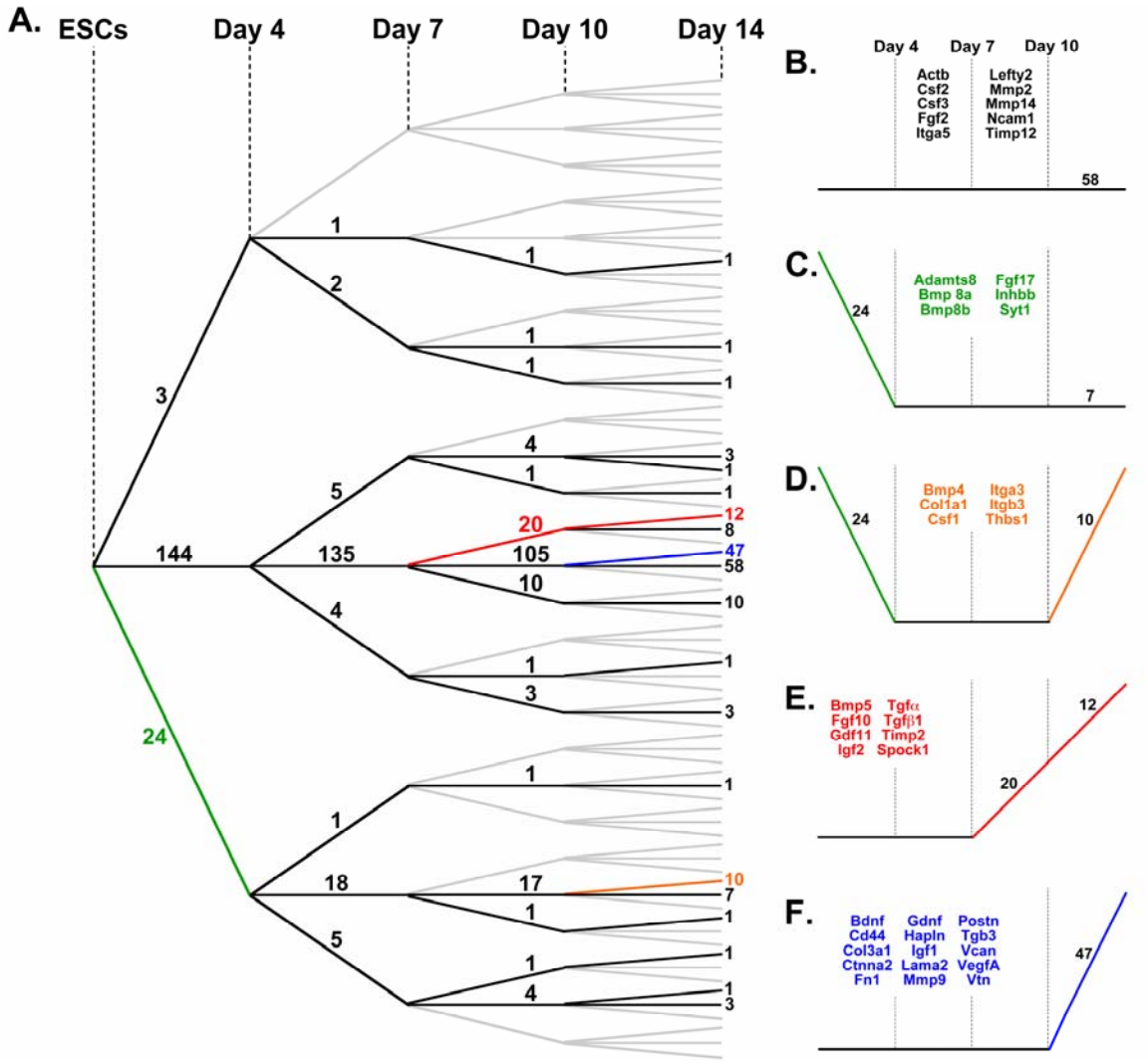

Figure 3.4. Statistical analysis of ECM and Growth Factor expression values. Parallel one-way ANOVAs were performed to evaluate the progressive statistical significance of gene expression values at each day compared to the previous time point (A). Branches with positive or negative slopes represent genes that respectively increased or decreased significantly ($p < 0.05$), while horizontal lines indicate no statistical significance. Particular trends are noted with corresponding molecules that fall into each specific group (B-F).

Table 3.3. List of genes represented in Figure 3.4B-F.

Figure 4B 58 genes		**Figure 4C** 24 genes	**Figure 4D** 10 genes	**Figure 4E** 20 genes	**Figure 4F** 47 genes	
Actb	Il18	Adamts8*	Bmp4	Bmp2	Adamts1	Hapln1
Adamts2	Il1a	Bmp4	Col1a1	Bmp5†	Bdnf	Igf1
Amh	Il1b	Bmp8a*	Csf1	Bmp7	Bmp1	Inha
Artn	Il2	Bmp8b*	Ctgf	Fgf10†	Bmp3	Itga2
Bmp10	Il3	Col1a1	Fgf13	Fgf14	Bmp6	Itga4
Cdh1	Il4	Csf1	Itga3	Gdf11†	Cd44	Lama1
Cdh2	Il6	Ctgf	Itgb3	Igf2†	Cntn1	Lama2
Cdh3	Il7	Fgf13	Itgb4	Itgb2	Col3a1	Lamb2
Cdh4	Inhba	Fgf17*	Lamc1	Kitl†	Col4a1	Lif
Csf2	Itga5	Fgf18	Thbs1	Lamb3	Col4a2	Mdk
Csf3	Itgae	Hprt1*		Mmp15	Col5a1	Mmp11
Ctnna1	Itgav	Icam1		Rabep1†	Col6a1	Mmp9
Ctnnb1	Itgax	Inhbb*		Sgce	Ctnna2	Ntf5
Egf	Itgb1	Itga3		Spock1†	Cxcl1	Pgf
Ereg	Lefty2	Itgal		Tgfa†	Cxcl12	Postn
Fgf11	Lep	Itgb3		Tgfb1†	Ecm1	Tgfb3
Fgf2	Mmp13	Itgb4		Tgfb2†	Emilin1	Tgfbi
Fgf22	Mmp14	Lama3		Timp2†	Entpd1	Timp3
Fgf6	Mmp2	Lamc1		Vegfb	Fbln1	Tnc
Fgf7	Mmp8	Pdgfa		Zfp91†	Fgf3	Vcam1
Fgf9	Ncam1	S100a6			Figf	Vcan
Gdf10	Ngfb	Spp1			Fn1	Vegfa
Gdf5	Ntf3	Syt1*			Gdnf	Vegfc
Gdf8	Sele	Thbs1				Vtn
Hc	Sell					
Hgf	Sparc					
Hsp90ab1	Tff1					
Il11	Thbs3					
Il12a	Timp1					

*Molecules that decrease significantly between days 4 and 7 and subsequently do not change significantly (black line Figure 4C).

†Molecules that increase significantly between days 7 and 10 and between days 10 and 14 (orange line Figure 4D).

Pathway Analysis

Based upon the parallel ANOVA analysis, only the genes that exhibited at least one significant change between consecutive time points in gene expression during EB differentiation were included in the Ingenuity Pathway Analysis (IPA). Thus, out of the 171 unique genes included in the ECM and growth factor SuperArrays, 57 genes were excluded from the pathway analysis due to their lack of significant fold change during the 14-day period of differentiation (Figure 3.4B). Of the 114 genes with significant fold change, 89 "focus" genes were eligible for generating "functions" and "networks" in IPA, determined by the association of a specific gene to other genes, either by interaction or in a functional annotation within IPA's knowledge base.

Using the IPA database that contains information on functions associated with specific genes, the top (Figure 3.5A) and bottom (Figure 3.5B) functions were generated from genes exhibiting more than two-fold changes in expression compared to ESCs. The functions were ranked highest to lowest according to day 4 EB results. Among the top 10 functions for each time point, 8 of the 10 were the same, including "cell growth & proliferation", "tissue development", "cell movement", and "cardiovascular system development & function". The lowest ranking functions (Figure 3.5B) were comprised of descriptions generally not directly related to development, such as "metabolic disease" or "ophthalmic disease". For all the lowest functions listed, the B-H significance was only slightly above threshold levels ($p < 0.01$), and some time points did not contain any genes in specific functions that met the fold-change cut-off value. To examine the interaction of certain molecules within the dataset, as well as with other known

molecules, IPA generated networks of these interactions based on literature available in IPA's database.

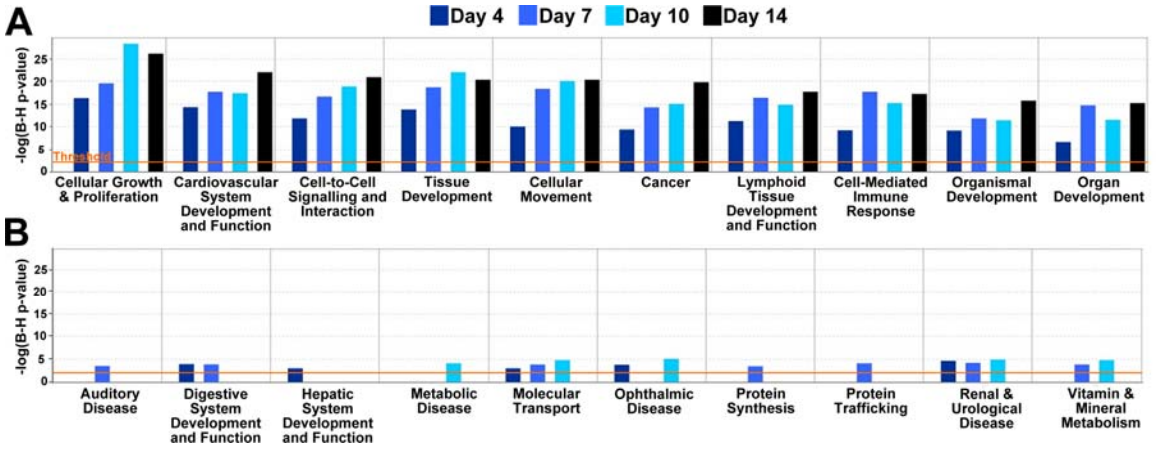

Figure 3.5. Assessment of EB functions associated with ECM and Growth Factor gene expression. Genes that exhibited at least one significant gene expression change between consecutive time points were included in the Ingenuity Pathway Analysis (IPA). Using the IPA database that contains information on functions associated with specific genes, the highest (A) and lowest (B) ranked functions were generated from genes exhibiting more than two-fold changes in expression compared to ESCs. In distinct contrast to the lowest ranked functions, top functions are generally associated with development and morphogenesis.

Networks at each time point were examined to determine relevant pathways involved at different stages of differentiation, with the top ranking network at each time point depicted in Figure 3.6. At day 4 (Figure 3.6A), the top network was generated with 15 focus molecules. A few genes within this network could be considered "nodes", or genes with numerous network connections, such as *Fn1*, *Csf1, and Vegfa*. Many of the extracellular factors included in this network were related to *p53*, which is a transcription factor that directly acts on the pluripotent marker *Nanog* by suppressing its expression to induce differentiation [131]. The top network at day 7 (Figure 3.6B) was generated using 17 of the "focus" genes, including nodal genes *Mmp9, Il1b,* and *Il6*. Similar to Figure 3.6A, several of the extracellular factors in Figure 3.4B were related to *p53*, which consequently affected *Nanog*. The top networks for days 10 (Figure 3.6C) and 14 (Figure 3.6D), used 35 and 39 "focus" genes, respectively. In the day 10 network, several nodal genes included *Vegfa*, *Igf1*, and *Tgfb1*, whereas the nodal genes within day 14's top network include *Fn1, Igf1,* and *Vegfa*. The appearance of *Tgfb1*, a mediator of ECM production, as a nodal gene at day 10, as well as its connection to other ECM molecules, such as *Col1a1* and *Sparc*, preceded the changes in day 14's top network, which included several more plasma membrane-associated molecules compared to the other networks, especially cell adhesion and ECM receptor molecules, such as *Vcam1*, *Itgb3*, and *Itgav*.

The differentiation of ESCs within EBs is depicted in the four networks of Figure 3.6. In the day 4 and 7 networks, the molecules included appear to be focused on decreasing ESC pluripotency based on the high connectivity of nuclear factor *p53,* which decreases Nanog expression, to extracellular molecules. At day 10, the network includes several more nuclear factors linked to extracellular factors, but the connectivity of the

nuclear factors is low. The increased number of nuclear factors with low connectivity suggests that the ESCs are continuing to differentiate, but along various lineages. In the day 14 network, the number of extracellular molecules is less than earlier time points, but the number of plasma membrane components increased with high connectivity. Overall IPA captures the progression of ESC differentiation in the resulting top networks generated.

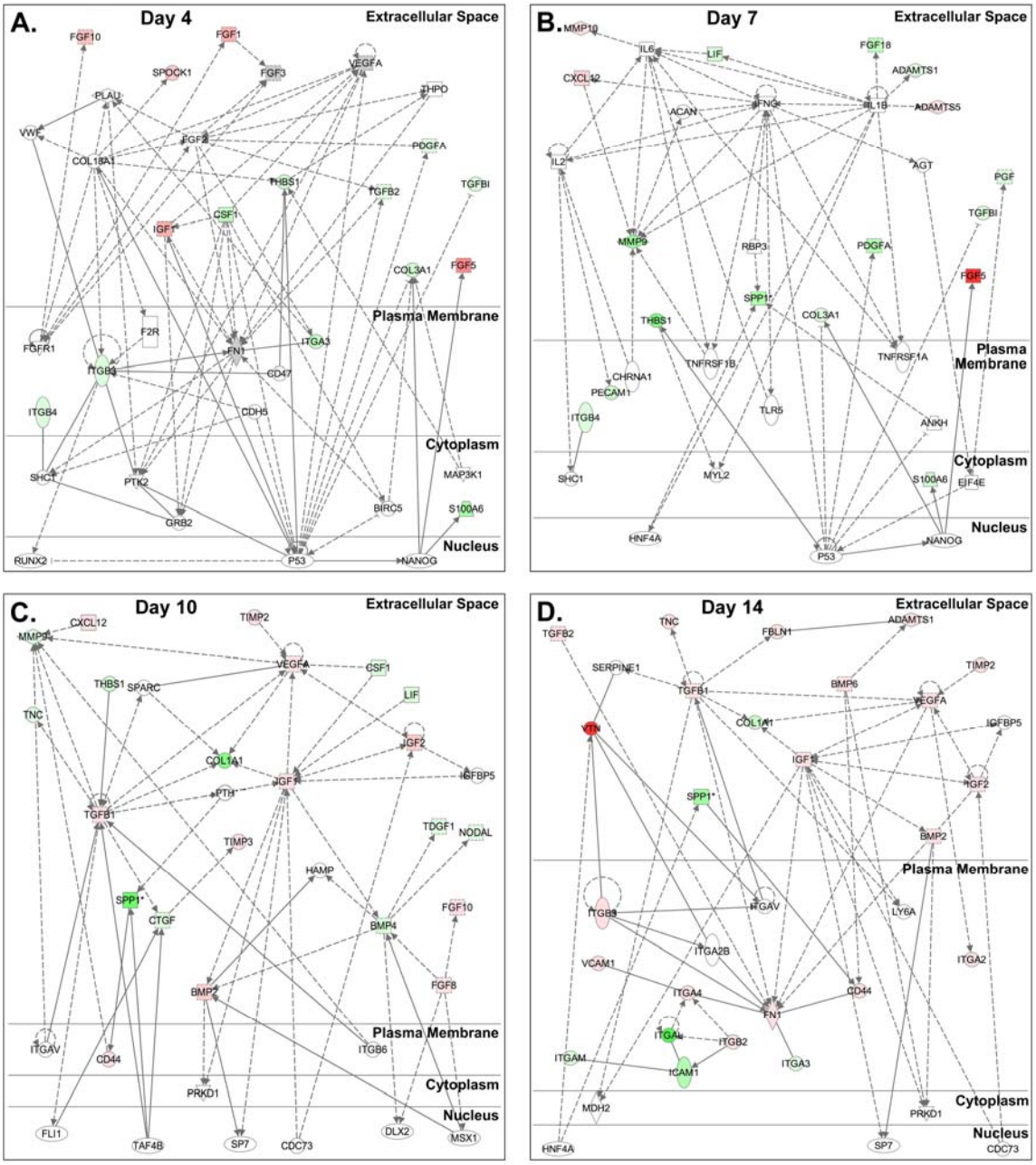

Figure 3.6. Network analysis over the course of differentiation. The top networks generated for day 4 (A), 7 (B), 10 (C), and 14 (D) EBs are depicted. Colors of the molecules indicate whether the corresponding expression value increased (red) or decreased (green) compared to ESCs. An increase in transcription factors appearing by day 10 of culture suggests the progression of heterogeneous differentiation within the EB population, while the appearance of cell adhesion molecules in day 14 EBs indicates the onset of signal transduction and cell movement.

Discussion

The overall objective of this study was to examine the global expression of ECM, receptor, and growth factor expression by differentiating ESCs. ESCs undergo progressive differentiation within EBs and correspondingly express differential amounts of a number of ECM and GF genes. Distinct sets of genes follow diverging patterns over the course of differentiation, suggesting that an increase or decrease of specific sub-groups of matrix molecules may be necessary for certain cell specification events. Although not typically used to examine differentiation patterns, variations in ECM and growth factor expression were indicative of more global changes occurring within the EB microenvironment. Low density analysis of extracellular factors in dynamic environments highlights the importance of such endogenous molecules and their utility in assessing the temporal shifts in the system.

As ESCs differentiate within the 3D EB environment, the expression patterns of molecules increase and decrease according to the phenotypic and morphological changes occurring within the cells. By analyzing a large number of molecules simultaneously, subtle changes in expression can be used collectively to analyze the system, in contrast to the traditional approach of focusing on the gene expression changes of one molecule at a time [65]. With a reduction in noise and a focused group of genes that can more readily be individually analyzed, low density arrays can offer some advantages over larger-scale gene arrays while still providing data for a subset of molecules of interest instead of individual ones. Importantly, ontological assessment of gene arrays can highlight not only relationships between the molecules within the array, but also connections to the existing literature. Such analysis of the extracellular genes (ECM and growth factors)

included in the arrays underscored key relationships with intracellular genes, such as receptors and transcription factors, that were indicative of morphogenic changes occurring within the EB microenvironment.

A number of analytical tools were used to evaluate the gene expression values obtained from the ECM and growth factor arrays: hierarchical clustering, k-means analysis, statistical analysis, and gene ontology mapping. Hierarchical clustering highlights general patterns of expression, which is useful for quick detection of subsets of genes that are generally increasing, decreasing, or remaining similar to baseline levels (in this case, undifferentiated ESCs). For the time-dependent data set presented here, two-way hierarchical clustering was useful for assessing whether non-consecutive time points exhibited any overall expression pattern similarities. K-means analysis was able to further parse out the temporal relationship across genes by isolating subsets of groups with distinct expression patterns. However, neither of these techniques incorporate statistical rigor into their algorithms. Mapping the results of parallel ANOVAs across all genes highlights the overall expression patterns adopted by the molecules over time, with each "branch" indicating the significant changes of the group of molecules compared to the previous time point. Apart from analyses based strictly on gene expression values, gene mapping tools using Ingenuity Pathways Analysis allows for the identification of established relationships between the input molecules and molecules available in the software database. Due to the relatively small number of molecules in the array, networks generated for each time point are inherently biased, although the inclusion of molecules from the database and external to the array allows for a more expanded network view.

These clustering, statistical, and gene mapping tools may be critical to further understanding the role of endogenous ECM and growth factors in differentiation. Some studies have begun to elucidate the role that specific molecules play in ESC differentiation [63, 65, 132-135], although analyses that include a broader range of extracellular factors have thus far been somewhat limited [69, 70]. In order to analyze the wide spectrum of matrix molecules in our study, distinct methods were used that either highlighted differences in expression patterns through clustering tools or focused on the relationships between the molecules via network analysis. Subsets of genes with diverging expression values (gene groups that between multiple time points had opposing trends) emerged from k-means and statistical analyses. The simultaneous increase and decrease of different sets of molecules may be necessary for the onset of a particular differentiation event, and the identification of these sub-groups could be critical for further understanding the coincident cell phenotype specification. While the clustering and statistical algorithms are based on the precise gene expression values, the only consideration of expression values when mapping networks in IPA is the fold-change threshold cutoff input by the user. Therefore, the combination of clustering/statistical analyses with network mapping provides a multi-faceted approach that enables a more in-depth understanding of the dynamic system. In contrast, studies that examine individual molecules largely remain one-dimensional and may lose the global view that contributes considerably to the fundamental understanding of the system.

In the EB system, a combination of the described analyses has provided a higher-level understanding of the influence of extracellular factors on morphogenic processes over the differentiation time course. The day 4 EB network (Figure 3.6A) was dominated

largely by growth factors and not ECM molecules. Similarly, k-means plots C and J (Figure 3.3C,J), which contain molecules that decrease sharply until day 4 prior to gradual increases, are composed primarily of ECM molecules. In addition, the molecules that appear in the day 4 network primarily act upon the transcription factor *p53* that in turn decreases the pluripotent marker *Nanog*. Together, these results suggest that in the early stages of EB culture, growth factors are the dominant factors necessary to prime the system for differentiation. However, there is likely some minimal matrix present in day 4 EBs that is absent from the network because the molecules did not meet the fold-change threshold cutoff or were not present in/associated with the arrays. These matrix molecules may serve as a reservoir for growth factors in the system. The ECM molecules present in the day 7 EB network are largely proteases, which may serve to remodel the little matrix present in the EBs and allow for the subsequent increase in molecules necessary for support of the differentiating cell phenotypes. By day 10, both ECM molecules and growth factors appear in the network, along with an increase in the number of connected transcription factors, suggesting the onset of signaling related to a variety of differentiation events. Finally, the appearance of a number of integrins by day 14 emphasizes the onset of cell movement and signal transduction events.

In addition to elucidating these global views of dynamic EB processes, low density extracellular array analyses offer insight into molecules that may otherwise have remained unstudied. For example, the uniquely sharp increases of molecules such as *Postn* and *Col3a1* by day 14 raise speculation as to their importance in EB differentiation, and subsequent knock-down studies may elucidate otherwise unknown mechanisms. In addition, with enough replicates, it could be possible to "reverse

engineer" networks, or to identify connections previously unknown. Key insights gained into the EB system from the array analyses highlighted that the earliest associated endogenous ECM and growth factor molecules are associated with regulators of self-renewal and differentiation. Additional array analyses examining matrices synthesized from directed differentiation schemes could further parse out the association of molecules with particular cell specification events. In addition to analyses of ESCs, parallel examination of induced pluripotent stem cells could highlight environmental cues that stimulate the reversion of somatic cells to a pluripotent state and could also identify novel candidates to promote or inhibit reprogramming. Global analysis of low density arrays elucidates the role of extracellular factors in modulating dynamic systems, which in turn is essential for understanding and manipulating the local microenvironment.

CHAPTER 4

SYNTHESIS AND ORGANIZATION OF HYALURONAN AND VERSICAN BY EMBRYONIC STEM CELLS*

Introduction

Pluripotent embryonic stem cells (ESCs), derived from the inner cell mass of pre-implantation blastocysts, have the ability to differentiate into all somatic cell types, as well as germ cells [1-4]. Differentiation of ESCs into ectoderm, mesoderm and endoderm derivatives can be induced *in vitro* via the aggregation of cells into three-dimensional clusters referred to as embryoid bodies (EBs), which serve as a model of peri-implantation development [35, 36]. For nearly 30 years, murine ESCs have provided an accessible *in vitro* model system for studying various aspects of early mammalian embryonic morphogenesis [136, 137], including the differentiation of ESCs into distinct functional cell types, such as cardiomyocytes, neurons, and endocrine cells (among many others) [137-139]. Although genetic and phenotypic changes of differentiating ESCs have been the primary focus of most studies, the associated dynamic changes in endogenous ECM synthesis and organization that occur coincidentally with differentiation have not been as rigorously examined.

During early development, the epithelial-mesenchymal transition (EMT) is a critical process in embryogenesis whereby epithelial progenitor cells transform into

---

* Modified from:
S Shukla†, R Nair†, MW Rolle, KR Braun, CK Chan, PY Johnson, TN Wight, and TC McDevitt. *Synthesis and organization of hyaluronan and versican by embryonic stem cells undergoing embryoid body differentiation*, submitted. † Both authors contributed equally to this work.

mesenchymal cells in order to migrate and facilitate tissue formation. This transition is typically characterized by a decreased expression of adherens junctions responsible for coupling the cells tightly together, thereby permitting an increase in cell motility. In an effort to further define the potential of using ESCs as an *in vitro* model of early development, researchers have studied the EMT in ESCs, including mouse [140], rhesus monkey [27, 141], and human ESCs [142-144]. ESCs that were differentiated using various strategies ranging from feeder-free conditions [142], definitive endoderm formation [143], monolayer [144], and spontaneous differentiation [140] have been shown to mimic aspects of EMT events, evidenced in part by the loss of E-cadherin and the tight junction associated proteins, as well as increased expression of N-cadherin and mesenchymal transcription factors. In addition to the differential expression of these cell junction markers and transcription factors, cell differentiation and tissue formation in the developing embryo are accompanied by spatially distinct alterations in the composition of the extracellular matrix (ECM) [145-147]. However, specific ECM molecules associated with EMT processes in ESCs have yet to be defined.

ECM molecules such as hyaluronan and versican are critically important in regulating EMT processes in various tissues [148-153]. Hyaluronan is a high molecular weight (10^6 – 10^7 Da) glycosaminoglycan (GAG) comprised of repeating disaccharide units of glucuronic acid and *N*-acetylglucosamine that can be synthesized by three independent hyaluronan synthases (HAS), HAS-1, -2, and -3 [154]. Hyaluronan has been implicated in several morphogenic cell and tissue events involving EMTs, including embryonic development, wound healing, and angiogenesis [155-159]. Versican is a chondroitin sulfate proteoglycan found in a variety of soft tissues and is capable of

binding to hyaluronan [160]. Four different isoforms of versican (V0, V1, V2, V3) exist as a result of alternative splicing of the two exons that encode the GAG attachment domains (α-GAG and β-GAG) in the core protein. Versican affects cell phenotypes associated with EMT processes, including proliferation and migration [160], suggesting that hyaluronan and versican together may play functional roles in EMTs occurring during embryonic development.

The objective of this study was to examine the temporal and spatial patterns of hyaluronan and versican expression, accumulation, and organization by mouse ESCs undergoing EB differentiation. The presence and spatial distribution of hyaluronan and versican within differentiating EBs was examined histologically, and hyaluronan and versican extracted from EBs were quantified as a function of differentiation time. The temporal gene expression profile of the individual hyaluronan synthase and versican isoforms was assessed over the course of early differentiation. In addition, the presence of primitive epithelial and mesenchymal cell populations was assessed relative to the spatial distribution of versican and hyaluronan within the ECM of EBs. These studies demonstrate that dynamic changes in hyaluronan and versican occur coincidentally with phenotypic changes observed during EB differentiation, indicative of EMT processes.

Materials and Methods

Cell culture

Mouse embryonic stem cells (D3 cell line, ATCC) were cultured on 0.1% gelatin-coated 100 mm polystyrene cell culture dishes (Corning, Corning, NY) with Dulbecco's modified eagle medium (Mediatech, Herndon, VA), supplemented with 15% fetal bovine

serum (HyClone, Logan, UT), 2mM L-glutamine (Mediatech), 1x MEM non-essential amino acids (Mediatech), antibiotic/antimycotics (Mediatech), and 0.1 mM β-mercaptoethanol (MP Biomedicals, LLC, Solon, OH). To maintain the undifferentiated cells, 10^3 U/ml leukemia inhibitory factor (LIF) (ESGRO, Temecula, CA) was added to the culture media, and the cells were passaged every 2-3 days before reaching >70% confluence. All of the described studies were performed with ESCs between passages 18-30. To initiate embryoid body (EB) cultures, a single cell suspension of $4x10^5$ ESCs/mL (in 10 mL) was added to 100 mm bacteriological grade Petri dishes (Corning) in culture media lacking LIF (differentiation media). Cultures were placed on rotary orbital shakers (Barnstead Lab-Line, Model 2314, Dubuque, Iowa) at 40 rpm at 37°C in 5% CO_2 for the entire duration of suspension culture, similar to previously described methods [124]. EBs were re-fed every other day after collecting the EBs via gravity-induced sedimentation in conical tubes and re-suspended in fresh differentiation media for additional culture.

Histological analysis of hyaluronan and versican

EBs collected at different stages of differentiation (4, 7, or 10 days) were fixed with 10% formalin for 30 minutes and embedded in Histogel® (Richard-Allan Scientific, Kalamazoo, MI). Each Histogel® block was processed for histological sectioning through a series of xylene and alcohol rinses prior to paraffin embedding. Sections of EB samples (5 μm each) were obtained from different depths (a minimum of 90 μm apart) within the paraffin block and stained with hematoxylin and eosin (H&E) using a Leica AutoStainer XL. ESCs fixed with formalin on tissue culture plates were similarly stained

for H&E, using the same reagents and incubation times as applied by the autostainer protocol. A minimum of three independent experiments, each containing roughly 3000 EBs, were examined by histological analyses. Paraffin-embedded EBs were also stained using Movat's Pentachrome staining procedure after de-paraffinization and hydration to distilled water. Sections were incubated in the following reagents, with intermittent rinses performed under running water or ultra-pure water: 1% alcian blue (20 minutes), alkaline alcohol (60^{o}C, 10 minutes), Weigert's stain (60 minutes), Crocein scarlet/acid fuchsin (1 minute), 5% phosptungsitic acid (5 minutes), 1% acetic acid (5 minutes), 95% ethanol (EtOH; 1 minute), 100% EtOH (2x; 1 minute), alcoholic saffron (7 minutes), and absolute EtOH (2x; 1 minute). Slides were then cleared in xylene and cover-slipped using Mount Quick mounting medium (Daido Sangyo Co., Ltd, Tokyo, Japan).

For immunohistochemical (IHC) staining, endogenous peroxidase activity was quenched using 0.75% hydrogen peroxide in 100% methanol (20 minutes), after which the samples were hydrated in a graded ethanol series (100% EtOH-35% EtOH) and rinsed in phosphate-buffered saline (PBS, pH 7.3). Slides from each block were then incubated in hyaluronidase reaction buffer (50 mM NaOAc, 150 mM NaCl, pH 6.0) for one hour at 37^{o}C; with or without hyaluronidase (Hyaluronan Lyase from *Streptomyces hyalurolyticus*, Sigma, St. Louis, MO), which was diluted to 20 U/mL in hyaluronidase buffer and added to negative control samples. Samples were then blocked in 1% bovine serum albumin (BSA) in PBS for 30 minutes before adding biotinylated hyaluronan binding protein (HABR-B, 2.5 µg/mL, Sigma) and incubating overnight at 4^{o}C. The Vector Elite ABC kit with Vector Red substrate (both from Vector Laboratories,

Burlingame, CA) was used to develop color, and the slides were counterstained with hematoxylin prior to cover-slipping.

For versican staining, sections were deparaffinized, rehydrated, and quenched as described above, then treated for 1 hour at 37°C with ABCase (Chondroitin ABC Lyase, MP Biomedicals; 0.2 U/mL in enriched TRIS buffer stock, final concentrations 50 mM TRIS, 60 mM NaAc, 50 mM NaCl, pH 8; with 0.1 mg/ml BSA) as an antigen retrieval step to degrade chondroitin sulfate GAGs and expose the versican core protein. Slides were rinsed in TBS and then blocked for one hour at room temperature in 5% Carnation non-fat dry milk. Primary antibody (rabbit anti-mouse versican β-GAG domain, Millipore, Billerica, MA; 7 µg/ml in 0.1% BSA in PBS) was added and incubated overnight at 4°C. After three PBS rinses, a biotinylated goat anti-rabbit secondary antibody (1:400 in 0.1% BSA/PBS, Invitrogen, Carlsbad, CA) was added for one hour at room temperature. Samples were developed with the Vector Elite ABC kit with Vector Red substrate, and the slides were counterstained with hematoxylin prior to cover-slipping. Negative control samples were prepared identically, with rabbit IgG isotype control (7 µg/ml in 0.1% BSA in PBS; Vector Laboratories) used in place of primary antibody.

To visualize hyaluronan and versican in the same section for co-localization studies, immunofluorescence (IF) was performed. De-paraffinized histological sections were blocked for 1 hour using 1.5% normal donkey serum (NDS). Samples were incubated with primary reagents HABR-B (2.5 µg/mL, Sigma) and versican (5 µg/mL beta-GAG domain, Millipore) together for one hour at room temperature or overnight at 4°C. After three PBS rinses, the samples were incubated with Alexa 488-streptavidin

(Invitrogen; 1:400 in 1.5% NDS; hyaluronan) and TRITC-labeled donkey anti-rabbit secondary antibody (Jackson ImmunoResearch, West Grove, PA; 1:400 in NDS; versican) for one hour at room temperature prior to Hoechst (10 μg/mL) counterstaining. Samples from all staining batches were then mounted with coverslips using either low viscosity mounting medium (IHC samples, Cytoseal™ 60, Richard-Allan Scientific) or aqueous mounting medium with anti-fading agents (IF samples, Gel/Mount™, Biomeda Corp., Foster City, CA). Note that antigen retrieval with ABCase was omitted in these samples; ABCase has hyaluronidase activity, which completely degraded hyaluronan in the samples (data not shown). Hyaluronidase treatment and incubation with rabbit IgG isotype in place of primary antibody served as negative controls for hyaluronan and versican staining, respectively.

Immunohistochemical analysis of ADAMTS-5, pan-cytokeratin, and N-cadherin

For ADAMTS-5 staining, de-paraffinized histological sections were blocked for 1 hour at room temperature using 2.5% NDS-2.5% BSA in PBS. Samples were incubated with rabbit anti-ADAMTS-5 JSCKNG (4 μg/mL in 0.1% BSA-PBS, Affinity BioReagents, Rockford, IL) overnight at 4^{o}C (negative IgG control: 4 μg/mL in 0.1% BSA-PBS). After three PBS rinses, the samples were incubated with Alexa Fluor 555 (5 μg/mL in 0.1% BSA-PBS) for one hour at room temperature prior to Hoechst (10 μg/mL) counterstaining. Samples were then mounted with coverslips using aqueous mounting medium with anti-fading agents (Gel/Mount™).

For pan cytokeratin and N-cadherin staining, the required antigen retrieval treatments damaged the versican epitope so that co-localization staining could not be

performed. Therefore, adjacent sections of each sample were stained for versican as described above. For pan cytokeratin, antigen retrieval was performed by incubating sections in 40 μg/mL proteinase-K (Fisher Scientific, Pittsburgh, PA) in 10mM Tris-HCl pH 8.0 (6 minutes, room temperature). Samples were then blocked for 1 hour at room temperature in 2% normal goat serum (NGS), followed by incubation with primary antibody recognizing pan cytokeratin (Dako, Carpinteria, CA, 1:10 dilution in 2% NGS; skin positive control) overnight at 4°C. For N-cadherin staining, heat-induced epitope retrieval was performed by boiling the samples in 10 mM citrate buffer at pH 6.0 for 20 minutes. Samples were blocked for 1 hour at room temperature in 2% NGS, then incubated with primary antibody recognizing N-cadherin (BD Biosciences, San Jose, CA, 1:30 dilution in 2% NGS; whole mouse embryo positive control) overnight at 4°C. Both pan cytokeratin and N-cadherin-stained samples were visualized by incubating with FITC-labeled goat anti-mouse secondary antibody (Southern Biotech, Birmingham, AL; 1:100 in 2% NGS) for one hour at room temperature prior to Hoechst (10 μg/mL) counterstaining. Samples were then mounted with coverslips using aqueous mounting medium with anti-fading agents (IF samples, Gel/Mount™, Biomeda Corp.).

Microscopy

Histological sections were imaged using a Nikon 80i microscope and a Spot Flex camera (Diagnostic Instruments, Inc., Sterling Heights, MI). For each antigen examined, images for all samples were acquired using the same exposure settings. Slight linear adjustments in brightness were made across entire images using SPOT Advanced software to enhance the contrast between signal and background.

Quantitative hyaluronan expression in EBs

Hyaluronan was isolated from ESCs, EBs (50,000 cells per sample; n=3 for each time point), or the media conditioned by the cells by digesting with Pronase (f.c. 500 μg/mL; 15 mg/mL stock in 0.5M Tris pH 6.5; Pronase from *Streptomyces griseus*, Roche Applied Science, Indianapolis, IN) at 37°C overnight. The enzyme was then heat-inactivated at 100°C for 20 minutes, and the samples were stored at -20°C prior to analysis. Hyaluronan was quantified using the Hyaluronan Test Kit (Corgenix, Denver, CO) by diluting the samples in 10 volumes of reaction buffer and adding 100 μL to hyaluronic acid binding protein (HABP)-coated micro-wells (1 hour, room temperature). Wells were then rinsed with PBS, and 100 μL of horseradish peroxidase (HRP)-conjugated HABP solution was added (30 minutes, room temperature). Each well was rinsed an additional four times prior to a 30-minute incubation (room temperature) with 100 μL of substrate solution (3, 3', 5, 5' – tetramethylbenzidine and hydrogen peroxide). Blue color developed in positive samples, and 100 μL of stopping solution (0.36 N sulfuric acid) was added to each well. The optical density for each well was read at 450 nm on a spectrophotometer (SpectraMax M2e, Molecular Devices, Sunnyvale, CA). A standard curve created from purified hyaluronan was used to calculate hyaluronan concentration in cell samples, which are presented normalized to cell number. Cell number was determined by dissociating EBs and counting individual cells on a hemacytometer.

Western blotting

Protein was isolated from ESCs and day 4, 7, and 10 EBs with extraction buffer (8M urea, 2 mM EDTA, 50 mM Tris, 0.5% Triton X-100, 0.25 M NaCl, Roche protease inhibitor cocktail). Protein concentrations were measured using a MicroBCA Assay (Pierce, Rockford, IL), and samples were stored at –80^{o}C prior to analysis. For versican blots, 300 μg total protein per sample were applied to diethylaminoethyl (DEAE) Sephacel® (Sigma) columns (0.3 mL bed volume), pre-equilibrated, and washed with 10 bed volumes wash buffer (8M urea, 2 mM EDTA, 50 mM Tris, 0.5% Triton X-100, 0.25 M NaCl). The samples were eluted with 3 bed volumes wash buffer containing 2 M NaCl. Chondroitin sulfate (f.c. 50 μg/mL; 10 mg/mL stock; Sigma) carrier was added, and protein was precipitated from the eluate by adding ethanol (95% ethanol/1.3% potassium acetate) for 2 hours at –80^{o}C. Precipitated protein was collected by centrifugation for 5 minutes at 14,000 rpm and rinsed twice with ethanol. Pellets were air-dried and then digested with 3 U/mL chondroitinase (10 U/mL stock; Seikagaku, Tokyo, Japan) in 20 mM Tris, 3.6 mM sodium acetate, pH 8.0 for 3 hours at 37^{o}C to remove chondroitin chains from the core proteins. Concentrated sample buffer (50 mM Tris-HCl pH 6.8, 1% SDS, 10% glycerol, 1.7% v/v 2-mercaptoethanol) was added, and the samples were boiled for 3-4 minutes prior to loading on a 15 cm x 12 cm 4-12% gradient polyacrylamide gel (3.5% stacking gel) and separated overnight at room temperature. Protein was transferred to nitrocellulose membranes and blocked for 2 hours at room temperature in blocking buffer (2% BSA in Tris-buffered saline, 0.1% Tween-20). Membranes were incubated overnight in blocking buffer containing 2% calf serum and 0.25 μg/mL rabbit anti-mouse versican β-GAG domain antibody (Millipore).

Membranes were then washed with TBS-T (Tris buffered saline with 0.1% Tween-20) and incubated for 2 hours at room temperature (1:20,000 goat anti-rabbit IgG antibody conjugated to alkaline phosphatase in blocking buffer; Jackson ImmunoResearch). After extensive washing in TBS-T, blots were incubated in assay buffer (0.1 M diethanolamine, 1 mM $MgCl_2$, 0.02% sodium azide, pH 10) for 10 minutes, followed by incubation with substrate (1:100 CSPD® substrate, 1:20 Nitro-Block™ enhancer in assay buffer; Applied Biosystems, Foster City, CA) for 5 minutes at room temperature. Blots were exposed to autoradiograph film (ISC BioExpress, Kaysville, UT) and developed in a film processor (Fischer Industries Inc., Geneva, IL). For DPEAAE blots, equal amounts of protein from each sample were ethanol precipitated and electrophoresed on 8% SDS-Page gel with 3.5% stacking gel. Proteins were transferred to nitrocellulose, probed with DPEAAE antibody (1 μg/mL, Affinity Bioreagents, Golden, CO), and detected using an enhanced chemiluminescence kit as described above. As a loading control, the same blot was also probed with an anti-actin N terminal antibody (Sigma).

Each lane on the Western blots reported represents protein lysates from an EB culture collected at the designated time point. Lysates from three separate cultures per time point were examined for each independent experiment.

Quantitative reverse-transcription polymerase chain reaction (qRT-PCR)

RNA was extracted from undifferentiated ESCs and EBs at days 4, 7, and 10 of differentiation using the RNeasy Mini Kit (Qiagen, Valencia, CA). Complimentary DNA was reverse transcribed from 1 μg of total RNA using the iScript cDNA synthesis kit (Bio-Rad, Hercules, CA), and real-time RT-PCR was performed using SYBR Green

technology on the MyiQ cycler (Bio-Rad). Beacon Designer software was used to design forward and reverse primers (purchased from Invitrogen; Table 1) for pluritpotency markers Oct-4 and Nanog, the three hyaluronan synthase (HAS) isoforms (HAS-1, HAS-2, HAS-3), the four versican splice variants (V0, V1, V2, V3), and glyceraldehyde-3-phosphate dehydrogenase (GAPDH), which were then validated with the appropriate positive controls. Gene expression of Oct-4 and Nanog were calculated relative to undifferentiated ESC samples using the Pfaffl method [125], while HAS and versican concentrations were calculated from standard curves prior to normalization to GAPDH expression levels. GAPDH was used as a normalization tool because it is stably expressed in ESCs over time, as demonstrated not only in literature [161], but when analyzed independently in these cultures. Gene expression data from two independent batches of ESCs and EBs each containing three replicates cultured at different times (n=6 for each time point) were combined prior to statistical analyses.

Table 4.1. qRT-PCR primer information.

Primer	Forward Sequence	Reverse Sequence	Hybridization T (^{o}C)
GAPDH	GCC TTC CGT GTT CCT ACC	GCC TGC TTC ACC ACC TTC	55.0
Oct-4	CCG TGT GAG GTG GAG TCT GGA G	GCG ATG TGA GTG ATC TGC TGT AGG	64.0
Nanog	GAA ATC CCT TCC CTC GCC ATC	CTC AGT AGC AGA CCC TTG TAA GC	64.0
V0	TTG AGG TCA GAG AAA ACA AGA CAG	TCT GTT TCT TCA CTG CAA GGT TCC	55.0
V1	AGC AGA TTT GAT GCC TAC TGC TTT	TCT TCA CTG CAA GGT TCC TCT TCT	55.0
V2	GAC CAA GTT CCA CCC TGA CAT AAA	GGT TTG TTT TGC AGA GAT CAG GTC	55.0
V3	AGC AGA TTT GAT GCC TAC TGC TTT	TGC ACA CAT AGG AAG TCT CGG TAG	55.0
HAS-1	ATG ACA GGC ACC TCA CCA AC	AAC CAA CGA AGG AAG GAG GA	55.0
HAS-2	CAA AAA TGG GGT GGA AAG AG	GAG GCA GGG TCA AGC ATA GT	55.0
HAS-3	GGC AAC TCA GTG GAC TAC	CAA CAC CTC CTA CTT GGG	55.0

For SuperArray RT^2 Profiler™ PCR array analysis, cDNA synthesis was performed using the SuperArray RT^2 First Strand kit (SABiosciences, Frederick, MD). First, the genomic DNA elimination mixture was prepared by mixing 0.5 μg RNA with the 5x gDNA Elimination Buffer and RNase-free water and incubating at 42°C for 5 minutes. The RT cocktail (5x RT Buffer 3, Primer & External Control Mix, RT Enzyme Mix 3, and RNase-free water) was prepared (10 μL) and added to the elimination buffer mixture. Each sample was then placed in the iCycler Thermal Cycler (Bio-Rad) for synthesis (15 minutes at 42°C, 5 minutes at 95°C) and diluted with RNase-free water. RT-PCR was performed by first preparing the experimental cocktail (1275 μL 2x SuperArray RT^2 qPCR Master Mix, 102 μL diluted first strand cDNA synthesis reaction, 1173 μL RNase-free water) and then distributing it across all wells of the PCR 96-well array. The array was tightly sealed with optical thin-wall 8-cap strips and run in the MyiQ cycler (Bio-Rad) with a two-step cycling program (1 cycle, 10 minutes, 95°C; 40 cycles, 15 seconds, 95°C; 40 cycles, 1 minute, 60°C) and melt curve. Fold changes in gene expression were analyzed using the $\Delta\Delta C_t$ method of quantitation, whereby samples of EBs from different time points (days 4, 7, and 10) were compared relative to undifferentiated ESC values after individual sample values were normalized to GAPDH levels.

Statistics

For paired comparisons, Student t-tests assuming unequal variances were used to determine statistical significance ($p < 0.05$). For comparisons across multiple groups, analysis of variance (ANOVA) was performed using a 95% confidence interval followed

by post-hoc Tukey analysis to determine significant ($p < 0.05$) differences between the different experimental groups.

Results

Embryoid body differentiation

Adherent colonies of undifferentiated mESCs were dissociated into single cells and re-aggregated in suspension culture to form cell spheroids constituting putative EBs (Figure 4.1). As expected, the resulting EBs increased in size and adopted a more differentiated morphology over the course of differentiation, indicated by the formation of a primitive endoderm layer on the periphery of EBs (denoted by solid arrows in Figure 4.1) as well as cystic cavities (hollow arrows, Figure 4.1) that developed in the interior of the EBs.

Phenotypic differentiation of the EBs was evidenced by a reduction in the expression of the pluripotent transcription factors Oct-4 and Nanog by EBs (Figure 4.2) and by opposing trends of E-cadherin and N-cadherin gene expression with time (Figure 4.3).

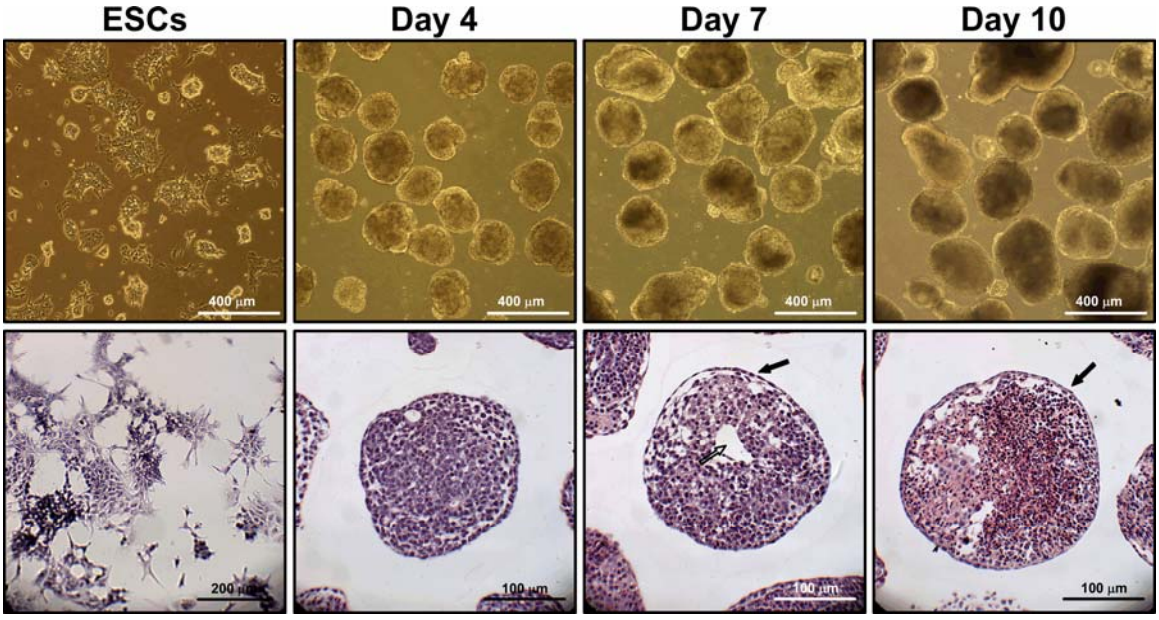

Figure 4.1. Embryoid body differentiation. Phase images were taken and histological staining was performed on ESCs and EBs cultured for 4, 7, and 10 days. EBs increased in size over the course of differentiation culture, and H&E staining showed pockets of differentiating cells visibly emerging by day 7. Solid arrows highlight differentiated endoderm layer, and hollow arrows indicate development of cystic cavities, both indicative of EB maturation.

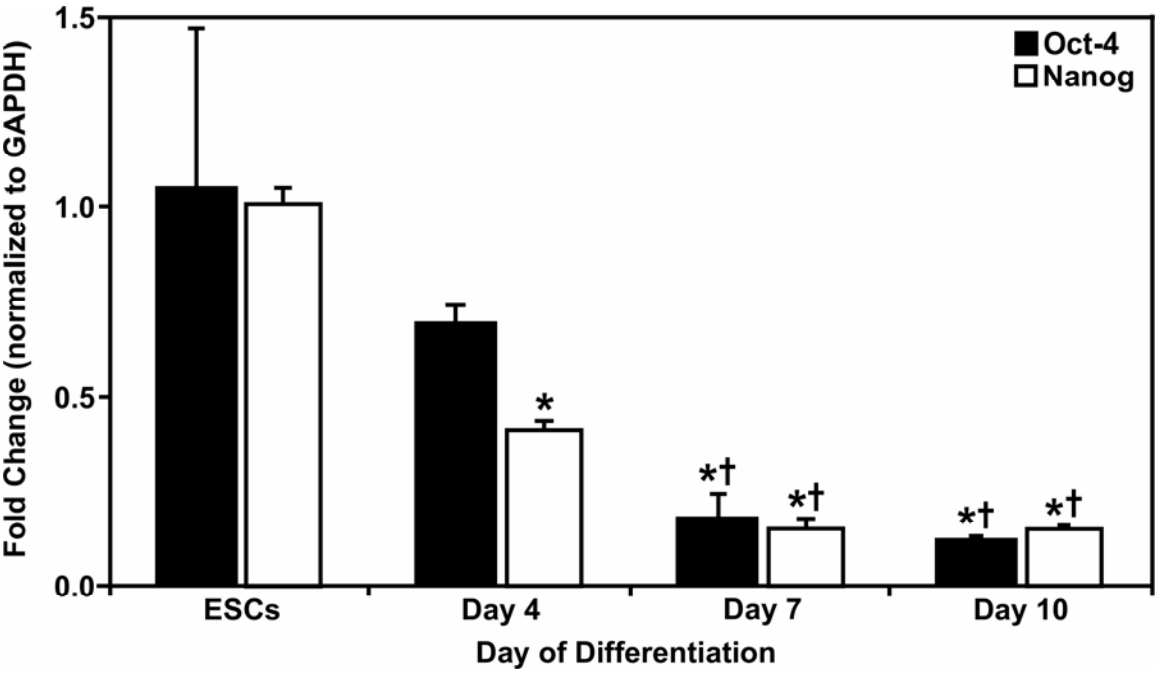

Figure 4.2. Pluripotency marker mRNA expression. Quantitative RT-PCR was performed to assess transcript abundance of two transcription factors, Oct-4 and Nanog. Both genes decrease steadily over the course of differentiation, indicating the expected loss of pluripotent markers as the ESCs differentiate. * indicates significant differences from ESCs, † from day 4, $p < 0.05$.

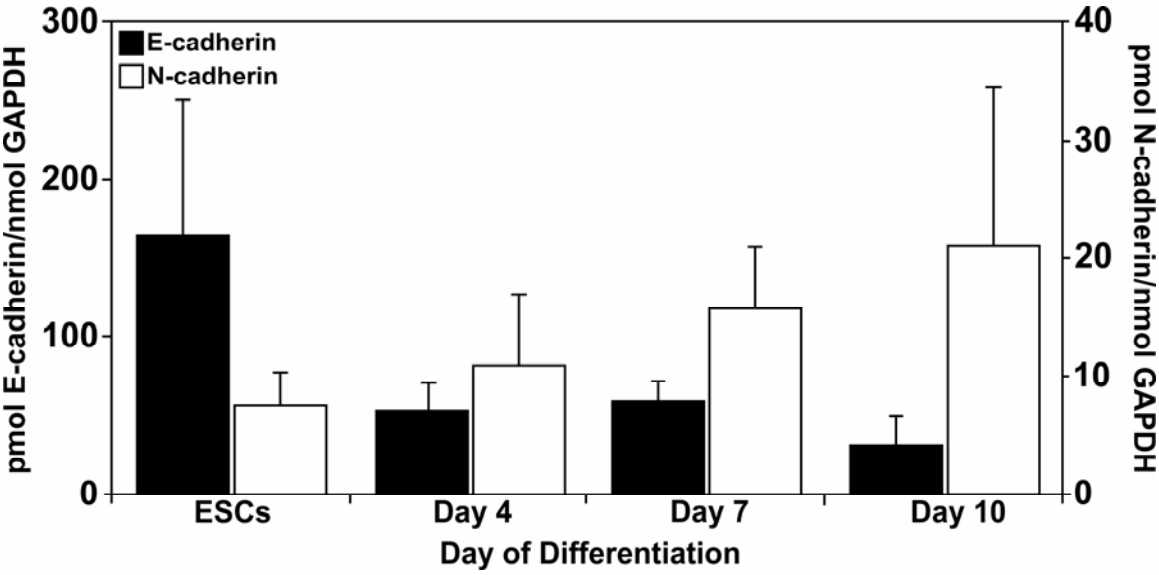

Figure 4.3. EMT marker mRNA expression. The gene expression of E-cadherin and N-cadherin was examined in ESCs and EBs differentiating for 4, 7, and 10 days. The opposing trends of E-cadherin and N-cadherin expression indicated the presence of an epithelial-mesenchymal transition in the differentiating EBs. The left scale on the y-axis corresponds to E-cadherin gene expression values, while the right scale corresponds to N-cadherin.

Movat's pentachrome staining of EBs revealed intense cytoplasmic staining (red) of densely-packed epithelial-looking cells at early stages of differentiation (days 4 and 7). After 10 days, a majority of cells within many EBs adopted a more mesenchymal appearance, and GAGs were detected in the extracellular space (light blue) throughout EBs (Figure 4.4), which appeared to be the primary ECM component synthesized at the times examined.

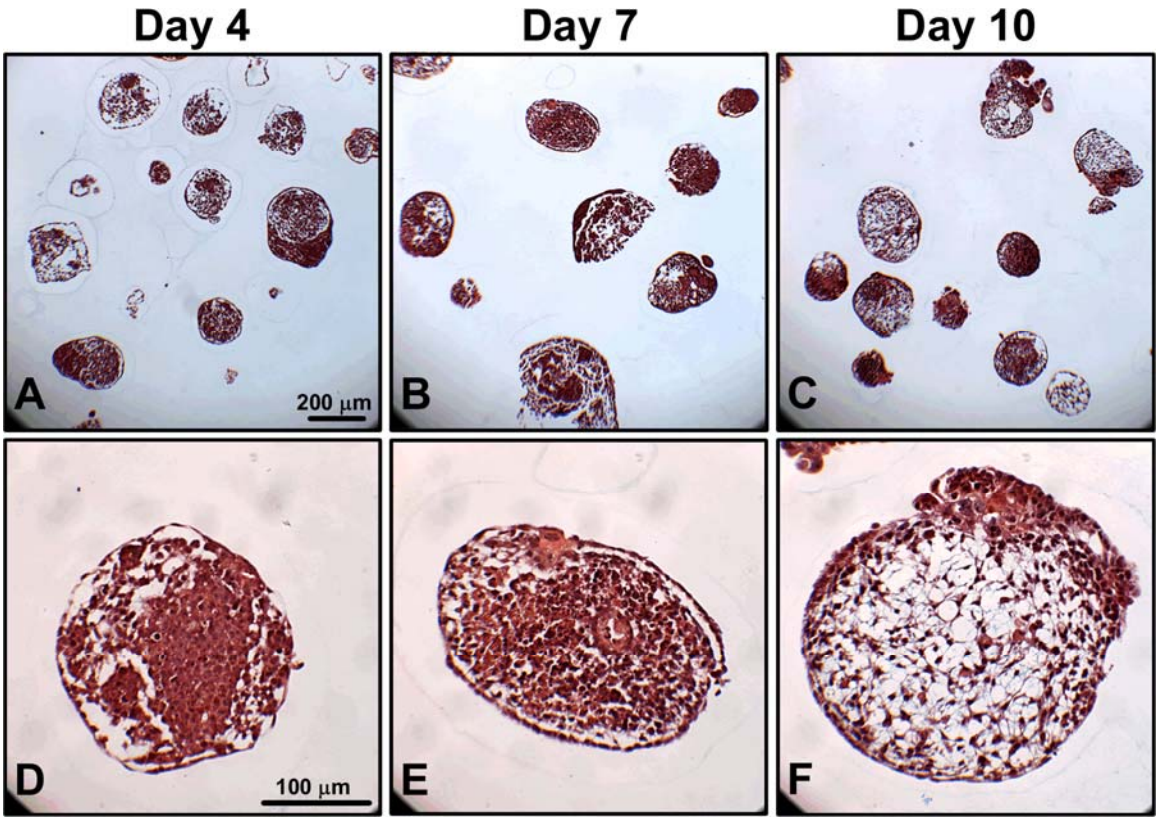

Figure 4.4. Embryoid body ECM synthesis. EBs were evaluated using Movat's pentachrome staining procedure, in which nuclei stain dark purple/black, cytoplasm stains pink/red, elastic fibers stain purple/black, collagen stains yellow/green, and non-collagenous ECM (primarily sulfated GAGs and proteoglycans) stains blue/green. EBs were primarily positive for cytoplasm (pink/red) staining, with some diffuse blue staining observed by day 10.

Hyaluronan and versican accumulation and distribution within differentiating EBs

In order to specifically examine the spatial distribution of hyaluronan and versican within EBs, immunohistochemistry was performed to examine EBs at different stages of differentiation (days 4, 7, 10). After only 4 days of differentiation, very little hyaluronan was detected in EBs (Figure 4.5A,D,G), but that which was present was predominantly localized around the periphery of most of the cell aggregates. By 7 days of differentiation, hyaluronan was clearly detectable more extensively throughout EBs and most often appeared to be enriched primarily on one side of an EB (Figure 4.5B,E,H). After 10 days, hyaluronan was found to be distributed throughout almost the entire interior of EBs (Figure 4.5C,F,I). Interestingly, the accumulation of hyaluronan appeared to be greatest in areas of lower cell density within EBs.

Similarly, versican (detected with an antibody recognizing the V0/V1 isoforms of versican) was minimally present within EBs at day 4 of differentiation (Figure 4.6A,D,G), but was distributed throughout a large portion of EBs by 7 days of differentiation (Figure 4.6B,E,H). After 10 days of differentiation, versican was detected throughout the majority of EBs and appeared most concentrated within less dense areas of cells (Figure 4.6C,F,I), similar to the patterns of hyaluronan localization observed. Thus, the expression of hyaluronan and versican within EBs exhibited similar temporal and spatial patterns over the course of differentiation.

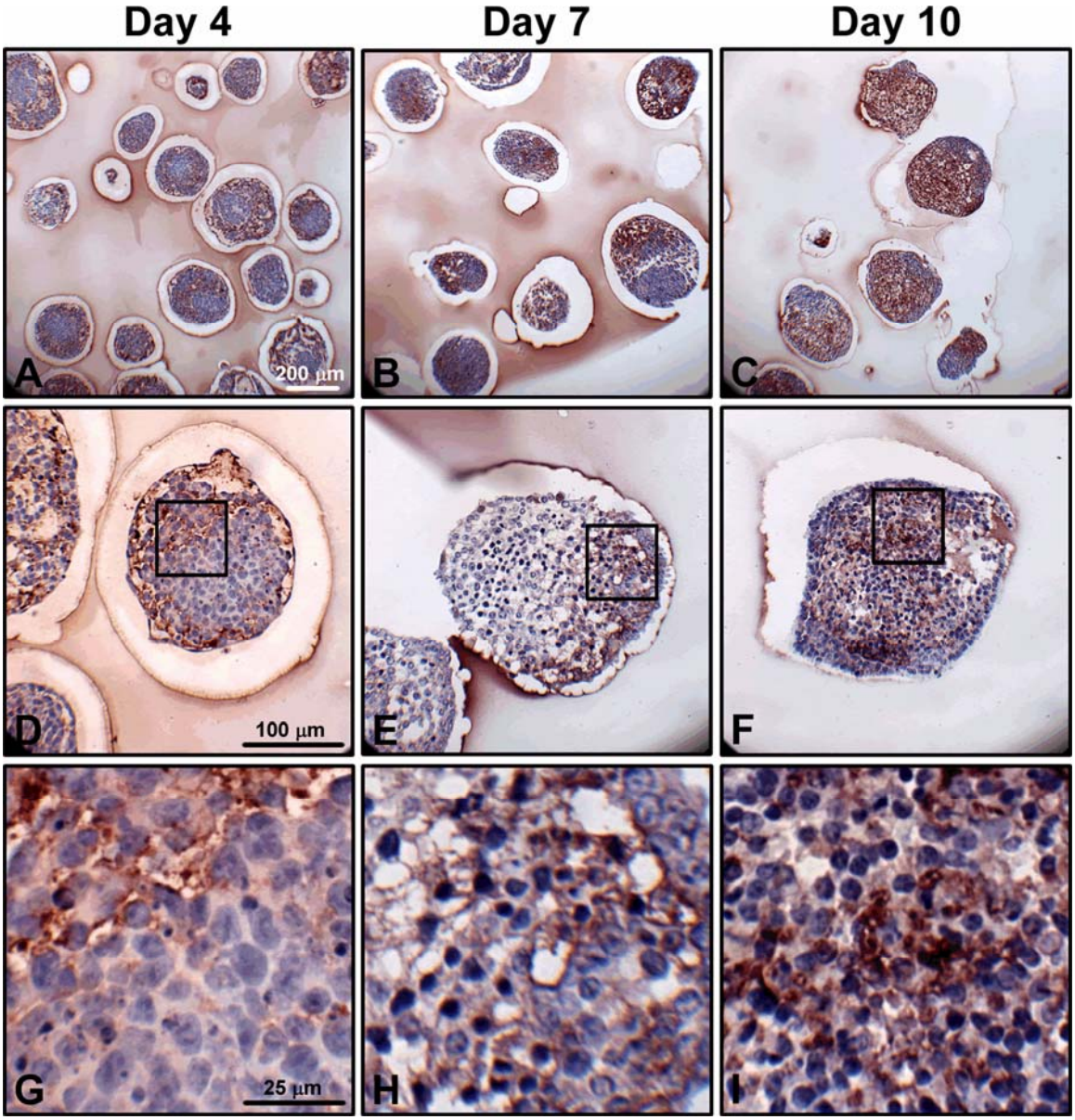

Figure 4.5. Hyaluronan accumulation during EB formation. Sections (5 μm) from day 4, 7, and 10 EBs were stained with hyaluronan binding protein (dark red color); hematoxylin-stained nuclei are shown in blue. Hyaluronan was increasingly prominent with differentiation time. Localized pockets of hyaluronan staining can be seen by day 7 (B,E), and higher magnification images (D-F, magnified view of boxes outlined in A-C) show hyaluronan surrounding individual cells. The magnification for each row is indicated by the scale bar defined in the left-most image.

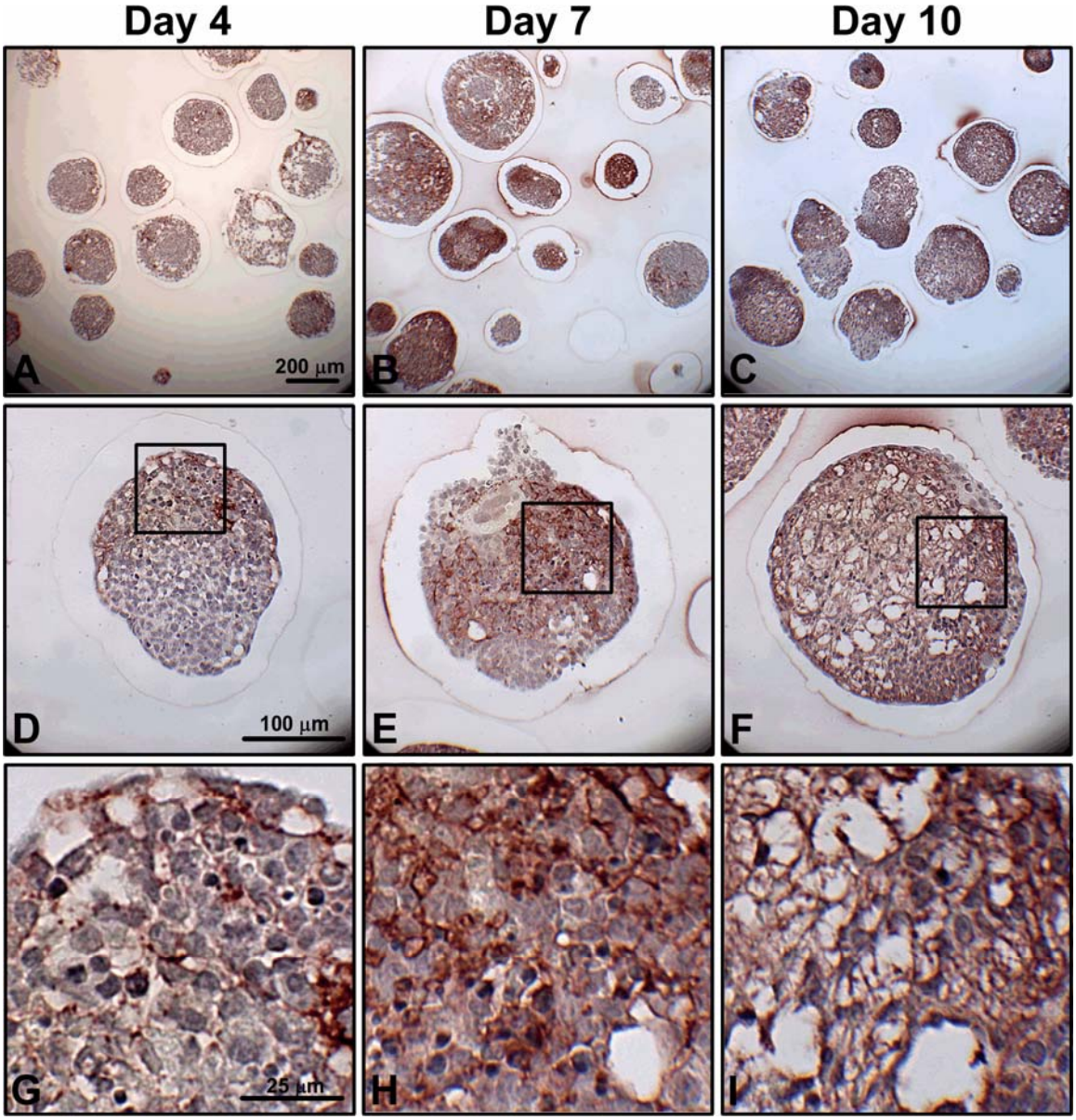

Figure 4.6. Versican accumulation during EB formation. Sections (5 μm) from day 4, 7, and 10 EBs were stained with an anti-versican antibody (dark red color); hematoxylin-stained nuclei are shown in blue. Some versican expression can be seen by day 4 (A,D), with increased quantities observed by days 7 (B,E) and 10 (C,F). Versican appears to localize in areas of lower cell density, while higher magnification images (D-F, magnified view of boxes outlined in A-C) reveal versican staining within acellular spaces. The magnification for each row is indicated by the scale bar defined in the left-most image.

Accumulation of hyaluronan during EB formation

To quantify the amount of hyaluronan synthesized and retained within EBs, and released into the media over the course of differentiation, hyaluronan produced by EBs was assessed using a hyaluronan binding protein quantification kit (Figure 4.7). Hyaluronan accumulated within EBs as a function of time, such that the relative amount of hyaluronan by day 10 of differentiation increased significantly compared to earlier time points (ESCs: $p = 0.002$; day 4: $p = 0.003$; 7: $p = 0.006$). The quantity of hyaluronan produced per cell and retained within day 10 EBs was almost 30-fold greater than the amount of hyaluronan retained in the cell layer by undifferentiated ESCs (0.090 ± 0.07 pg/cell to 2.680 ± 1.11 pg/cell) (Figure 4.7A). Likewise, the concentration of hyaluronan secreted into the culture media increased almost four-fold from 0.898 ± 0.13 μg/mL at day 2 to 3.572 ± 0.59 μg/mL by day 10 of EB culture. For the first six days of differentiation, ESC- and EB-conditioned media contained similar concentrations of hyaluronan, between 0.898 ± 0.13 μg/mL and 1.594 ± 0.32 μg/mL (Figure 4.7B). However, hyaluronan content significantly increased at days 8 and 10 of differentiation (2.769 ± 0.42 μg/mL and 3.572 ± 0.59 μg/mL, respectively) compared to the earlier time points examined. On a per cell basis, proportionally less hyaluronan was secreted into the media than retained within the EBs over time. Media conditioned by day 4 and 7 EBs contained 0.354 ± 0.072 pg hyaluronan/cell and 0.157 ± 0.0058 pg hyaluronan/cell, respectively, compared to 0.167 ± 0.06 pg hyaluronan/cell (day 4) and 0.480 ± 0.22 pg hyaluronan/cell (day 7) retained within the EBs. Altogether, these results indicate that EBs synthesize and secrete increasing amounts of hyaluronan as a function of differentiation and an increasing amount of hyaluronan is retained within EBs over time.

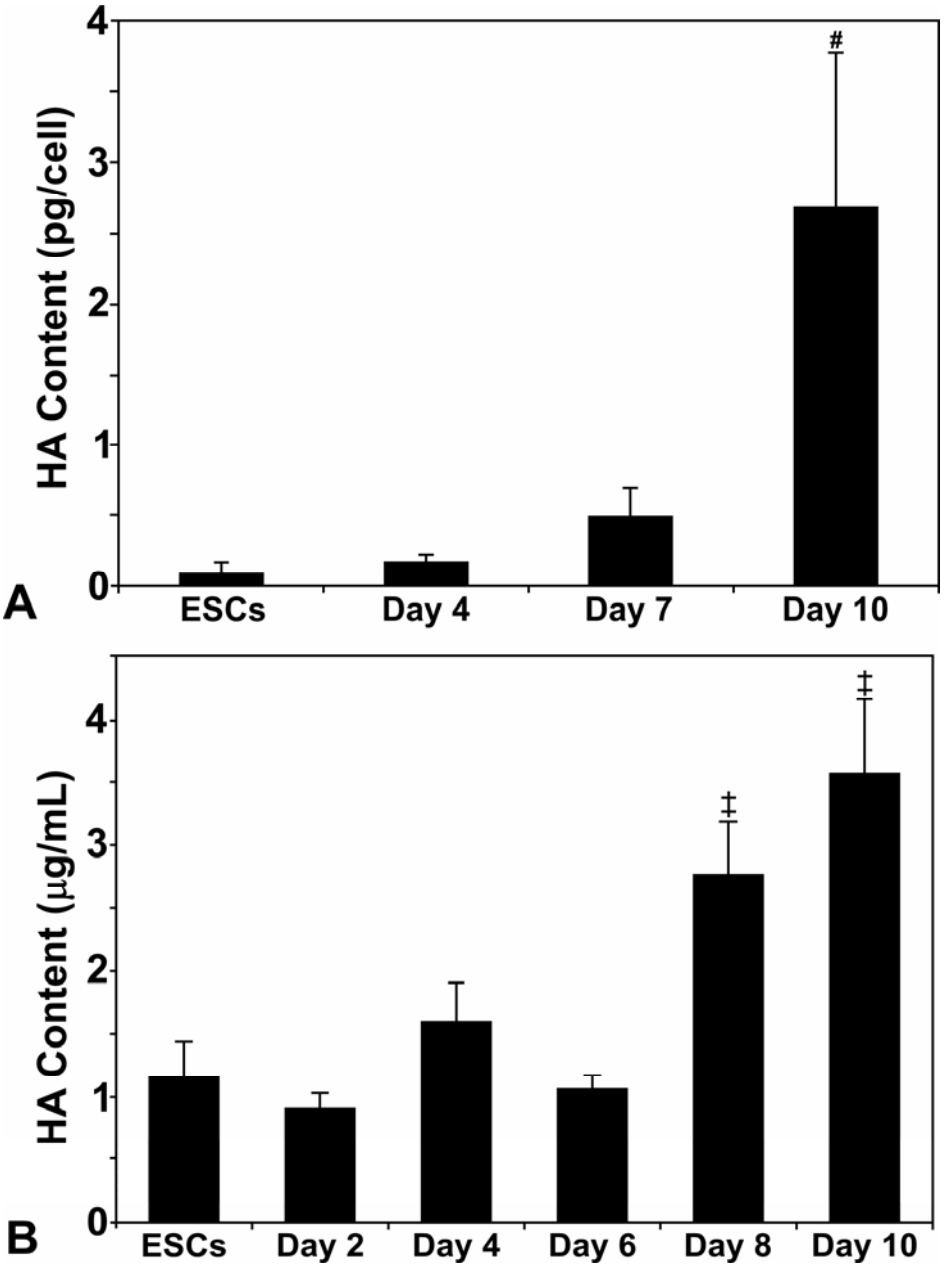

Figure 4.7. Quantification of hyaluronan synthesis by EBs. A quantitative hyaluronan (HA)-binding protein-based kit was used to measure hyaluronan retained within ESCs and day 4, 7, and 10 EBs (A) as well as hyaluronan secreted in media conditioned by ESCs and day 2, 4, 6, 8, and 10 EBs (B). Hyaluronan content in ESCs, EBs, and conditioned media samples progressively increased over the course of differentiation. Day 10 EBs and day 8- and 10-conditioned media samples contained significantly greater amounts of hyaluronan than samples collected from all other time points examined. # in (A) indicates significant differences from ESCs, day 4, and day 7, $p < 0.01$; ‡ in (B) indicates significant differences from ESCs and days 2 – 6, $p < 0.01$.

Versican accumulation and proteolytic processing during EB formation

To further analyze versican synthesis by differentiating EBs, proteoglycans were isolated and examined by Western blot analysis using a primary anti-mouse versican β-GAG domain antibody, which detects only the V0 and V1 versican isoforms. V0 and V1 appear as two high molecular mass products that migrate in the 350-450 kDa range on SDS PAGE gels [162-164]. V0 and V1 were not detected in the ESCs or EBs after 4 days of differentiation. However, V1 appeared at day 7 in the EBs and persisted at day 10 (Figure 4.8A). Although a distinct band for V0 was not clearly visible, positive immunoreactivity was detected at a higher molecular weight than the V1 product. Several bands also appeared at lower molecular weights than V1 in the 10 day EB cultures, which most likely represent degradation products of versican [162-164], such as the 70kDa DPEAAE neoepitope generated by proteolytic cleavage of versican by ADAMTS-1 [163]. Therefore, to assess whether versican proteolysis occurred during EB differentiation, immunoblotting was performed using an antibody that specifically recognizes DPEAAE. Parallel to the expression patterns of V0 and V1, the neoepitope was not detected in undifferentiated ESCs, but appeared at day 4 of differentiation, and increased in signal intensity through day 10 (Figure 4.8B). Similarly, gene expression of ADAMTS-1 [163] and ADAMTS-5 [165] (known versicanases) increased significantly by 10 days of differentiation compared to ESCs (Figure 4.8C), particularly for ADAMTS-5. In contrast, gene expression of ADAMTS-8, which is not implicated in versican degradation, did not change significantly during EB differentiation. Immunostaining for ADAMTS-5 indicated minimal expression in day 4 EBs (data not shown), but the protease was distributed throughout different regions of day 7 and day 10

EBs (Figure 4.8D,E). Altogether, these results indicate that increased expression and proteolytic processing of versican occurs during EB differentiation.

Hyaluronan synthase and versican gene expression

To evaluate the potential sources of hyaluronan and versican in differentiating EBs, gene expression analysis was performed. The relative expression levels of the different hyaluronan synthase genes remained fairly consistent over the course of early EB differentiation (Figure 4.9A), with expression of HAS-2 significantly greater than either HAS-1 or HAS-3 at each of the time points examined (undifferentiated ESCs and days 4, 7 and 10 of EB differentiation). In contrast, no significant differences were found between HAS-1 and HAS-3 expression at any stage of ESC differentiation. In addition, by 10 days of differentiation, HAS-2 expression was significantly increased ($p < 0.01$) compared to the levels measured at all of the earlier time points of analysis.

Similar to the patterns of HAS expression, the relative expression levels of the different versican isoforms were consistent over time (Figure 4.9B). Undifferentiated ESCs and differentiating EBs expressed relatively high levels of V0 and V1 that were each significantly greater than V2 and V3 at all of the time points examined ($p \leq 0.003$ in all cases), except for 10 days, when V0 and V3 were not statistically different. The expression of V0, V1 and V3 increased significantly by day 10 of EB differentiation compared to any of the earlier time points ($p < 0.01$). However, the expression of V2 remained relatively low compared to the other versican isoforms and did not change significantly over the course of EB differentiation.

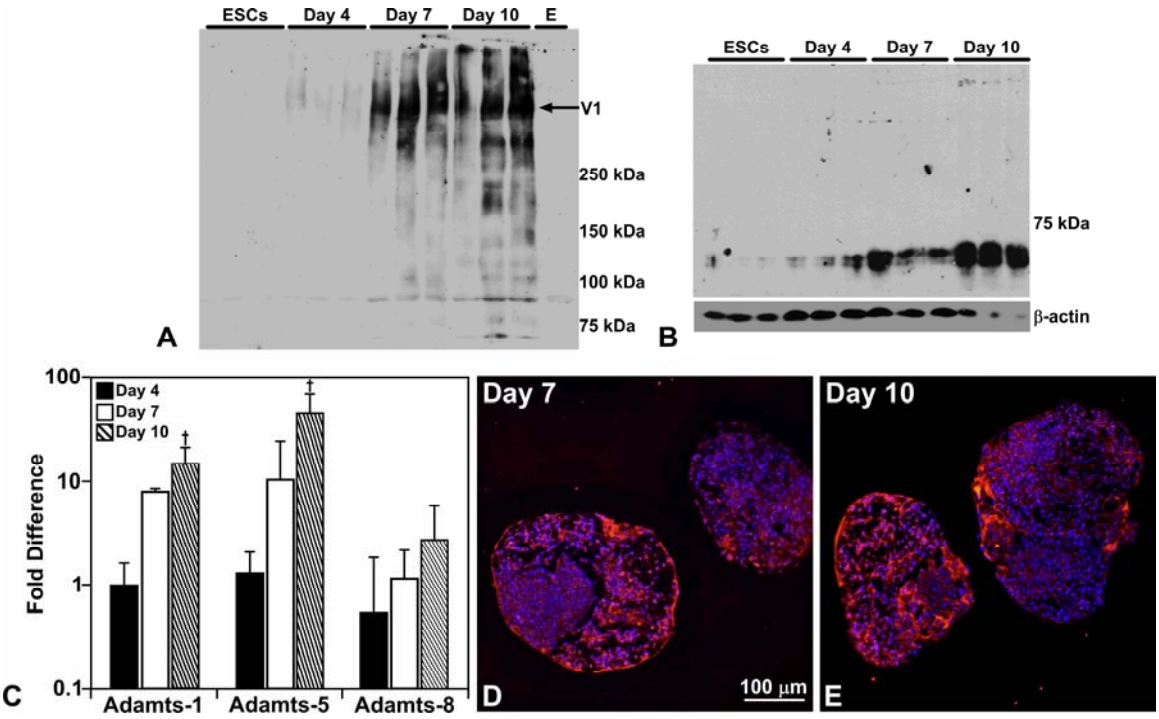

Figure 4.8. Analysis of versican synthesis and proteolysis in differentiating EBs. Purified, chondroitinase-treated protein lysates from triplicate samples of ESCs and day 4, 7, and 10 EBs were probed with rabbit anti-mouse versican β-GAG domain antibody (A). Versican core proteins V0 and V1 (~450 and 350 kDa respectively) were apparent after 7 and 10 days of differentiation in triplicate samples and were not detected in ESCs and EBs after 4 days of differentiation. Protein lysates were also examined for the versican cleavage product, known as the DPEAAE fragment, generated by ADAMTS-1 over the course of EB culture (B). The 70 kDa DPEAAE fragment was present at day 4 and appeared to increase with differentiation time through day 10. Beta actin was used as a loading control. ADAMTS-1 and -5, known versicanases, were examined via SuperArray RT-PCR arrays, and each gene was found to increase significantly by day 10 compared to day 4 of differentiation, while ADAMTS-8, a protease unrelated to versican degradation, remained unchanged (C). ADAMTS-5 immunofluorescent staining detected protease expression with day 7 (D) and day 10 (E) EBs. † indicates significant differences from day 4 EBs, $p < 0.05$.

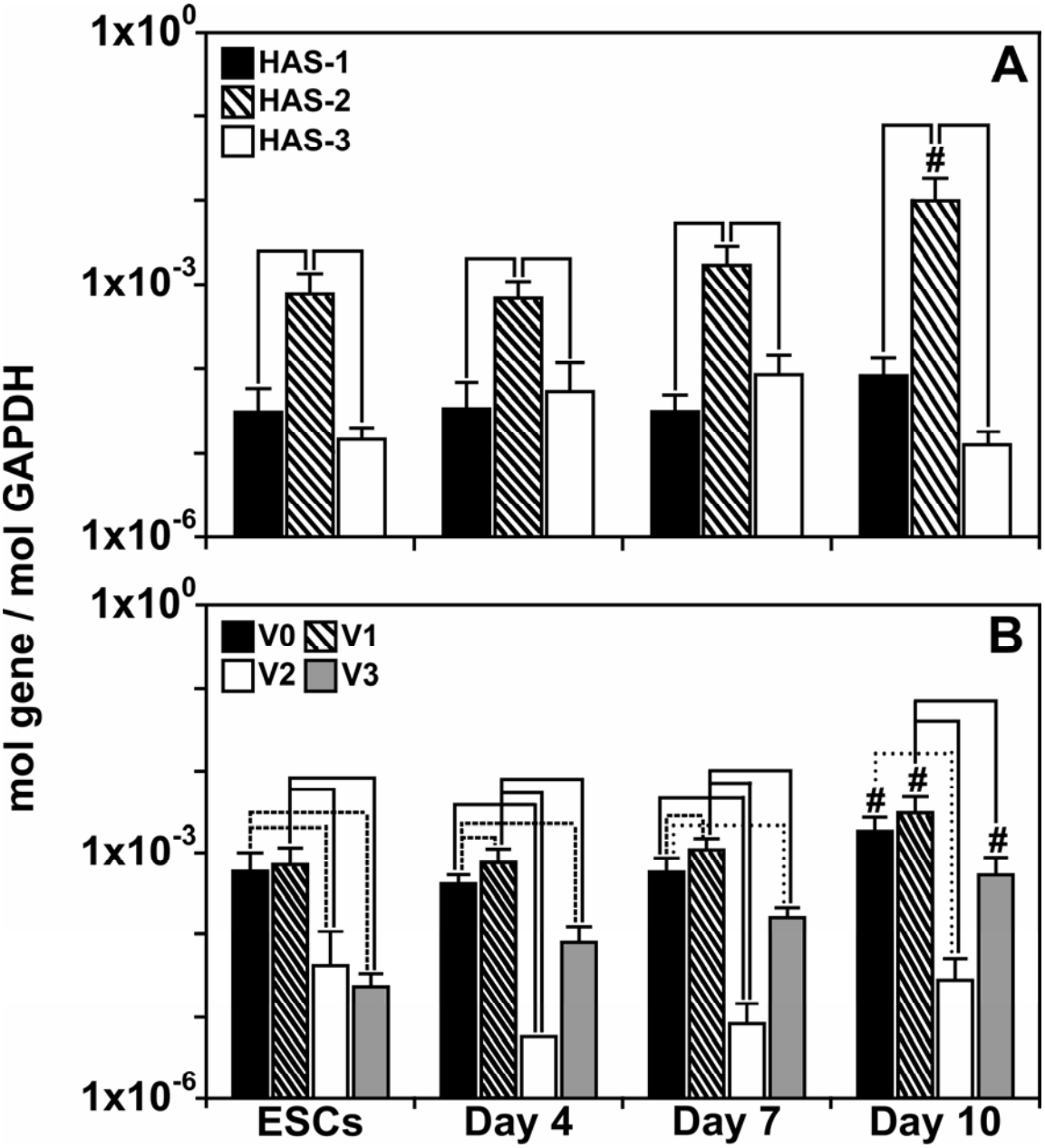

Figure 4.9. Quantification of hyaluronan synthase and versican gene expression. Quantitative RT-PCR was used to compare expression levels of hyaluronan synthase (HAS) isoforms 1, 2, and 3 and versican splice variants V0, V1, V2, and V3 during the course of EB differentiation. HAS-2 increased with time and was consistently expressed at significantly higher levels than either HAS-1 or HAS-3. V0, V1, and V3 increased by 10 days of differentiation, while V2 was consistently expressed at relatively low levels. # indicates significant differences from ESCs, day 4, and day 7, $p < 0.02$; ▬ indicates $p < 0.01$, ▬▬ $p < 0.02$, and . . . $p < 0.05$.

Hyaluronan and versican co-localization

Immunofluorescent affinity labeling of both hyaluronan and versican within the same sections confirmed that hyaluronan and versican were not detectable in most EBs at 4 days of differentiation, although when present, hyaluronan co-localized with versican (Figure 4.10A,D,G,J). By day 7, hyaluronan and versican co-localized in regions of the EBs that primarily contained a lower density of cells (Figure 4.10B,E,H,K). The appearance of a largely fibrillar network of overlapping hyaluronan and versican was clearly distinguishable by 10 days of differentiation throughout much of the interior of EBs (Figure 4.10C,F,I,L). Thus, at each of the time points examined, hyaluronan and versican were consistently distributed in a similar spatial pattern within differentiating EBs.

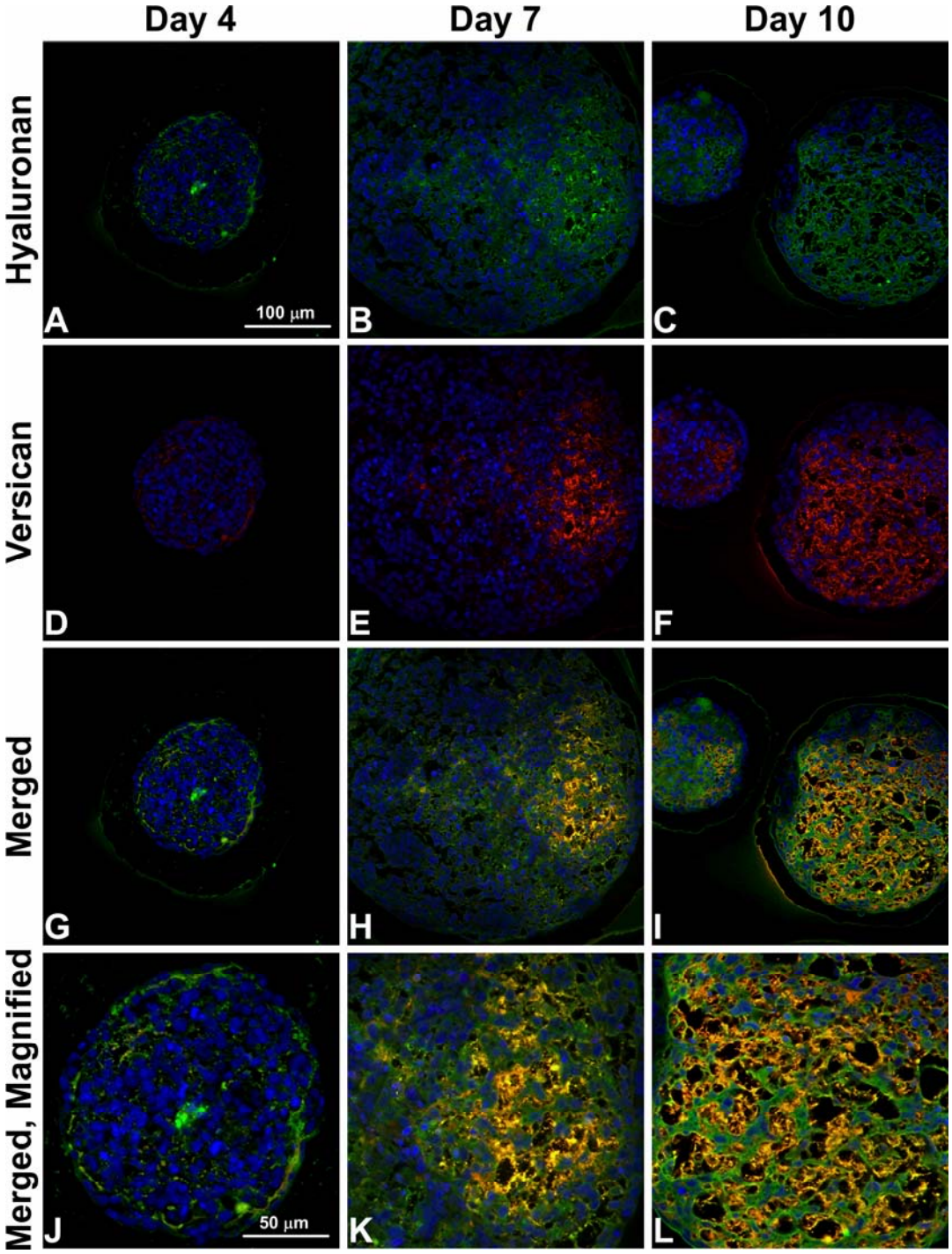

Figure 4.10. Hyaluronan and versican co-localization. EBs were stained for both hyaluronan (green; A-C) and versican (red; D-F); merged images show co-localization of the two molecules in yellow (G-I; higher magnifications J-L). Hyaluronan and versican appear to co-localize in areas of lower cell density, and deposition of both molecules increases over the course of differentiation. Images A-I are shown at the same magnification, with the scale bar shown in the upper left image; the scale bar for J-L is shown in J.

Epithelial and mesenchymal phenotypes within EBs

Based on the observed accumulation and co-localization of hyaluronan and versican in EBs during differentiation, as well as differences in cell morphology in regions containing hyaluronan and versican, the spatial distribution of epithelial (cytokeratin+) and mesenchymal (N-cadherin+) cells within EBs were examined relative to versican-rich regions. After 10 days of differentiation, EBs clearly contained distinct populations of cytokeratin+ and N-cadherin+ cells. Cytokeratin+ cells were primarily localized around the periphery of EBs, and versican appeared to be completely excluded from such areas within the same EB (Figure 4.11A,B). In contrast, N-cadherin+ cells were predominantly found within the interior of EBs in regions that overlapped with the presence of versican (Figure 4.11C,D). Taken together, these results suggest that versican (and likely hyaluronan based on their apparent co-localization and known binding interactions) may influence epithelial-mesenchymal transitions that occur within EBs during ESC differentiation.

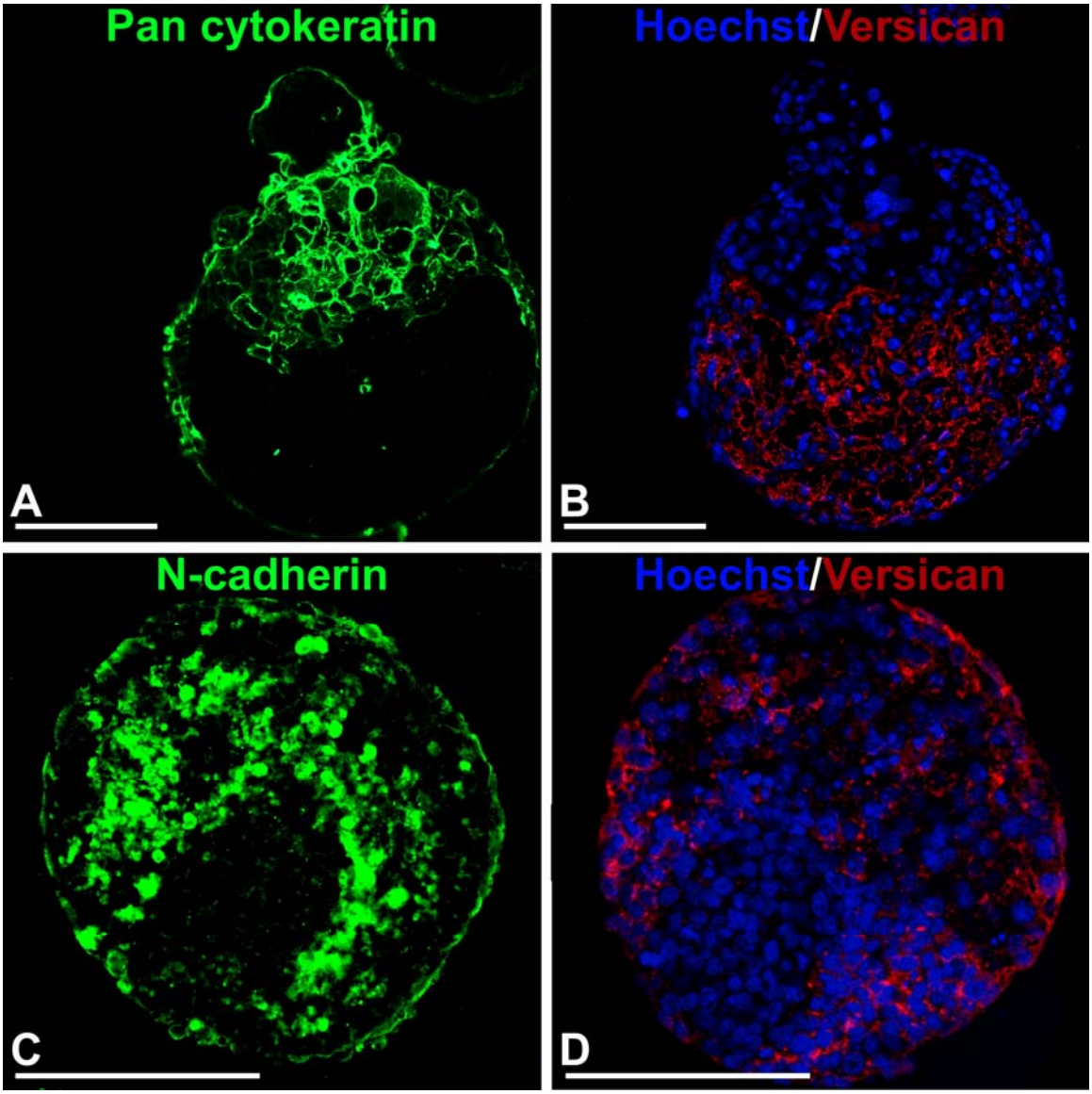

Figure 4.11. Cellular expression of epithelial-mesenchymal phenotypic markers relative to versican localization. Adjacent 5 μm sections from day 10 EBs were fluorescently stained with pan-cytokeratin or N-cadherin primary antibody (FITC-labeled secondary; green) and versican (TRITC-conjugated secondary antibody; red); nuclei were counterstained with Hoechst dye (blue). Cytokeratin localized primarily in the periphery of the EBs, with some evidence of invasion into the EB interiors, while versican was localized exclusively in cytokeratin-negative areas (A,B). In contrast, N-cadherin localized to areas occupied by versican (C,D). Staining was performed on adjacent sections of the same EBs, which were matched based on morphology and location on each slide. Scale bar = 100 μm.

Discussion

These studies provide evidence that spatial and temporal patterns of hyaluronan and versican accumulation and organization by ESCs within EBs are associated with epithelial-mesenchymal transitions occurring within the aggregates of differentiating cells. ESCs express several hyaluronan synthase and versican isoforms throughout the course of EB differentiation, concomitant with increasing accumulation of hyaluronan and versican over the first ten days of differentiation. The overlapping spatial patterns of expression suggest that hyaluronan and versican are physically associated within EBs, and moreover, the overlapping patterns of accumulation of these molecules are found predominantly in regions of EBs containing cells actively undergoing EMT differentiation. Overall, these results not only suggest a specific role for hyaluronan and versican in the morphogenesis of primitive pluripotent stem cells, but also demonstrate that dynamic changes in the endogenous expression, accumulation, and processing of ECM molecules by differentiating ESCs occur coincidentally with cell phenotype changes. These results indicate that an improved understanding of the molecular composition of embryonic extracellular matrices could yield new insights into developmental biology and provide novel strategies for the directed differentiation of stem cells.

The most significant and novel finding of the present study is that the timing and spatial distribution of hyaluronan and versican expression within EBs correlates with the appearance and localization of mesenchymal (N-cadherin+) cell phenotypes and is excluded from regions of epithelial (cytokeratin+) cells (Figure 4.11). Previous studies have demonstrated that ESC differentiation within EBs recapitulates many aspects of

gastrulation, including the transformation of epithelial pluripotent cells (resembling primitive ectoderm) into migratory mesenchymal cells (resembling primitive streak) [27, 140-144]. Thus far, however, dynamic changes in prevalent ECM molecules produced within EBs, such as hyaluronan and versican, have not been directly examined or correlated with distinct populations of cells. It has been previously demonstrated that coincident expression of hyaluronan and versican can stimulate cell migration by creating a visco-elastic, hyaluronan-versican-rich, malleable extracellular environment [155, 160], [166, 167]. Furthermore, a hyaluronan-versican matrix may influence cell fate by enriching for signaling molecules and growth factors that regulate cell proliferation and differentiation. The importance of hyaluronan and versican in directing EMT processes is clear from a number of examples in cell and developmental biology. Whereas HAS-2$^{-/-}$ mouse embryos fail to undergo EMT during cardiac morphogenesis [153], over-expression of hyaluronan by HAS-2 recombinant adenoviral infection of normal epithelial cells induces an EMT [150]. In addition, versican plays an essential role in the EMT of the endocardial mesenchymal cushion [148, 152], as well as mesenchymal condensation and hair induction [168]. Thus, hyaluronan and versican appear to regulate the transformation of epithelial cells to mesenchymal phenotypes at various stages of development.

As noted above, the expression of HAS isoforms, in particular HAS-2, and the synthesis of hyaluronan play important roles in early embryological development of numerous tissues. Although targeted inactivation of both HAS-1 and HAS-3 genes result in viable animals [169], knock-out of the HAS-2 gene is embryonic lethal by E9.5. In addition, HAS-2$^{-/-}$ E9.5 embryos almost completely lack hyaluronan, suggesting that

HAS-2 is the primary isoform responsible for hyaluronan synthesis during early organogenesis [153]. In the present study, HAS-2 was the dominant synthase isoform expressed by ESCs in EBs, and HAS-2 expression increased significantly by ten days of differentiation. The distribution of hyaluronan within murine EBs increased over time such that after ten days, differentiating cells produced ~30-fold more hyaluronan than undifferentiated ESCs (Figure 4.7A). Similar results have been reported in differentiating human EBs. Specifically, HAS-2 and its binding receptor RHAMM were highly up-regulated in human EBs and pre-implantation human embryos compared to ESCs, and a 24-fold enhancement of total hyaluronan was found in day 4 EBs (17.2 ng/10^6 cells) compared to ESCs (0.7 ng/10^6 cells) [69, 170]. However, compared to both HAS-1 and HAS-3, increased expression of HAS-2 by human ESCs only occurred upon EB differentiation, whereas in the present study, HAS-2 expression was significantly greater than HAS-1 or HAS-3 in undifferentiated mESCs, as well as in EBs at all time points examined. These subtle differences in HAS expression could be due to different culture methods utilized for the propagation and differentiation of mouse and human ESCs, as well as intrinsic differences between pluripotent cells derived from the two species [171].

In addition to changes in HAS expression and hyaluronan synthesis, differentiating ESCs also exhibit temporal changes in versican isoform expression, associated with increasing versican content within EBs over the course of differentiation. In the developing embryo, versican plays an important role in early cell migration events during neural crest formation and cardiac morphogenesis [172], [151]; thus it is not surprising that versican is expressed by EBs undergoing similar differentiation processes

in vitro. Compared to several other hyaluronan-binding proteoglycans, including aggrecan, neurocan and brevican, previous work demonstrated that versican (unspecified variant, presumably V0) was the only transcript to show a considerable enhancement in EBs compared to ESCs [69]. In the present study however, gene expression of each of the four different versican isoforms was independently examined. V0 and V1 were consistently expressed at greater levels than V2 and V3 throughout EB differentiation, and by ten days of differentiation, expression of V0 and V1 was significantly increased compared to earlier stages of differentiation. V0 and V1 isoforms uniquely contain the β-GAG chain, and immunostaining and Western blotting results with an anti-β-GAG antibody clearly indicated accumulating versican (V0, V1) protein within EBs after 7 days of differentiation. Specific expression of β-GAG isoforms (V0, V1) has previously been linked to developmental processes such as chondrogenic differentiation and neural crest migration [172-175], thus V0 and V1 could be exerting similar effects in early ESC morphogenesis. Furthermore, proteolytic cleavage of versican by ADAMTS enzymes to expose the DPEAAE epitope has been associated with EMT during cardiac cushion formation in the mouse embryo [148] and has been reported to play an important signaling function in EMT processes in various tissues [176], [177]. In addition, expression of ADAMTS-5 was limited prior to 11.5 days (E11.5) of mouse embryogenesis, but specifically found in developing nerves and limbs after E11.5, suggesting the potential importance of ADAMTS-5 in mid-stage development [178]. Therefore, the coincident increase in DPEAAE epitope exposure with the expression of ADAMTS-1 and ADAMTS-5 during EB differentiation indicates that similar remodeling processes are involved in pluripotent stem cell morphogenesis.

Differentiating embryonic stem cells offer a unique model system for studying various aspects of developmental biology. Analyzing the dynamics of ECM synthesis, accumulation, and organization during development may yield new insights into the molecular regulatory mechanisms responsible for stimulating morphogenic processes, such as EMT, important for embryonic cell differentiation and organ development. In a broader context, these results also indicate that phenotypic differences between differentiating ESCs may be associated with the local composition of the ECM, reflecting either the differentiation of specific cell types or the possibility of regulating endogenous ECM production within EBs to provide a novel approach to directing ESC fate.

CHAPTER 5

EFFICACY OF SOLVENT EXTRACTION METHODS FOR DECELLULARIZATION OF EMBRYOID BODIES*

Introduction

Embryonic stem cells (ESCs) are pluripotent cells with the ability to self-renew indefinitely *in vitro* and differentiate into all cell types comprising the ectoderm, endoderm, and mesoderm lineages. The pluripotent differentiation capacity of ESCs suggests that these cells may be used for a variety of different regenerative cell therapies. However, in experimental models of ESC transplantation, tissue repair has been observed even in the absence of significant cell differentiation [179-182]. This suggests that in addition to the differentiated cells ESCs may become, they may also be capable of producing molecular factors that might alter the local tissue microenvironment and modulate tissue repair processes. This notion is further supported by *in vivo* studies wherein delivery of local soluble factors by exogenous embryonic stem cells was capable of treating genetic defects or injuries in rodents [47, 48]. In order to determine the exact mechanisms whereby stem cells contribute to tissue morphogenesis (i.e. cell differentiation versus molecular delivery), it is vital to be able to physically separate the cells from their extracellular microenvironment.

One approach commonly used to extract extracellular matrices from cells and

---

* Modified from:
R Nair, AV Ngangan, and TC McDevitt, *Efficacy of solvent extraction methods for acellularization of embryoid bodies*. J Biomater Sci Polym Ed., 2008, 19(6): 801-819.

tissues is decellularization. Various types of tissues have successfully been decellularized, including intestine [71], bladder [183, 184], nerve grafts [83, 185], esophagus [84], heart valves [92, 186-188], placenta [77], skin [75], and pericardium [74]. Typical decellularization protocols include a variety of means to eliminate cellular components and retain extracellular matrix, including physical disruption, chemical treatments, and enzymatic digestions. Decellularization procedures typically yield extracellular matrices consisting of structural and adhesive proteins, such as collagens, laminins, elastin and fibronectin, other proteoglycans and growth factors, and glycosaminoglycans. These native ECM components retain bioactivity even after the decellularization process, evidenced by the ability of exogenous cells to invade, proliferate within, and remodel the acellular tissue [189-192]. Acellular products have been broadly applied to regenerate a variety of tissues, including infarcted myocardium [193], ruptured Achilles tendon [80], and injured skin [81], as well as to replace vascular grafts [71, 194] and tissues of the lower urinary tract [190]. Acellular tissues are capable of stimulating neovascularization, eliciting a minimal host immune response, and promoting functional tissue regeneration *in vivo* [83-85]. Several acellular products approved by the FDA for regenerative therapies and presently in clinical use include Surgisis® (Cook Surgical) [195], Alloderm® (LifeCell, Corp.) [196] and Synergraft® (CryoLife, Inc.) [186]. However, none of the currently commercially available acellular products are derived from tissue sources dynamically undergoing morphogenic processes. On the other hand, acellular matrices derived from embryonic stem cells could provide a robust clinical product capable of being tailored for different regenerative therapies due to the pluripotent nature of the cells and their ability to be differentiated towards different

lineages. The development of different acellular products requires individual optimization of treatment conditions, such as combinations of chemical concentrations and durations, in order to efficiently inhibit cell viability while preserving extracellular matrix composition of the native tissue.

Inherent biochemical and structural differences between diverse tissues necessitate the use of different decellularization chemical solvent regimens that vary in their ability to disrupt and extract cellular elements. The chemicals that have been used to decellularize different tissues can be generally categorized into alkaline or acid solvents, non-ionic or ionic detergents, and enzymatic treatments [86]. Acid/alkaline treatments, including acetic acid, peracetic acid (PAA), and ammonium hydroxide, are intended to solubilize cellular cytoplasmic components and disrupt nuclei. PAA in particular has been found to be effective as a disinfectant and at removing cellular material while maintaining ECM proteins, GAGs, and growth factors of thin tissues [80, 89, 197, 198]. Ionic detergents, such as sodium dodecyl sulfate (SDS), can efficiently solubilize nuclear and cytoplasmic membranes; however, SDS can also solubilize proteins, such as native ECM components [91]. Non-ionic detergents, which disrupt lipid-lipid and lipid-protein interactions, can also disrupt cell membranes, yet perturb protein-protein interactions less than ionic detergents. One of the most common non-ionic detergents, Triton X-100, has exhibited variable success in removing cellular material without significantly disrupting ECM composition [91-93]. Finally, enzymatic treatments, such as trypsin and DNase, have been used to cleave peptide bonds or digest nucleotides [85, 92]. The varying success of comparable decellularization treatments on dissimilar tissues suggests that reagent protocols must be optimized for each tissue by

controlling the concentrations and durations of treatments and analyzing the effects on the composition and function of the acellular product obtained.

The objective of this study was to determine the ability of different types of chemical solvent extraction methods to effectively decellularize aggregates of mouse embryonic stem cells undergoing differentiation, commonly referred to as "embryoid bodies" (EBs). By directly comparing chemical reagents previously used to decellularize other types of tissues, a set of conditions capable of yielding acellular matrices from mouse EBs was established. Initially, treatment with peracetic acid, SDS, and Triton X-100, either alone or in combination with DNase, were compared directly. Based on quantitative assays of cell viability, DNA content, mass retention, protein content, and qualitative histological analysis, a combination of Triton X-100 and DNase was found to effectively yield an acellular product derived from EBs. Subsequent studies therefore focused solely on the concentration and duration of Triton X-100 and DNase treatment, as well as ratios of the volumetric amounts of each reagent to the number of EBs in an attempt to optimize conditions for EB decellularization. These results provide the initial proof-of-principle that acellular proteinaceous matrices can be derived from differentiating ESCs and establish the basis for future studies to examine the molecular composition and biological function of novel stem cell-derived acellular matrices, which may have implications for tissue repair and wound healing applications in the field of regenerative medicine.

Materials and Methods

Cell Culture

Mouse embryonic stem cells (D3) were cultured on gelatin-coated dishes with ESGRO Complete™ Clonal Grade Medium (Millipore). Cells were passaged every two to three days before reaching ~70% confluence. For the described studies, cells were used between passages 20-30. To initiate embryoid body (EB) culture, ESCs were dissociated using ESGRO Complete™ Accutase™ and removed from the gelatin-coated dishes. A density of 400,000 cells/mL was used to inoculate 10 mL EB cultures in differentiation media composed of Dulbecco's modified eagle medium (Mediatech), supplemented with 15% fetal bovine serum (HyClone), 2 mM L-glutamine (Mediatech), non-essential amino acids, antibiotic/antimycotics, and 0.1 mM β-mercaptoethanol. The EB suspension cultures were inoculated in 100 mm bacteriological grade polystyrene Petri dishes (Corning) on day "0" of differentiation and placed on rotary orbital shakers (Barnstead Lab-Line, Model 2314) at 40 rpm at 37^{o}C in 5% CO_2. Recent work from our lab has indicated that placing a suspension culture of mESCs in differentiation media on a rotary shaker at 40 rpm results in greater yields of homogeneously-sized EBs [199]. EBs were re-fed every other day by collecting the EBs via gravity sedimentation in 15 mL conical tubes, aspirating the old media, and replenishing the cultures with 10 mL of fresh differentiation media, before being placed back in the Petri dishes and onto the rotary orbital shakers.

Decellularization

For all of the described studies, embryoid bodies were collected at day 7 of differentiation. Input EB number was determined by performing a 10x dilution of one culture plate of EBs into 8 wells of a 24-well plate and counting the EBs under a microscope. Analysis performed on triplicate samples indicated an average of ~6200 EBs/100 mm plate (inoculated with $4x10^6$ cells initially). Unless otherwise specified, approximately 2000 EBs (~1/3 culture plate) were aliquoted into individual samples in 1.5 mL microcentrifuge tubes for decellularization assays. For mass retention analyses, each tube was weighed before addition of the sample. Untreated EBs were either rinsed in phosphate buffered saline (PBS) and stored in 4^oC for subsequent analyses or kept in serum-free media for up to three hours at 37^oC for cell viability measurements. Reagents tested were combinations of peracetic acid (PAA, Aldrich), sodium dodecyl sulfate (SDS, Fisher), Triton X-100 (VWR), and DNase (~2,000 Kunitz units/mg, Worthington Biochemical Corp.). Treatment groups were centrifuged at 18,000 × g (Microfuge® 18 Centrifuge, Beckman-Coulter) for two minutes before addition of the reagent being tested. Samples were rotated in a LabQuake Rotisserie for 30 – 90 minutes, spun down at 18,000 × g for two minutes, rinsed twice with PBS, and, if applicable, rotated in DNase between 15-60 minutes. At the end of the treatment, samples were centrifuged for two minutes at 18,000 × g and rinsed twice in PBS prior to additional analysis.

Histology

EBs were harvested from suspension by gravity-induced sedimentation within a 15 or 50 mL conical tube. EBs or acellular products were incubated in formalin fixative

for 30 minutes, rinsed twice with PBS, and embedded in Histogel®. Samples were then processed for histological sectioning through a series of xylene and alcohol rinses and embedded in paraffin. Embedded samples were sectioned into 5 μm slices and de-paraffinized prior to staining. Histological samples were either stained with hematoxylin and eosin (H&E) using a Leica Autostainer XL, or incubated in Hoechst fluorescent dye (10 μg/mL) for five minutes to stain for nuclei. Coverslips were mounted on each sample using either low viscosity mounting medium (H&E samples, Cytoseal™ 60, Richard-Allen Scientific) or aqueous mounting medium with anti-fading agents (fluorescent samples, Gel/Mount™, Biomeda Corp.) and imaged using a Nikon 80i Upright Microscope and a Sony Cyber-shot (DSC-W1) camera.

Cell Viability

Immediately after collection and decellularization treatment, untreated EBs and acellular samples were incubated in a 10% alamarBlue (Biosource) solution in serum-free media for four hours at 37°C with 5% CO_2. A 100 μL sample of the sample-conditioned alamarBlue solution was added to a 96 well plate, and fluorescent measurement values were taken (ex: 545 nm, em: 590 nm) using a SpectraMax M2e plate reader. Fluorescent measurements of the treated samples were normalized to values obtained for untreated EBs collected prior to decellularization treatment from the same batch of EBs. The acellular sample values were reported as the relative percent reduction of alamarBlue normalized to the untreated EB values (100% viable) from within the same experimental batch.

DNA Quantification

DNA content of untreated EBs and acellular samples was quantified using the Quant-iT™ PicoGreen® dsDNA Assay kit (Molecular Probes). Samples were solubilized using 6M GuHCl for two hours in a sonicating water bath and added to 20x TE buffer (200mM Tris-HCl, 20mM EDTA, pH=7.5) and PicoGreen dye solutions at a ratio of 43 μL sample : 107 μL buffer : 150 μL dye. Fluorescent measurements of experimental samples were taken using a SpectraMax M2e plate reader (ex: 485 nm, em: 528 nm), and the absolute DNA concentrations were determined by comparing experimental values to standard curve readings obtained using calf thymus DNA solutions ranging between 30 – 5000 ng/mL.

Mass Retention

The percent mass of the EBs retained after decellularization treatment was determined for both hydrated and lyophilized samples. Hydrated samples were weighed after removing excess liquid with a micropipette prior to and after treatments. For greater accuracy, dry weight measurements were also taken for untreated and decellularized EBs after rinsing the samples twice in distilled water and storing overnight at -80^{o}C. Samples were then freeze-dried for 24 hours using a lyophilizer (Freezone® 4.5, Labconco), and the final mass was weighed (AX205 DeltaRange®, Mettler Toledo). For both hydrated and lyophilized samples, individual tube mass was subtracted from total mass to obtain the net sample weight. Mass retention was recorded as the percent of the average acellular material mass (hydrated or dry) compared to the average starting EB sample mass.

Protein Quantification

In order to assay total protein content, the untreated EBs and acellular samples were solubilized with 6M guanidine hydrochloride (GuHCl), and total protein content was assessed using the bicinchoninic acid (BCA) assay kit (Pierce). A standard titration curve using bovine serum albumin (BSA) was generated for concentrations ranging from 20 – 2000 μg/mL. Samples were incubated in the BCA solution for 30 minutes at 37°C, and absorbance readings were taken at 562 nm on a SpectraMax M2e plate reader. The protein concentrations of the experimental samples were normalized to the BSA titration standard curve.

Statistics

For paired comparisons, student t-tests assuming unequal variances were used to determine statistical significance ($p<0.05$). For comparisons across multiple experimental groups, analysis of variance was used with post-hoc Tukey analysis to determine significant ($p<0.05$) differences between the different groups.

Results

Solvent extraction comparison

Multiple reagents were analyzed for their effects on EB decellularization. Peracetic acid (PAA, 0.1%, v/v), sodium dodecyl sulfate (SDS, 0.1% w/v), and Triton X-100 (1%) were used alone, and in conjunction with 1 mg/mL DNase, based on their reported ability to decellularize other types of tissues [71, 75, 77, 78, 84, 200]. Relative

cell viability was significantly decreased by all of the different solvent treatments (typically < 1% of untreated EBs), indicating that each of the chemicals effectively inhibited cell viability within the EBs (Figure 5.1A). Addition of DNase reduced DNA retention in both PAA- and Triton-treated samples on average by ~55-65% ($p = 0.02$ and $p = 0.09$, respectively), but did not have a significant effect ($p = 0.19$) when combined with SDS (Figure 5.1B). SDS alone, sequential treatments of SDS and DNase (S+D), and Triton and DNase (T+D) were most effective at removing DNA, resulting in only ~3-9% retention, compared to the initial, viable EBs. Mass retention (relative to the starting mass of EBs) varied amongst the different treatments, with PAA (70.3±1%) and its combination with DNase (P+D, 48.8±7%) demonstrating significantly greater retention ($p = 1.46E-4$ compared to S+D; $p = 9.62E-5$ compared to T+D) than treatment with other decellularization reagents (Figure 5.1C). For all groups treated with DNase, the additional treatment appeared to reduce the final mass of acellular material retained by ~30-60%, presumably due to enzymatic digestion of cellular DNA. On average, ~2000 untreated EBs contained a total of 745 μg of protein. Treatment with PAA resulted in the greatest amount of residual protein content (508.6±56 μg/2000 EBs) and was not affected by DNase treatment (501.2±92 μg/2000 EBs) (Figure 5.1D). Triton and T+D treatments maintained lower, but moderate concentrations of protein (132.7±2 μg/2000 EBs and 92.2±52 μg/2000 EBs, respectively), while SDS and S+D had the least protein retention (on average, ~14-31 μg/2000 EBs).

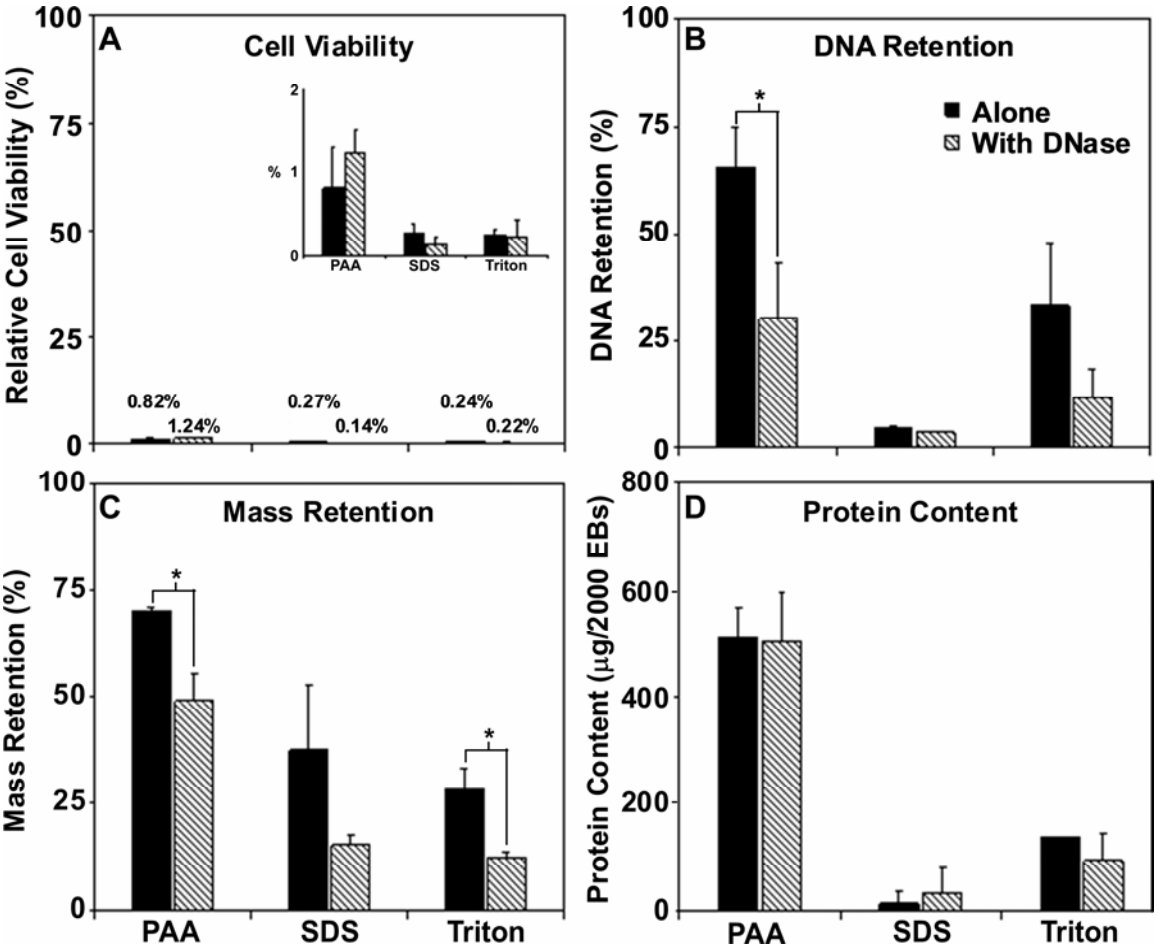

Figure 5.1. Solvent comparison. Cell viability (A), DNA retention (B), mass retention (C), and protein content (D) were assessed in samples treated for 30 minutes with 0.1% peracetic acid (PAA), 0.1% sodium dodecylsulfate (SDS), 1% Triton X-100, and combinations of these reagents with 1 mg/mL DNase (15 minutes) in order to assess their relative decellularization potential (* indicates significance across paired comparisons, $p \leq 0.03$). PAA was the least effective at reducing DNA content; the Triton X-100 and DNase combination was able to eliminate appreciable quantities of DNA, while maintaining a significantly higher mass:protein ratio than SDS-treated samples ($p = 0.02$). The inset in (A) depicts the identical set of data with a smaller y-axis range to more clearly demonstrate the lack of differences in cell viability between the different experimental groups.

In addition to the quantitative population assays, histological analysis was performed to directly assess the morphological effects of the different solvent treatments on individual EBs (Figure 5.2). PAA-treated EBs looked most similar to untreated EBs and exhibited a relatively high number of distinct cell nuclei, both with and without DNase treatment. The PAA treatment also did not appear to cause the agglomeration of individual EBs into a compact, continuous mass, as observed for both SDS and Triton X-100 treatments. SDS treatment appeared to completely extract cell nuclei (corroborating the PicoGreen DNA assay results, Figure 5.1B), even without the addition of DNase. EBs treated with Triton X-100 alone resulted in a complete disruption of intact cell nuclei, although DNA appeared to remain bound to the acellular material, as indicated by relatively bright Hoechst staining throughout the material. However, DNase treatment following Triton X-100 exposure reduced most of the Hoechst signal from the acellular material, suggesting that the cellular DNA associated with the matrix could be efficiently degraded and removed by enzymatic DNase treatment. Hematoxylin and eosin staining (Figure 5.2 insets) corroborated the results of the Hoechst staining, showing mostly basophilic staining (nuclear material) for PAA-, P+D-, and Triton-treated samples, whereas SDS, S+D, and T+D treatments lacked such staining. Furthermore, SDS-treated EBs histologically showed little evidence of structural or material complexity. Thus, based on the sum of these quantitative and qualitative measures, a combination of Triton and DNase treatment appeared to most effectively inhibit cell viability and remove DNA, while at the same time retain some of the original mass and protein content of mouse EBs.

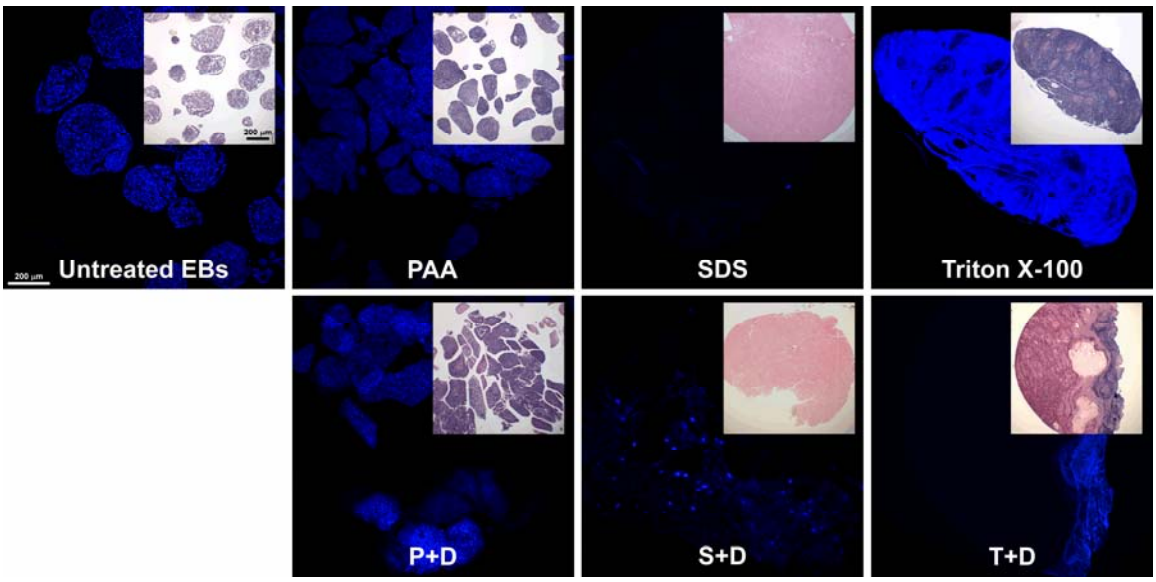

Figure 5.2. Histological analysis. Hoechst staining of cell nuclei was used for qualitative assessment of the various acellular samples treated for 30 minutes with 0.1% peracetic acid (PAA), 0.1% sodium dodecylsulfate (SDS), and 1% Triton X-100 (top row), or combinations of these reagents with 1 mg/mL DNase for 15 minutes (bottom row). Hematoxylin and eosin staining of adjacent sections of the corresponding acellular samples was also performed (inset images). Scale bar = 100 μm. PAA-treated samples retained DNA, while the addition of DNase to SDS and Triton samples reduced DNA content. Untreated EBs and PAA samples looked similar, while SDS and Triton treatments resulted in a compact, continuous mass of material.

Variable Triton and DNase Concentrations and Durations

To further optimize the efficiency of EB decellularization, additional experiments were performed using variations of Triton X-100 and DNase combinations. A matrix of different Triton concentrations (0.1%, 1%, 10%) and durations (30, 60, 90 minutes) were applied in combination with different DNase concentrations (0.5 mg/mL, 1 mg/mL, 2 mg/mL) and durations (15, 30, 60 minutes) in order to assess the effects of varying the extraction conditions on cell viability, mass retention, and DNA and protein content. Cell viability (Figure 5.3) and mass retention (Figure 5.4) did not change appreciably across the different treatment groups. In all samples, viability was inhibited to less than ~1% of the untreated EB values, while in some cases, trends suggested a slight increase in mass retention with an increase in DNase concentration. For the concentration ranges examined, there were few noticeable differences between the treatments, although 10% Triton resulted in significantly greater DNA retention (Figure 5.5) and protein content (Figure 5.6), as did 0.5 mg/mL DNase-treated samples. Although a higher total protein content may reflect a greater retention of desired ECM protein components, the corresponding higher DNA values do not meet the criteria of low cellular remnant levels expected for acellular tissues. Under most conditions, an increase in DNase concentration resulted in a slight decrease in DNA (Figure 5.5). For the treatment durations examined, increasing the length of Triton treatment significantly decreased the total protein content of the final acellular material (Figure 5.6). DNase duration did not have a significant effect on protein content (as expected); however, for 30- and 60-minute treatments, total protein increased slightly as DNase duration increased for all concentrations examined. Values from all concentration and duration analyses are listed

in Table 5.1. Overall, Triton- and DNase-treated samples typically retained less than 7.5% of the original DNA content and possessed an average of 14.2±6% of the initial protein content. Based on these findings, a 30-minute treatment of 0.1-1% Triton and 15 minutes of 1-2 mg/mL DNase provided the most efficient and convenient method of removing DNA while maintaining protein content from mouse EBs.

Ratios of Triton and DNase to EBs

The effect of different ratios of reagent volume to the input number of EBs was also analyzed by fixing the input of EBs and varying the volume of reagent used, and also by varying the EB input with a fixed solution volume. Similar to the previously described types of multi-parametric analyses, cell viability, DNA retention, mass retention, and protein content of acellular EBs were assessed with 1% Triton X-100 (30 minutes) and 1 mg/mL DNase (15 minutes). Neither cell viability nor mass retention varied significantly with the different volumetric ratios of Triton X-100 and DNase examined (Figure 5.7A,C), but increasing the volumes of Triton X-100 and DNase generally decreased the amount of DNA and protein remaining in the treated samples (Figure 5.7B,D). With a fixed volume of 0.25 mL of 1% Triton, both protein content and DNA retention significantly decreased with an increase in DNase volume ($p = 0.018$ and $p = 0.001$, respectively). A combination of 0.25 mL of 1% Triton X-100 and 0.25 mL of 1.0 mg/mL DNase resulted in 11.9±1% relative cell viability, 3.4±0.4% DNA retention, and 772.9±88 μg/2000 EBs protein content, while a four-fold increase in Triton X-100 and DNase volume decreased cell viability to 3.1±5%, DNA retention to 0.81±0.5%, and protein content to 29.1±192 μg/2000. As EB input increased (from ~1500 to 6200 EBs)

with constant treatment volumes of Triton X-100 (1 mL) and DNase (0.5 mL), no significant differences were observed in relative cell viability, mass retention, or protein retention with the varying input number of EBs (Figure 5.8), although these values increased steadily for untreated EBs (Figure 5.9). These results suggested that a minimum of 1.0 mL of 1% Triton X-100 and 0.5 mL of 1 mg/mL DNase were sufficient to decellularize ~3000-6000 EBs.

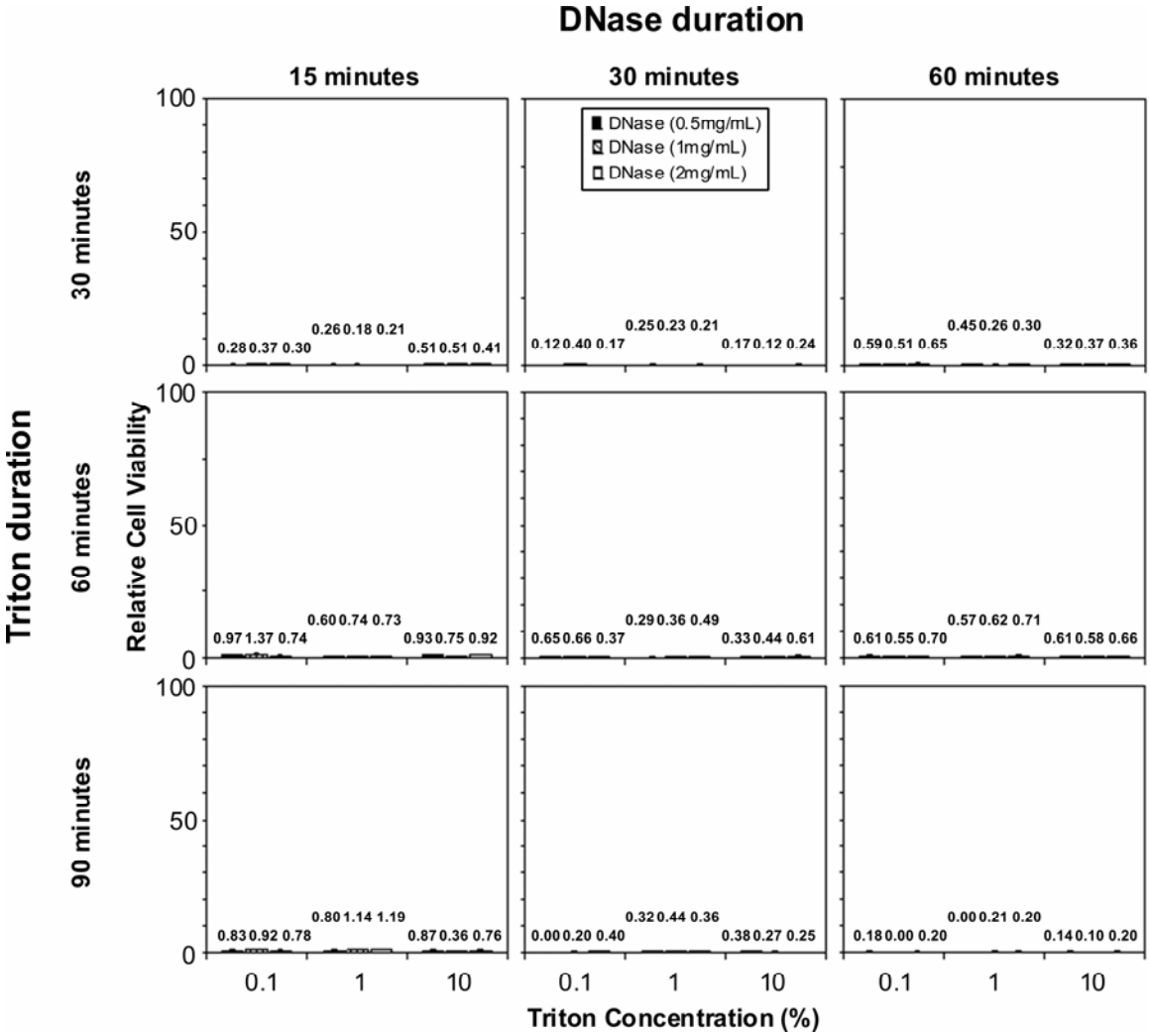

Figure 5.3. Relative cell viability analysis. Relative cell viability was assessed for combinations of sequential Triton X-100 and DNase treatments. Triton X-100 (0.1%, 1%, 10%) durations varied between 30, 60, and 90 minutes, while DNase (0.5 mg/mL, 1 mg/mL, 2 mg/mL) was varied between 15, 30, and 60 minutes. All of the experimental conditions examined reduced cell viability to negligible levels (~<1%).

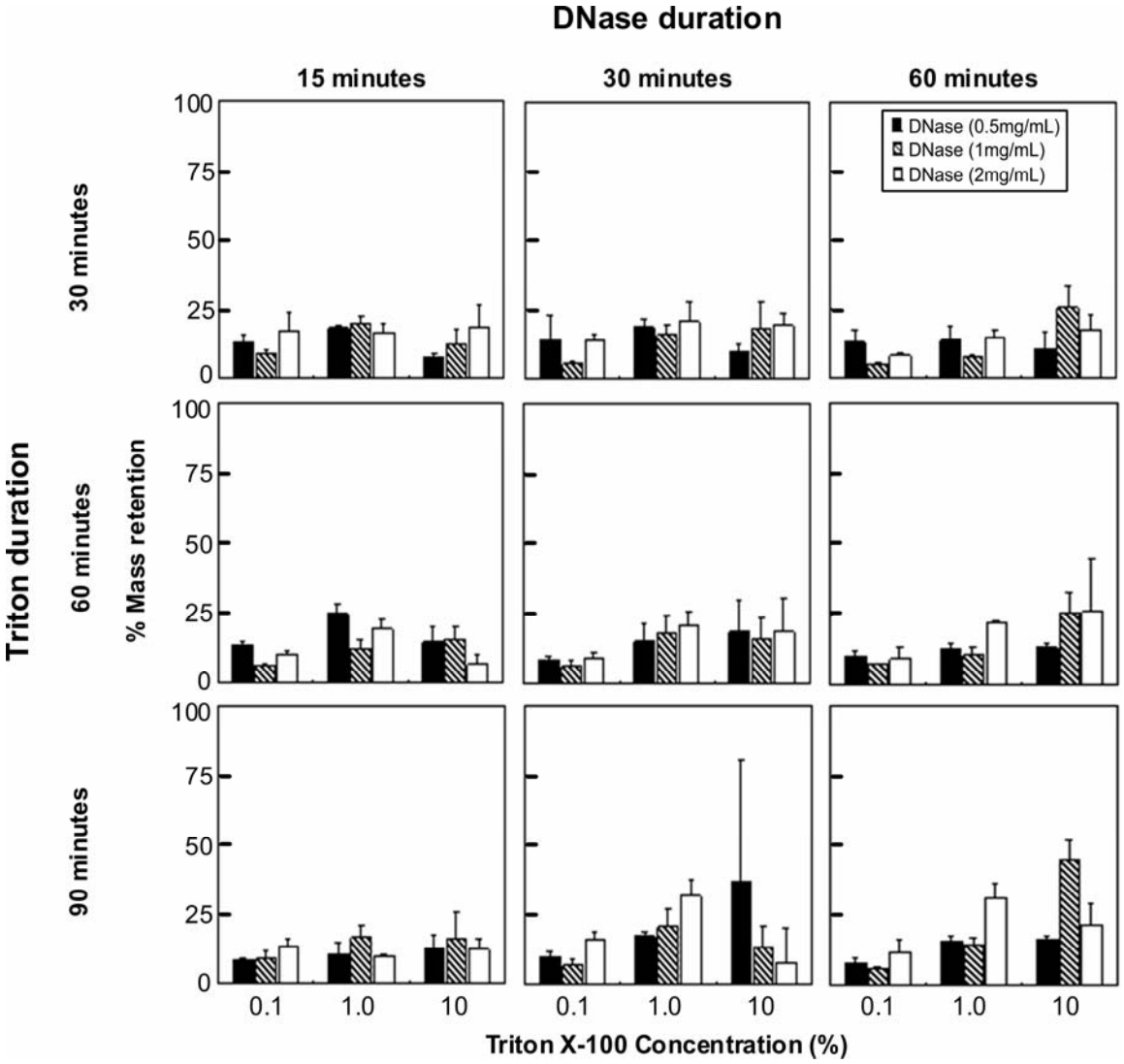

Figure 5.4. Mass retention analysis. Mass retention was assessed for combinations of sequential Triton X-100 and DNase treatments. Triton X-100 (0.1%, 1%, 10%) durations varied between 30, 60, and 90 minutes, while DNase (0.5 mg/mL, 1 mg/mL, 2 mg/mL) was varied between 15, 30, and 60 minutes. No noticeable differences between the groups were observed for different treatment durations, but increases in concentration of Triton X-100 and DNase, in some cases, resulted in slight increases in mass retention.

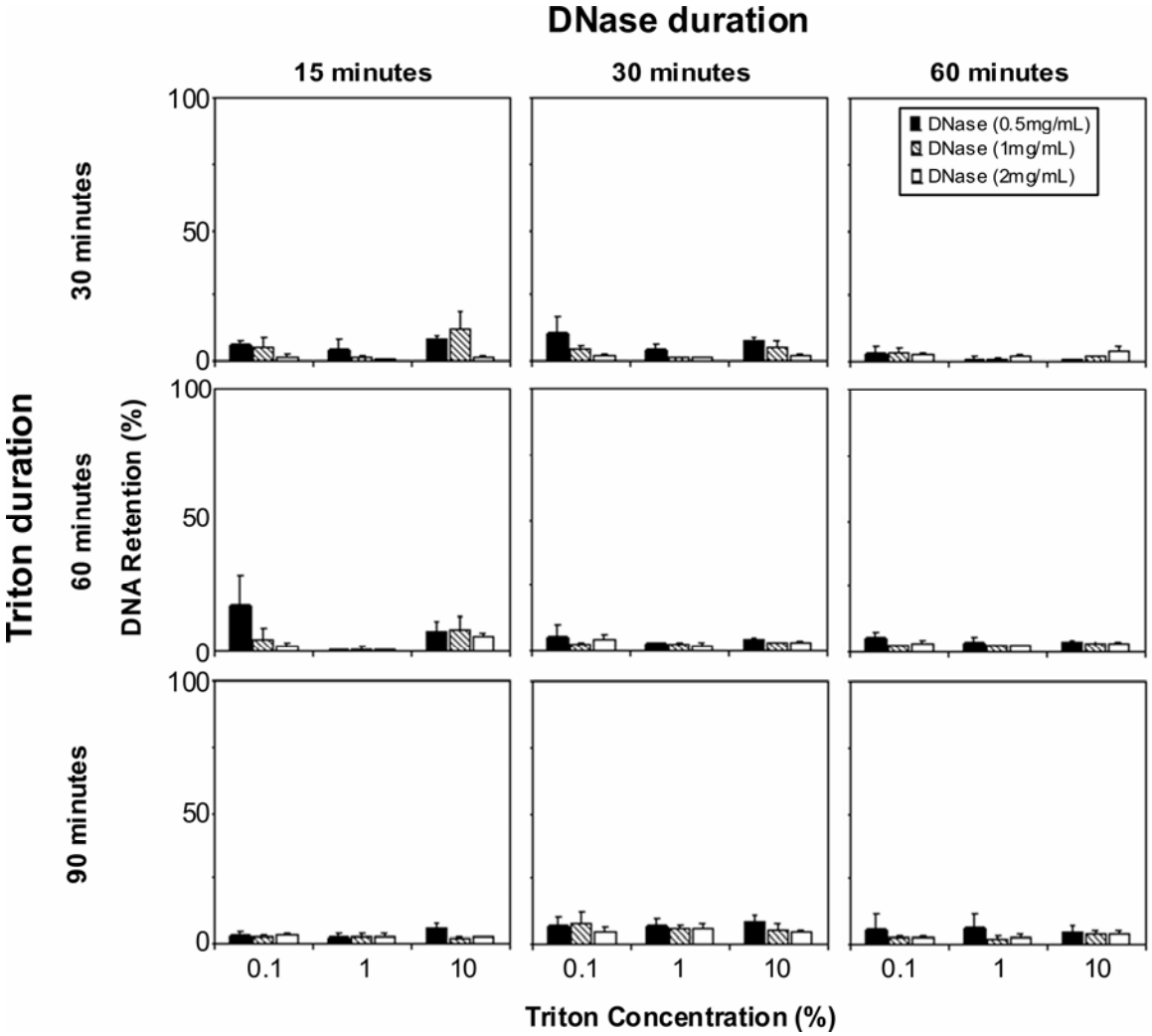

Figure 5.5. DNA retention analysis. DNA retention was assessed for combinations of sequential Triton X-100 and DNase treatments. Triton X-100 (0.1%, 1%, 10%) durations varied between 30, 60, and 90 minutes, while DNase (0.5 mg/mL, 1 mg/mL, 2 mg/mL) was varied between 15, 30, and 60 minutes. In general, increasing DNase concentrations led to slight decreases in DNA retention, but no statistically significant trends between the different experimental groups were observed.

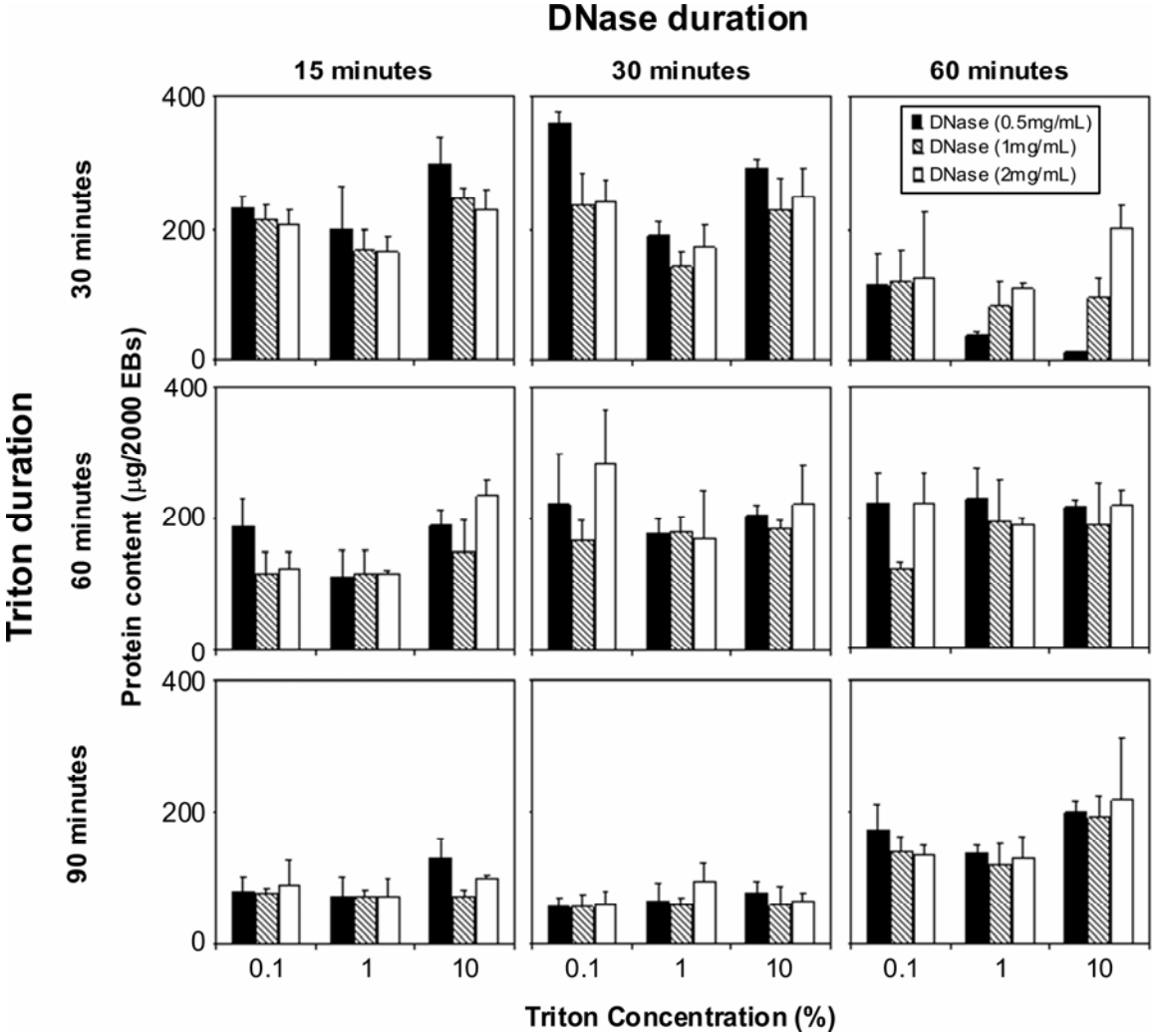

Figure 5.6. Protein content analysis. Protein content was assessed for combinations of sequential Triton X-100 and DNase treatments. Triton X-100 (0.1%, 1%, 10%) durations varied between 30, 60, and 90 minutes, while DNase (0.5 mg/mL, 1 mg/mL, 2 mg/mL) was varied between 15, 30, and 60 minutes. Overall, increases in Triton duration led to significant decreases in total protein content ($p<0.05$), but no significant trends were observed for the different Triton concentrations.

Table 5.1. Values from concentration and duration optimization analyses.

Time	Triton conc. (%)	DNase conc. mg/mL	Viability		Mass Retention		DNA Retention		Protein Content	
			Avg	Std Dev	Avg	Std Dev	Avg	Std Dev	Avg	Std Dev
30 min. Triton/ 15 min. DNase	0.1	0.5	0.28	0.14	12.62	2.91	0.58	0.11	231.12	18.00
	0.1	1	0.37	0.11	8.69	1.20	0.45	0.31	214.50	20.93
	0.1	2	0.30	0.06	16.48	6.81	0.14	0.06	206.73	22.80
	1	0.5	0.26	0.06	18.29	0.50	0.37	0.33	198.36	66.00
	1	1	0.18	0.16	19.27	2.80	0.13	0.05	165.97	33.91
	1	2	0.21	0.06	16.27	3.47	0.08	0.00	162.39	24.17
	10	0.5	0.51	0.14	7.34	1.21	0.70	0.14	296.60	40.18
	10	1	0.51	0.10	12.21	5.14	1.08	0.59	246.17	15.68
	10	2	0.41	0.13	18.13	7.99	0.14	0.04	229.89	30.30
30 min. Triton/ 30 min. DNase	0.1	0.5	0.12	0.06	13.84	8.91	0.85	0.48	360.89	15.26
	0.1	1	0.40	0.39	5.77	0.50	0.32	0.11	235.49	49.29
	0.1	2	0.17	0.05	14.02	1.81	0.15	0.03	242.63	31.90
	1	0.5	0.25	0.15	18.42	2.63	0.34	0.12	189.84	22.71
	1	1	0.23	0.02	15.74	3.26	0.09	0.03	139.71	24.81
	1	2	0.21	0.12	20.76	6.50	0.08	0.01	170.83	35.83
	10	0.5	0.17	0.06	9.33	3.06	0.61	0.09	292.68	11.58
	10	1	0.12	0.11	17.68	9.61	0.40	0.18	228.10	48.19
	10	2	0.24	0.10	19.03	4.11	0.15	0.06	248.71	43.08
30 min. Triton/ 60 min. DNase	0.1	0.5	0.59	0.20	13.04	4.04	0.19	0.12	112.95	48.28
	0.1	1	0.51	0.15	5.04	0.77	0.18	0.08	118.89	47.20
	0.1	2	0.65	0.42	8.02	0.81	0.13	0.05	124.03	101.49
	1	0.5	0.45	0.21	13.74	4.73	0.05	0.05	38.10	3.83
	1	1	0.26	0.14	7.31	0.69	0.05	0.03	82.93	34.94
	1	2	0.30	0.18	14.36	3.05	0.10	0.03	107.93	7.19
	10	0.5	0.32	0.16	10.64	5.95	0.05	0.00	12.96	0.00
	10	1	0.37	0.13	25.60	7.18	0.09	0.02	95.03	28.74
	10	2	0.36	0.18	16.95	6.03	0.21	0.08	201.95	35.60
60 min. Triton/ 15 min. DNase	0.1	0.5	0.97	0.22	13.35	1.17	0.38	0.24	187.35	43.53
	0.1	1	1.37	0.17	6.07	0.74	0.09	0.10	118.14	31.37
	0.1	2	0.74	0.28	9.67	1.37	0.04	0.02	124.31	26.31
	1	0.5	0.60	0.10	24.66	3.04	0.01	0.01	111.35	40.38
	1	1	0.74	0.00	12.30	2.89	0.02	0.02	117.20	35.72
	1	2	0.73	0.11	19.12	3.34	0.01	0.01	118.02	5.60
	10	0.5	0.93	0.08	14.43	5.61	0.17	0.08	189.30	22.83
	10	1	0.75	0.06	15.36	4.38	0.18	0.10	151.22	45.32
	10	2	0.92	0.16	6.87	3.18	0.13	0.03	234.80	23.45
60 min. Triton/ 30 min. DNase	0.1	0.5	0.65	0.19	8.60	0.94	0.30	0.22	223.13	74.15
	0.1	1	0.66	0.15	6.08	2.37	0.13	0.05	168.28	29.65
	0.1	2	0.37	0.34	8.62	2.60	0.22	0.10	281.33	82.78
	1	0.5	0.29	0.15	14.95	6.57	0.15	0.03	177.36	21.50
	1	1	0.36	0.05	18.20	6.00	0.14	0.02	180.82	21.79
	1	2	0.49	0.22	20.75	5.05	0.11	0.05	170.01	71.34
	10	0.5	0.33	0.09	18.57	11.19	0.23	0.04	206.15	14.52
	10	1	0.44	0.14	16.07	7.13	0.16	0.02	185.54	11.87
	10	2	0.61	0.53	18.41	12.13	0.16	0.05	223.27	57.15

Time	Triton conc. (%)	DNase conc. mg/mL	Viability		Mass Retention		DNA Retention		Protein Content	
			Avg	Std Dev	Avg	Std Dev	Avg	Std Dev	Avg	Std Dev
60 min. Triton/ 60 min. DNase	0.1	0.5	0.61	0.29	10.07	1.85	0.23	0.10	222.08	44.56
	0.1	1	0.55	0.05	7.07	0.33	0.11	0.03	124.02	9.21
	0.1	2	0.70	0.12	9.16	3.85	0.14	0.05	222.51	44.92
	1	0.5	0.57	0.18	12.65	1.86	0.16	0.08	229.22	44.68
	1	1	0.62	0.25	10.77	2.25	0.11	0.03	192.78	63.84
	1	2	0.71	0.18	21.80	0.96	0.09	0.01	188.13	10.46
	10	0.5	0.61	0.05	13.00	1.48	0.16	0.03	215.45	9.84
	10	1	0.58	0.10	25.60	7.18	0.13	0.05	188.78	63.60
	10	2	0.66	0.18	26.26	18.36	0.12	0.02	219.45	21.92
90 min. Triton/ 15 min. DNase	0.1	0.5	0.83	0.38	8.30	0.73	0.09	0.04	81.05	22.43
	0.1	1	0.92	0.07	8.87	3.06	0.09	0.02	78.54	7.27
	0.1	2	0.78	0.15	12.77	2.93	0.09	0.03	90.60	36.07
	1	0.5	0.80	0.08	10.19	4.19	0.09	0.03	73.70	28.65
	1	1	1.14	0.03	16.49	4.52	0.08	0.03	73.56	10.03
	1	2	1.19	0.26	9.41	0.68	0.09	0.03	73.63	25.56
	10	0.5	0.87	0.18	12.21	5.07	0.18	0.06	129.40	31.85
	10	1	0.36	0.16	15.88	9.77	0.07	0.00	72.10	11.47
	10	2	0.76	0.13	12.16	3.51	0.08	0.01	100.60	3.75
90 min. Triton/ 30 min. DNase	0.1	0.5	-0.02	0.08	9.72	2.29	0.10	0.05	54.11	16.02
	0.1	1	0.20	0.12	6.59	0.96	0.11	0.06	56.01	19.82
	0.1	2	0.40	0.09	15.70	5.15	0.07	0.03	57.67	22.14
	1	0.5	0.32	0.10	17.07	1.59	0.10	0.04	65.63	25.77
	1	1	0.44	0.07	20.70	3.15	0.08	0.02	59.50	9.64
	1	2	0.36	0.11	32.06	5.76	0.08	0.03	94.03	27.26
	10	0.5	0.38	0.20	36.71	44.29	0.11	0.04	77.02	17.04
	10	1	0.27	0.05	13.27	5.97	0.08	0.03	57.80	30.73
	10	2	0.25	0.02	7.89	0.91	0.06	0.01	65.02	11.25
90 min. Triton/ 60 min. DNase	0.1	0.5	0.18	0.23	8.09	1.52	0.27	0.27	172.53	38.06
	0.1	1	-0.14	0.21	6.05	0.24	0.11	0.03	140.76	21.41
	0.1	2	0.20	0.28	11.43	4.74	0.12	0.04	133.95	16.41
	1	0.5	-0.47	0.38	15.50	0.93	0.32	0.22	138.00	11.44
	1	1	0.21	0.30	14.54	1.59	0.11	0.04	121.21	31.79
	1	2	0.20	0.32	31.10	5.37	0.12	0.06	128.86	33.22
	10	0.5	0.14	0.28	16.20	4.85	0.22	0.10	200.18	14.45
	10	1	0.10	0.19	44.68	33.47	0.19	0.07	191.72	30.35
	10	2	0.20	0.29	21.60	7.82	0.18	0.06	217.38	92.02

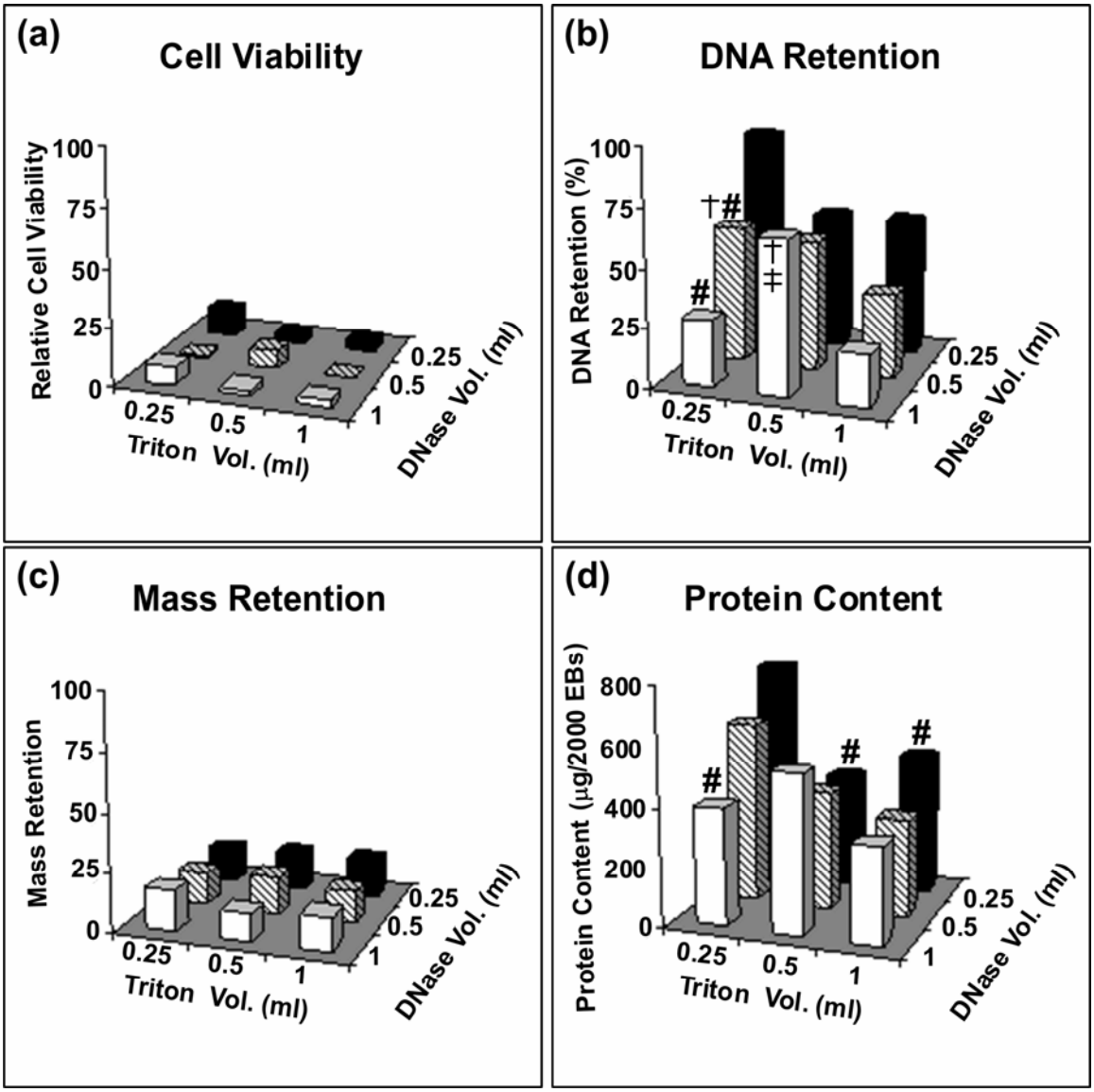

Figure 5.7. Reagent volume:EB ratio. The effect of reagent volume on decellularization efficiency was assessed by assaying for cell viability (A), DNA retention (B), mass retention (C), and protein content (D). Combinations of 0.25 mL, 0.50 mL, and 1 mL of both Triton and DNase were analyzed, with a fixed input of approximately 2000 EBs. The combination of 0.25 mL of each reagent resulted in significantly greater protein content and DNA retention than EBs treated with larger volumes. # indicates significant differences from 0.25 mL Triton/0.25 mL DNase; † indicates significant differences from 0.25 mL Triton/1 mL DNase; ‡ indicates significant differences from 1 mL Triton/1 mL DNase; $p < 0.05$. Note: different bar graph patterns indicate different DNase volumes used.

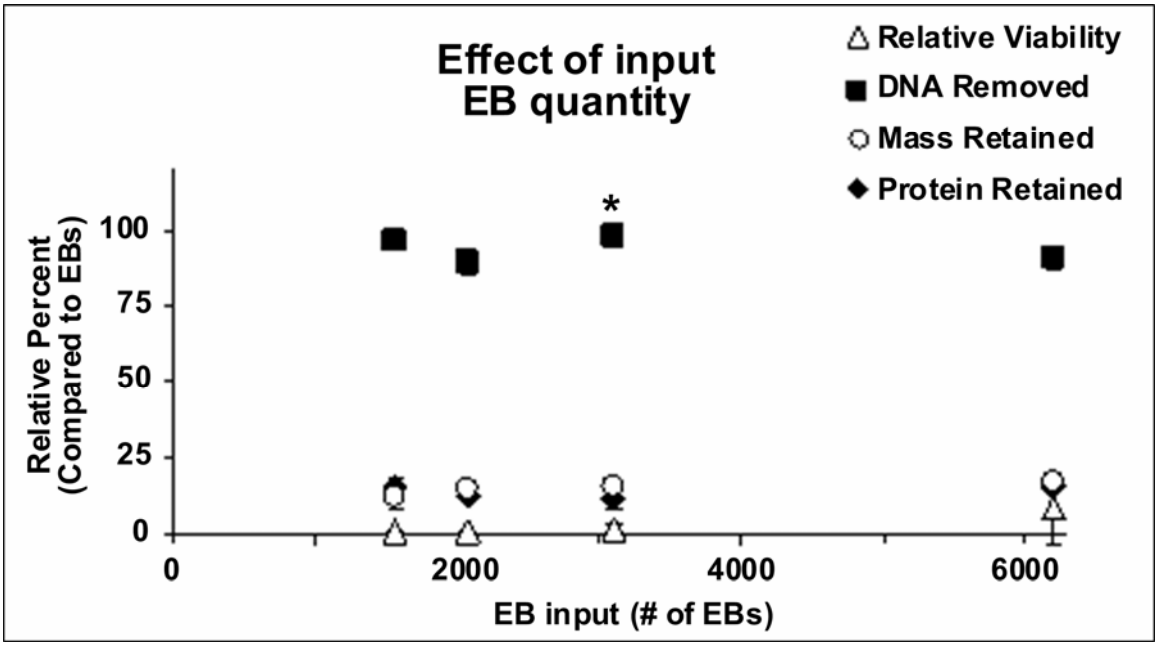

Figure 5.8. Variable EB input. The effect of EB input with a fixed reagent volume on decellularization efficiency was assessed by assaying for relative cell viability and DNA, mass, and protein retention. The number of initial EBs varied from 1500 – 6200, with all samples treated with 1 mL of Triton and 0.5 mL of DNase. With the exception of DNA removal, no statistically significant trends were observed in the parameters examined. *indicates significance ($p < 0.05$) compared to ~2000 and 6200 EB samples (Note: Error bars are too small to be displayed).

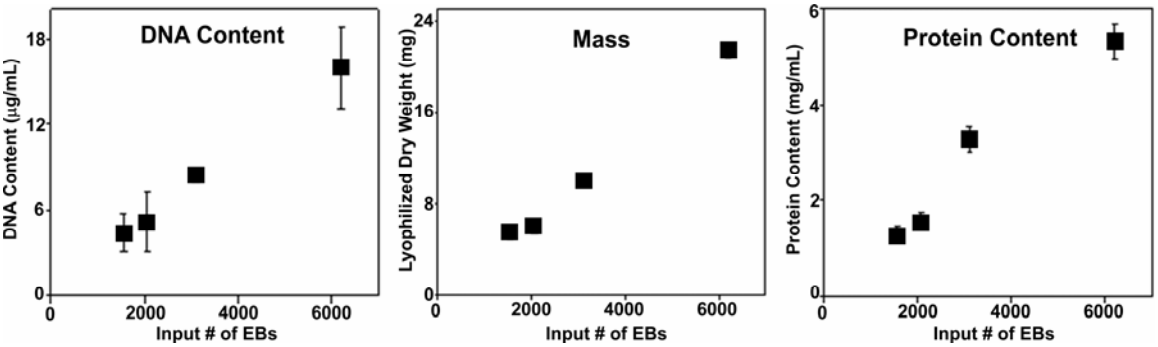

Figure 5.9. Variable native EB input. DNA, mass, and protein were analyzed as a function of increasing number of EBs. As expected, each of the different measures increased with increasing EB input. DNA content increased from 4.47±1.4 µg/mL to 15.94±2.9 µg/mL, mass increased from 5.50±1.0 mg to 21.46±1.7 mg, and protein increased from 1.32±0.1 mg/mL to 5.32±0.4 mg/mL as EB input was varied from 1550 to 6200 EBs. (Note: Some error bars are too small to be displayed.)

Discussion

In these studies, multiple chemical solvents were examined for their ability to effectively decellularize differentiating ESCs. A combination of Triton X-100 and DNase was found to reduce cell viability and DNA content while maintaining a greater protein:mass ratio more so than PAA or SDS treatments. Further optimization studies indicated that longer Triton durations significantly reduced protein content, and lower DNase concentrations were less efficient at removing DNA. In addition, for a fixed number of EBs, larger solvent volumes were more effective for decellularization, although significant differences were not detected when EB input was varied with constant solvent treatment volumes. The combination of lower concentrations of Triton X-100 (0.1 -1 %) and higher concentrations of DNase (1 - 2 mg/mL) applied for relatively short durations (15 – 30 minutes) was found to be sufficient for decellularizing thousands of EBs at once.

Decellularization technologies have evolved using a variety of reagents, depending largely on their suitability to effectively treat different tissue sources. The choice of solvent is critical, as it can eliminate desirable components in addition to the intended removal of cellular elements. The judicious selection of chemical solvents and the net effects on the composition and yield of the final acellular product must be defined experimentally since most common solvents, such as detergents, cannot accurately discriminate between cell and non-cell material. In these studies, a combination of cell viability, mass and DNA retention, and protein content were assessed to determine conditions for successful decellularization of EBs. Cell viability was used to globally examine residual cellular activity after chemical treatment, while DNA retention studies

provided a specific measure of nuclear material remaining. Analysis of mass retention was essential to evaluate the relative amount of non-specific material retained after decellularization treatment of the EBs. Total protein content was examined to obtain more specific information about the final content of the acellular material, and to potentially reflect the amount of ECM protein retained, although the non-specific nature of the assay renders it incapable of discriminating between intracellular and extracellular proteins. Additional properties, such as specific biomolecule content and bio-functionality are logical parameters to analyze after the aforementioned assays and are the focus of ongoing studies. Although the range of experimental conditions and values examined in the current study could be viewed as somewhat limited, they provided sufficient information about the trends to be expected with varying concentrations, durations, and ratios of solvent volumes to EBs. Many cell parameters are interrelated such that they uniformly decrease with chemical treatment, suggesting the need to prioritize, for example, the importance of DNA removal versus protein retention if both are to be considered essential metrics to evaluate the effectiveness of decellularization treatments. Despite such limitations, the comprehensive nature of studying multiple parameters of decellularization efficiency in parallel is clearly advantageous compared to assessing single parameters individually.

During the initial studies, multiple reagents typically used in various decellularization protocols were investigated, both alone and in conjunction with DNase. Use of peracetic acid (PAA) was found to maintain a higher level of protein content than all other treatments investigated, but PAA was also ineffective at removing DNA compared to other solvent treatments. These results differ from published reports where

PAA was used to successfully decellularize tissues such as SIS and urinary bladder [80, 201], although it has also been used primarily as a sterilization agent at the end of decellularization procedures by others [200]. This difference, however, simply attests to the variable effectiveness of different solvents based on the original tissue source and type of matrix attempting to be obtained. Sodium dodecyl sulfate (SDS), as well as successive treatments of Triton X-100 and DNase, significantly reduced DNA content, but both also reduced total protein content. However, EBs treated with Triton and DNase retained a significantly larger percentage of protein when related back to initial hydrated weight (30.0±17%) than those treated with SDS (1.4±2%) ($p = 0.018$). This result is relatively consistent with previously published reports that SDS significantly disrupts native extracellular matrix tissue composition and structure [75, 202]. Based on these criteria, the additional optimization studies conducted focused on varying combinations of Triton X-100 and DNase as an effective means to decellularize EBs.

The initial solvent comparisons provided a broad contrast of the effects that different reagents can have on the decellularization of EBs at fixed concentrations, durations, and ratios of the various chemicals to EBs. Thus, in order to develop a more refined decellularization protocol, the duration, concentration, and ratios of Triton X-100 and DNase to the original mass of EBs were systematically analyzed. Cell viability (Figure 5.3) and mass retention (Figure 5.4) did not change appreciably across the different treatment groups. Increasing the duration of Triton treatment, independent of the Triton concentration, decreased the total protein content retained in the final acellular product. On the other hand, increasing the duration of DNase treament appeared to increase protein content, suggesting that DNase was possibly becoming incorporated

within the acellular material with prolonged exposure time. These data suggested that minimizing the duration of solvent treatments would most likely yield the greatest amount of endogenous extracellular protein content, while still effectively inhibiting cell viability and extracting cellular DNA.

All combinations of Triton and DNase reduced DNA content significantly. In an attempt to investigate differences resulting from possible variances in initial conditions, the effect of either a solvent volume or EB input change on cell viability, and the retention of mass, DNA, and protein was examined. While increasing the volume resulted in lower DNA retention and protein content, varying the number of input EBs did not significantly affect cell viability, protein content, or mass retention. The larger solvent volumes presumably enhanced the access of the reagents to act on the EB samples. Although DNA, total mass, and protein of untreated EBs increased with an increase in input EB number, the decellularized mass maintained similar values regardless of initial conditions, suggesting that the combination of centrifugation and solution treatments was sufficient for the range of input EBs tested (1500-6000). Thus, based on the summation of the various studies performed, efficient decellularization of up to ~6200 EBs can be achieved using 1 mL of 0.1 - 1% Triton X-100 for 30 minutes and 1 mL of 1 - 2 mg/mL DNase for 15 minutes.

The combination of Triton X-100 and DNase treatment described by these studies can now be used to assess the specific molecular composition and function of acellular matrices derived from differentiating ESCs. This step is especially important as it has been suggested that excessive disruption of the native ECM is the primary cause of poor cellular repopulation and ultimate bioactivity of acellular tissues [203]. Further refinements could be integrated within the developed protocol, including the use of

protease inhibitors to prevent degradation of the final acellular product or antibiotics to minimize potential bacterial contamination [91]. Additional experiments could also be performed to develop methods for increasing ECM production by ESCs, possibly through the addition of soluble factors, such as ascorbic acid, or other means [204, 205]. These studies demonstrate that it is possible to decellularize differentiating aggregates of embryonic stem cells and retain protein content, suggesting that such methods could yield a novel biomaterial containing a complex assembly of morphogenic molecules naturally produced and localized within the embryoid body microenvironment. The ability of the initial pluripotent source to differentiate into cells comprising the three germ layers, as well as the homogeneity resulting from the EB rotary suspension culture [199], suggests that decellularization of differentiating ESCs could yield a unique, complex mixture of morphogenic cues that could be clinically relevant for a number of different regenerative medicine applications. The development of a decellularization protocol could also permit functional analysis of the molecular cues present in an embryonic environment actively undergoing cell differentiation and tissue morphogenesis and potentially have direct applications in efforts to regenerate diseased and injured tissues.

CHAPTER 6

ACELLULAR MATRICES DERIVED FROM DIFFERENTIATING EMBRYONIC STEM CELLS*

Introduction

Embryonic stem cells (ESCs), derived from the inner cell mass of pre-implantation blastocysts [1-4], are pluripotent cells capable of differentiating into all somatic cell types. The ability of ESCs to differentiate into various phenotypes, such as cardiomyocytes, neurons, and endocrine cells [137-139] suggests they could be useful in a number of applications where cells are irreversibly lost due to injury or disease. Therefore, ESCs are being investigated in a number of regenerative therapies including myocardial repair, neurodegenerative diseases, and diabetes [206-212]. Conventional methods of initiating ESC differentiation *in vitro* rely on suspension culture systems in which the cells spontaneously aggregate to form clusters of differentiating cells typically referred to as embryoid bodies (EBs) [35, 36]. Individual EBs recapitulate the temporal sequence of molecular signaling and cell differentiation events of embryonic pre-gastrulation tissues, culminating in the differentiation of the cells into the three germ lineages (ectoderm, endoderm, and mesoderm) from which all other somatic cells are subsequently formed [6, 37-40].

---

* Modified from:
R Nair, S Shukla, and TC McDevitt, *Acellular matrices derived from differentiating embryonic stem cells.* J Biomed Mater Res A, 2008. 87(4): 1075-1085.

In addition to their ability to differentiate into progenitor and somatic cells, recent studies have suggested that molecular factors synthesized and released locally by ESCs *in vivo* may be primarily responsible for observed tissue regenerative events [47, 48]. This significant observation suggests that biomolecules produced by stem cells may be at least as important as differentiation of the cells to achieve cell restoration and functional tissue repair. In order to separate cells from the natural biomolecules present locally in the tissue microenvironment, decellularization protocols have been developed to successfully extract extracellular matrix (ECM) from an array of tissue sources. The variety of tissues that have been decellularized include, but are not limited to, small intestinal submucosa, skin, pericardium, gall bladder, placenta, and tendon [71, 74, 75, 77, 213, 214], but thus far acellular matrices derived directly from stem cells and tissues actively undergoing morphogenic differentiation have not been reported.

The objective of this study was to develop a decellularization technique to isolate the biomolecules produced by embryonic stem cells actively undergoing tissue morphogenesis at different stages of differentiation. Previous studies were performed to establish an efficient method of extracting cells from EBs by assessing a combinatorial matrix of different chemicals and enzymes, reagent concentrations, and treatment durations. Such studies found that sequential treatment of Triton X-100 and DNase could effectively decellularize EBs differentiated for seven days, supported by multi-parametric analyses of cellularity [215]. Based on those previous findings, additional studies were performed to decellularize EBs at different stages of differentiation in order to potentially temporally regulate the molecular composition of acellular matrices. Decellularization of EBs differentiated for different periods of time was examined via histological analysis of

cellularity and quantitative assessments of cell viability, total mass, DNA, and protein content. The retention of ECM molecules produced by ESCs undergoing differentiation was assessed by immunohistochemical detection of adhesive ECM proteins and glycosaminoglycans before and after decellularization of EBs. This novel approach provides a unique method to examine the composition of the ECM produced by cells undergoing morphogenesis and could have significant implications in the development of future regenerative medicine therapies to stimulate tissue repair.

Materials and Methods

Cell Culture

Mouse embryonic stem cells (D3) were cultured on 0.1% gelatin-coated 100 mm polystyrene cell culture dishes (Corning) with Dulbecco's modified eagle medium (Mediatech), supplemented with 15% fetal bovine serum (HyClone), 2 mM L-glutamine (Mediatech), 1x MEM non-essential amino acid solution (Mediatech), antibiotic/antimycotics (Mediatech), and 0.1 mM β-mercaptoethanol (MP Biomedicals, LLC). To maintain the cells in their undifferentiated state, 10^3 U/mL leukemia inhibitory factor (LIF) (ESGRO) was added to the culture media upon each re-feeding. Cells were passaged every two to three days before reaching ~70% confluence. For the described studies, cells were used between passages 20-30. To initiate embryoid body (EB) culture, ESCs were dislodged from the gelatin-coated dishes and dissociated with 0.05% Trypsin/0.53 mM EDTA (Mediatech). A density of 400,000 cells/mL was used to inoculate 10 mL EB cultures in 100 mm bacteriological grade polystyrene Petri dishes (Corning) using differentiation media (media without LIF). Cultures were placed on

rotary orbital shakers (Barnstead Lab-Line, Model 2314) at 40 rpm at 37°C in 5% CO_2 for the entire duration of suspension culture. Previous work from our lab has demonstrated that rotary orbital suspension culture methods result in greater yields of homogeneously-sized EBs [124]. EBs were cultured in suspension for up to 10 days and re-fed every other day by collecting the EBs via gravity sedimentation in 15 mL conical tubes. Old media was aspirated and the cultures were replenished with 10 mL of fresh differentiation media before being placed back in the Petri dishes and onto the rotary orbital shakers.

Decellularization

Embryoid bodies were harvested after 4, 7, or 10 days of differentiation in rotary orbital suspension culture. The number of EBs at the different time points was determined by performing a 10x dilution of one culture plate of EBs into 8 wells of a 24-well plate and counting the number of EBs with an inverted phase microscope (Nikon Eclipse TS100). Analysis performed on triplicate samples indicated an average of ~6200 EBs/100 mm plate (inoculated with $4x10^6$ cells initially). Unless otherwise specified, approximately 3000 EBs (~1/2 culture plate) were distributed into individual samples in 1.5 mL microcentrifuge tubes for decellularization assays (Figure 6.1). For mass retention analyses, each tube was weighed before addition of the experimental sample. Native EBs were rinsed in phosphate buffered saline (PBS) and stored at 4°C for subsequent mass, DNA, and total protein content analyses or kept in serum-free media for up to three hours at 37°C for cell viability measurements. Experimental samples were centrifuged at 18,000 × g (Microfuge® 18 Centrifuge, Beckman-Coulter) for two minutes

before addition of 1% Triton X-100 (VWR). Samples were rotated on a LabQuake Rotisserie for 30 minutes, spun down at 18,000 × g for two minutes, rinsed twice with PBS, and rotated in 1 mg/mL DNase (~2,000 Kunitz units/mg, Worthington Biochemical Corp.) for 15 minutes at room temperature. At the end of the Triton X-100/DNase treatments, samples were centrifuged for two minutes at 18,000 × g to obtain the final acellular product and rinsed twice in PBS prior to additional characterization studies. EBs were deemed "acellular" based upon significant reductions of cell viability (<1%) and DNA content, compared to equivalent numbers of native EBs.

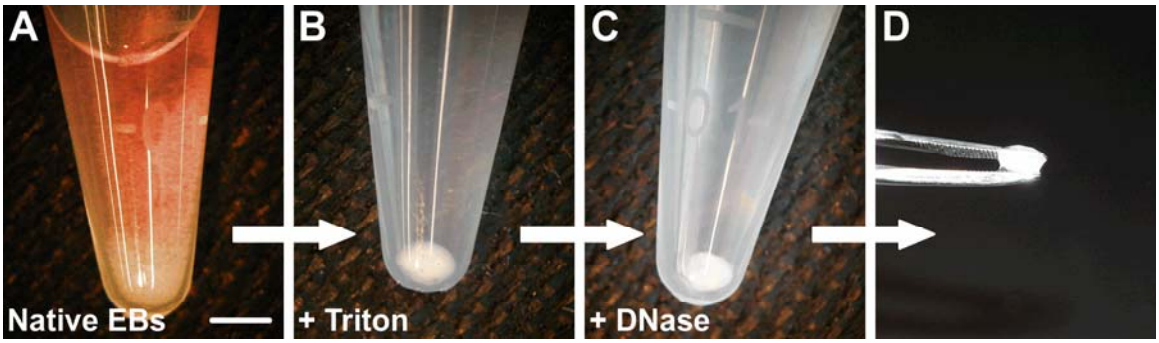

Figure 6.1. Decellularization protocol steps. (A) Equal numbers of native EBs were distributed into separate microcentrifuge tubes. Samples were then centrifuged (18,000 x g) and treated with (B) 1% Triton X-100 (30 minutes) followed by (C) treatment with 1 mg/mL DNase (15 minutes). The resulting viscous mass of consolidated EBs (D) could be easily held and manipulated with a pair of tweezers. Scale bar = 3 mm.

Immunostaining and Histology

Native or Triton/DNase-treated EBs were fixed in Methyl Carnoy's fixative (for collagen IV staining) or formalin (for all other staining) for 30 minutes, rinsed twice with PBS, and embedded in Histogel® (Richard-Allan Scientific). Samples were processed through a series of xylene and alcohol rinses and embedded in paraffin. Paraffin-embedded samples were sectioned into 5 μm slices, placed onto glass slides and de-paraffinized prior to staining. Samples to be analyzed for histology and nuclei content were either stained with hematoxylin and eosin (H&E) using a Leica Autostainer XL, or incubated in Hoechst fluorescent dye (10 μg/mL) for five minutes to stain for nuclei. For immunofluorescent staining, sections were permeabilized and blocked for 45 minutes using 0.05% Triton X-100 and 2% goat serum. Samples were incubated with collagen IV, laminin, or fibronectin primary antibodies (polyclonal rabbit) overnight at 4°C (1:80 dilution), rinsed with PBS, and then incubated with FITC-conjugated goat anti-rabbit secondary antibody (1:100 dilution) before counterstaining using Hoechst. For immunohistochemistry analysis of hyaluronan, endogenous peroxidase activity of EB sections was quenched using hydrogen peroxide (0.75% in 100% methanol) after de-paraffinization and before staining. IHC samples were incubated in 1% bovine serum albumin for 30 minutes before addition of the hyaluronan binding protein (2-4 μg/mL PBS/0.1% BSA, overnight, 4°C). The Vector Elite ABC kit (Vector Labs) was used for color staining development prior to counterstaining in hematoxylin. All samples were mounted with coverslips using either low viscosity mounting medium (H&E and IHC samples, Cytoseal™ 60, Richard-Allan Scientific) or aqueous mounting medium with anti-fading agents (fluorescent samples, Gel/Mount™, Biomeda Corp.) and imaged using

a Nikon 80i Upright Microscope and a Spot Flex camera (Diagnostic Instruments, Inc.). Sections stained with Hoechst dye were then analyzed quantitatively for intact nuclei by counting punctate fluorescent cells in three fields from at least three sections in triplicate samples. The cross-sectional area of the EBs or acellular samples being counted was quantified using NIH ImageJ software in order to compute the number of cells per unit area.

Cell Viability

Native and Triton/DNase-treated EBs were incubated in a 10% alamarBlue (Biosource) solution in serum-free media for four hours at 37°C with 5% CO_2 to assess cell viability. A 100 μL sample of each of the sample-conditioned alamarBlue solutions was individually added to a 96 well plate, and fluorescent measurement values were taken (ex: 545 nm, em: 590 nm) using a SpectraMax M2e plate reader. The Triton/DNase-treated samples' fluorescent values were reported as the relative percent reduction of alamarBlue normalized to the native EB values (assumed to be 100% relative viability) from within the same experimental batch.

Mass Retention

The mass of the EB samples before and after decellularization treatment was determined from dry weight measurements of the different samples. Native and Triton/DNase-treated EBs were rinsed twice in distilled water and stored overnight at -80°C prior to lyophilization. Samples were then freeze-dried for 24 hours using a lyophilizer (Freezone® 4.5, Labconco), and the final mass of the dry samples was taken

(AX205 DeltaRange®, Mettler Toledo). The mass of each of the empty tubes was recorded prior to lyophilization and subtracted from the final mass of each sample to obtain an accurate measure of the net sample weight.

DNA Quantification

DNA content of native EBs and Triton/DNase samples was quantified using the Quant-iT™ PicoGreen® dsDNA Assay kit (Molecular Probes). Samples were completely solubilized in a 6M guanidine hydrochloride (GuHCl) solution for two hours in a sonicating water bath and added to 20x TE buffer (200mM Tris-HCl, 20mM EDTA, pH=7.5) and PicoGreen dye solutions at a ratio of 43 µL sample : 107 µL buffer : 150 µL dye. Fluorescent intensity values of experimental samples were acquired using a SpectraMax M2e plate reader (ex: 485 nm, em: 528 nm), and the absolute DNA concentrations were determined by comparing experimental values to standard curve readings obtained using a range of calf thymus DNA solutions (30 – 5000 ng/mL).

Protein Quantification

Native EBs and Triton/DNase EBs were solubilized with 6M GuHCl (as described above), and total protein content was quantified using the bicinchoninic acid (BCA) assay kit (Pierce). A standard titration curve using bovine serum albumin (BSA) was generated for concentrations ranging from 20 – 2000 µg/mL. Samples (25 µL) were incubated in the BCA solution (200 µL) for 30 minutes at 37°C, and absorbance readings were taken at 562 nm on a SpectraMax M2e plate reader. The reported protein

concentrations of the experimental samples were obtained from the BSA titration standard curve.

Scanning Electron Microscopy

Native and Triton/DNase-treated EBs were fixed in gluteraldehye (2.5% in 0.2M cacodylate buffer) and post-fixed in 1% osmium tetroxide (Electron Microscopy Sciences). Samples were rinsed three times in 0.2M cacodylate buffer and transferred into acetone immediately prior to drying using a critical point dryer (E3000 series, Quorum Technologies). Native and acellular EBs were impregnated for one hour with liquid CO_2 and passed through the CO_2 critical point (31.5^{o}C, 1100 psi). Each sample was gold sputter coated for 90 seconds in a Polaron Sputter Coater SC 7640 (Quorum Technologies) and examined using the Hitachi S800 Field Emission Gun Scanning Electron Microscope and iXRF EDS2004 image acquisition software.

Statistics

For paired comparisons, student t-tests assuming unequal variances were used to determine statistical significance ($p<0.05$). For comparisons across multiple groups, analysis of variance was performed followed by post-hoc Tukey analysis to determine significant ($p<0.05$) differences between the different experimental groups.

Results

Decellularization Steps

EBs were equally distributed among different microcentrifuge tubes (Figure 6.1A) prior to decellularization using the previously optimized combination of Triton X-100 and DNase treatment [215]. After high speed (18,000 x g) centrifugation and 1% Triton X-100 treatment for 30 minutes, the original population of individual EBs agglomerated into a compacted mass of tissue (Figure 6.1B). Subsequent treatment with 1 mg/mL DNase for 15 minutes yielded a pellet of consolidated EBs of comparable size (Figure 6.1C). The resulting acellular product of Triton/DNase-treated EBs was able to be easily handled and manipulated with tweezers prior to further analyses (Figure 6.1D).

Histological Assessment

Native EBs adopted a more differentiated morphological phenotype over the course of differentiation (Figure 6.2, top row), as expected. EBs from days 4 and 7 were comprised of cells that were more densely packed than those from day 10 of differentiation, but localized regions of more differentiated cells began to appear at about day 7 of differentiation (note black rectangles outlining such areas in Figure 6.2). At each of the time points examined, the individual EBs were relatively homogeneous in size and shape as a result of the rotary orbital suspension culture method [124] (Figure 6.2, top row insets). In contrast, Triton/DNase-treated EBs at each of the time points consistently showed a lack of distinct cell nuclei and formed a continuous mass of acellular tissue with a dissimilar appearance to that of individual native EBs. The

macroscopic shape of the acellular matrix (Figure 6.2, bottom row insets) was dictated by the shape of the microcentrifuge vessel in which the EBs were decellularized and compacted, which suggested that the inherent pliability of the acellular matrix enables it to be potentially manipulated into various geometric configurations.

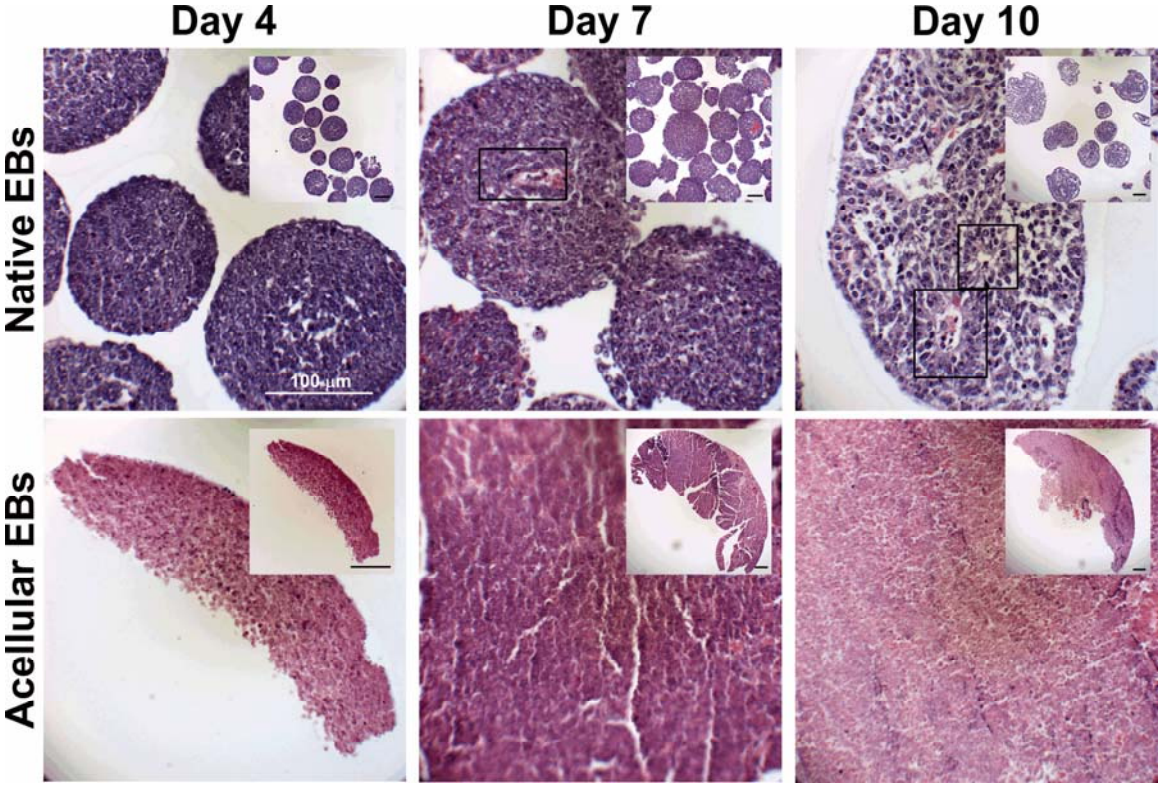

Figure 6.2. Histological analysis. Native and Triton/DNase-treated EBs from days 4, 7, and 10 of differentiation were stained with hematoxylin and eosin. Pockets of differentiated cells were present in untreated (native) EBs by day 7 (black rectangular outlines). Individual EBs agglomerated with decellularization treatment, and little evidence of intact nuclei was observed. Insets show a broader view of the samples; image and inset scale bars = 100 μm.

As noted in the hematoxylin and eosin stained sections, native EBs stained with Hoechst dye exhibited slightly greater nuclei density at days 4 and 7 of differentiation than at 10 days of differentiation (Figure 6.3A). For Triton/DNase-treated EBs, all remnants of Hoechst fluorescent signal were included in nuclei quantification (Figure 6.3B), although most spots in acellular samples were much smaller than native intact cell nuclei. Nuclei content was significantly decreased in all acellular EB samples (Figure 6.3B, $p < 1E-24$), with only some diffuse fluorescence observed in EBs decellularized at day 10 of differentiation culture. Quantitative analysis indicated that the decellularization treatment removed approximately 95% of the total nuclei content in day 4 samples, 97% in day 7, and 99% in day 10.

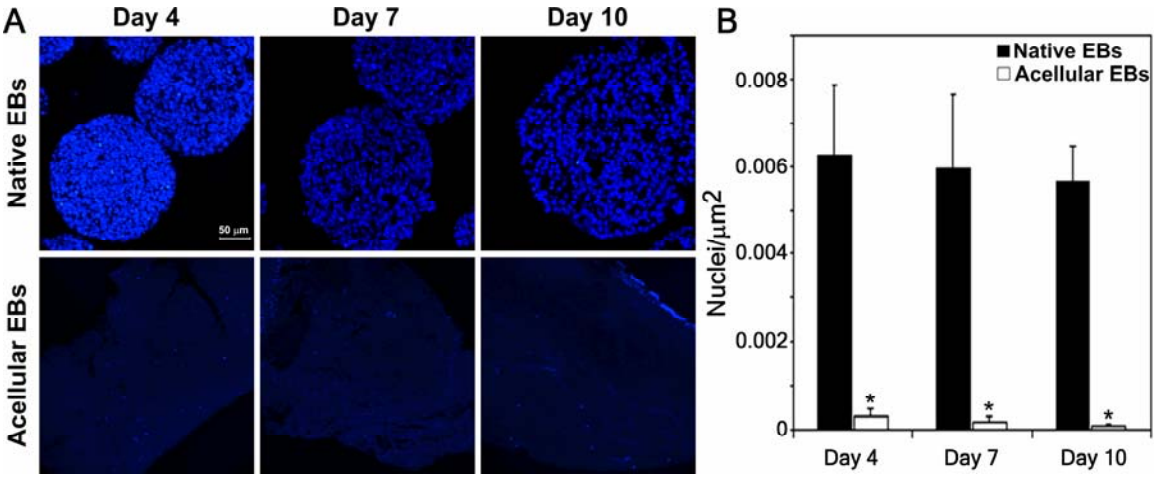

Figure 6.3. Quantification of cell nuclei. Native and acellular EBs from days 4, 7, and 10 of differentiation were stained with Hoechst (A) for nuclei quantification (B). Hoechst staining was negligible in acellular EBs, with only some diffuse staining observed at day 10. Quantification of punctate nuclei was performed on triplicate sections per experimental sample (n=3) and a minimum of three fields of view per section. The number of intact cell nuclei was significantly reduced for each of the acellular samples examined at different time points of differentiation (*p<1E-24).

Quantitative Multi-Parametric Analysis

A multi-parametric approach was used to quantify the extent of decellularization as a function of time, based on cell viability and DNA content, as well as the final amount of material retained. Cell viability was completely inhibited (>99%) in all treatment groups, suggesting efficient decellularization at all of the time points examined (Figure 6.4A). The mass of native EBs increased significantly with differentiation ($p = 0.002$), along with a mass increase of the corresponding acellular matrix from the same time points (Figure 6.4B). The lyophilized mass of the acellular samples indicated that a sizable portion of the original EB mass was retained after the cellular extraction process after 4 (17±3%), 7 (22±5%), and 10 days of differentiation (31±12%) (Figure 6.4B). DNA content of native EBs increased slightly, but not significantly ($p = 0.055$), over the course of differentiation, while protein content increased significantly ($p = 0.001$) between days 4 and 10 of differentiation. DNA content was significantly reduced by decellularization at each time point (69-75% removed; $p \leq 0.002$; Figure 6.4C). Despite some loss presumably due to extracted cellular protein elements, a fraction (15-25%) of the original protein content was retained in each of the Triton/DNase-treated EB samples (Figure 6.4D). The summation of the results from the quantitative assays demonstrated that populations of EBs at different stages of differentiation can be effectively decellularized by solvent extraction methods to yield proteinaceous matrices.

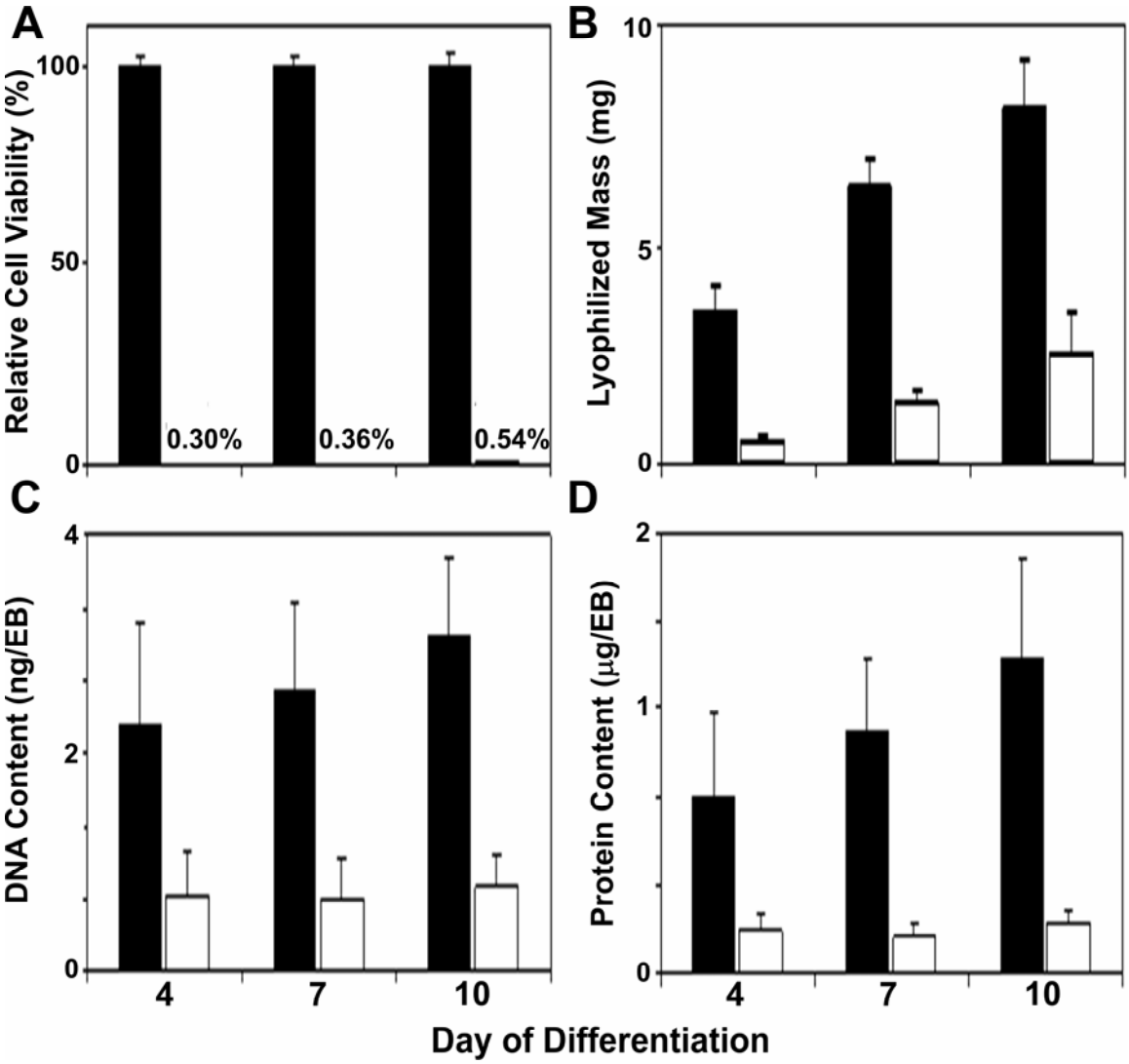

Figure 6.4. Multi-parametric characterization. Native EBs and decellularized samples from days 4, 7, and 10 of differentiation were analyzed for cell viability (A), mass retention (B), DNA content (C), and protein content (D). Cell viability was inhibited (>99%) in all treated samples. As expected, lyophilized mass, DNA and protein content gradually increased with time in the native EBs. While mass of the acellular sample increased along with the native EBs, DNA and protein content maintained similar values during the course of differentiation. (black bars = native EBs, white bars = acellular EB-derived matrix)

Ultrastructure Analysis

Scanning electron microscopy (SEM) was performed to elucidate differences between the ultrastructure of native EBs and acellular EB-derived matrices at a range of magnifications (Figure 6.5). At low magnification, distinct, individual EBs were clearly observed (Figure 6.5A), whereas the acellular EBs formed a larger cohesive material with a relatively smooth exterior appearance (Figure 6.5D). Higher magnification views clearly indicated that tightly aggregated cells comprised the individual native EBs (Figure 6.5B,C), while the cross-sectional morphology of the acellular EBs lacked distinct cells (Figure 6.5E,F). EBs and acellular samples from days 4 and 10 of differentiation were also analyzed by SEM (data not shown) and exhibited comparable morphological attributes to day 7 differentiated samples.

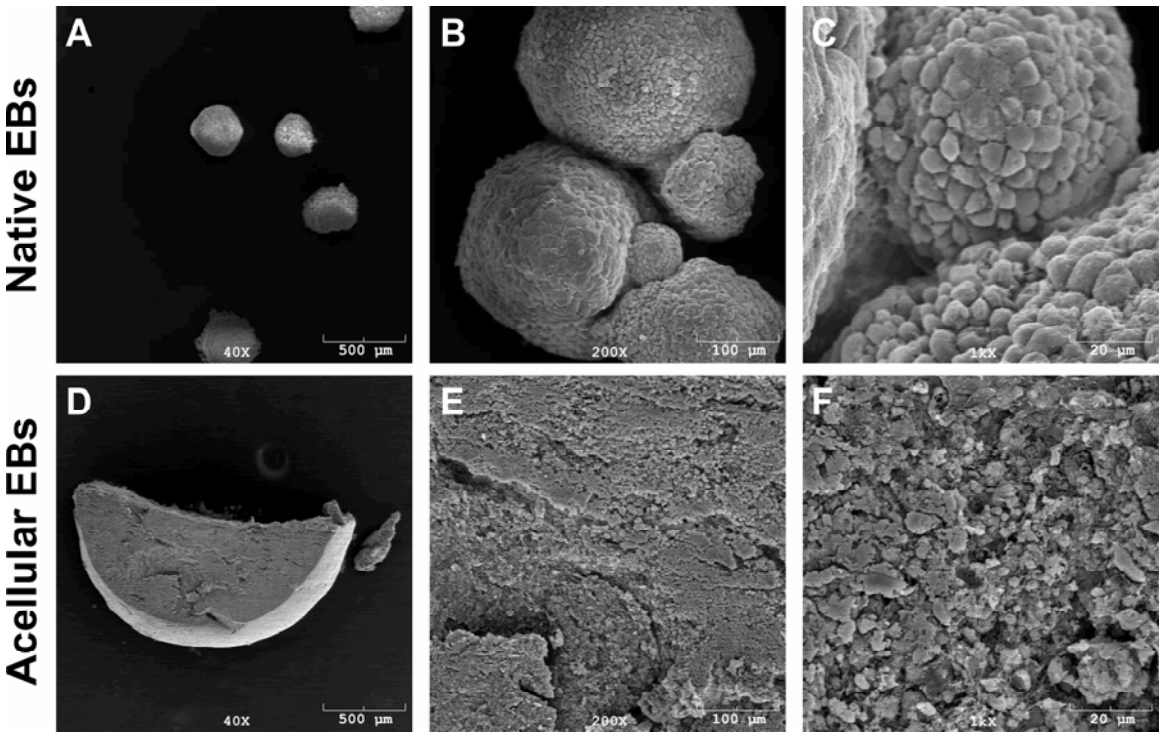

Figure 6.5. Ultrastructure analysis. Scanning electron micrographs (SEM) display ultrastructural details of the surfaces of day 7 native EBs and cross-sections of the acellular material at magnifications of 40x (A), 200x (B), and 1000x (C). Individual cells were clearly seen in magnified untreated EBs, while distinct cells were not visible in the acellular EBs.

ECM Component Retention

In order to confirm the presence and retention of extracellular matrix components synthesized within EBs, immunostaining analysis of EBs and acellular EB-derived matrices was performed for samples collected after 4, 7 and 10 days of differentiation. Although the spatial distribution of different ECM components varied over time with differentiation of the native EBs (Hiatt, Shukla, *et al.*, unpublished observations), acellular matrices derived from EBs retained ECM molecules that were present at each of the time points examined (Figure 6.6 – day 7; days 4 & 10, data not shown). For example, ECM molecules such as collagen IV, laminin, fibronectin, and hyaluronan were all expressed within native EBs differentiated for 7 days and were retained following decellularization (Figure 6.6). In general, positive immunostaining of ECM molecules appeared more diffuse throughout native EBs, whereas the intensity of immunostaining seemed more concentrated in particular regions of the acellular EB-derived matrices.

Scalability

The scalable production of acellular matrices derived from EBs was assessed as a function of the input number of EBs used for decellularization (Figure 6.7). As expected, an increase in the final mass and total protein content was achieved by increasing the initial numbers of EBs. The increasing amounts of acellular EB-derived matrix linearly correlated with the input number of EBs for both overall mass (r^2 = 0.982) and total protein content (r^2 = 0.993). This evidence strongly suggested that the quantity of acellular matrix material derived from EBs can be simply controlled by the initial batch size of EBs.

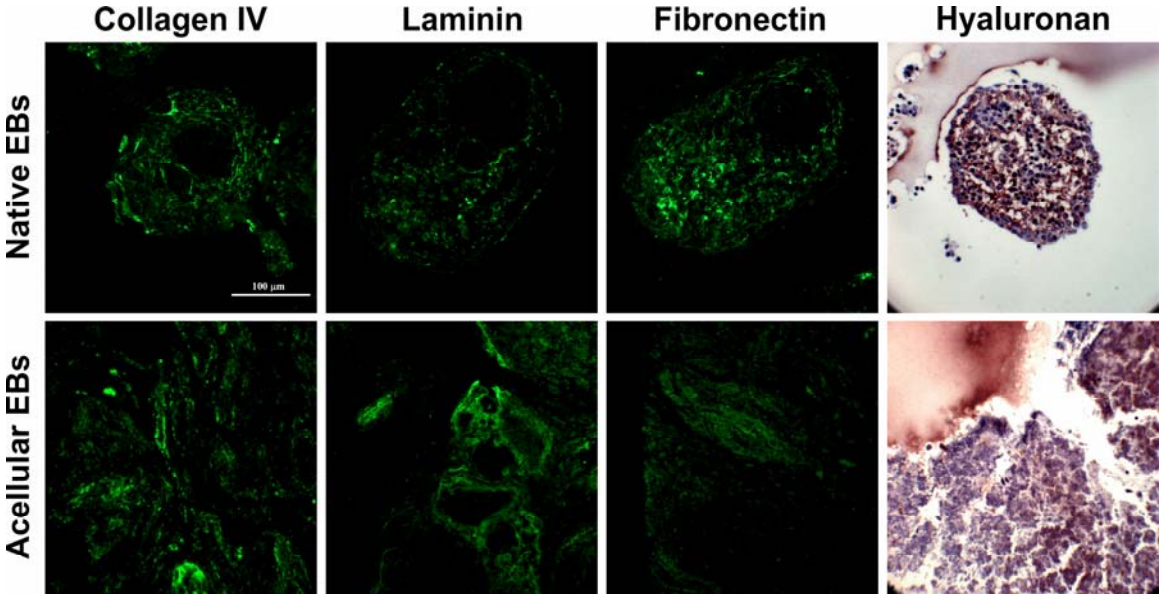

Figure 6.6. ECM molecule immunostaining. Immunostaining for collagen IV, laminin, fibronectin, and hyaluronan was performed in day 7 native and acellular EBs. Each of the ECM components was present in the native EBs as well as the acellular matrix, indicating that the solvent extraction process does not completely remove ECM components from the final acellular matrix product. All images are shown at the same magnification (scale bar = 100 μm).

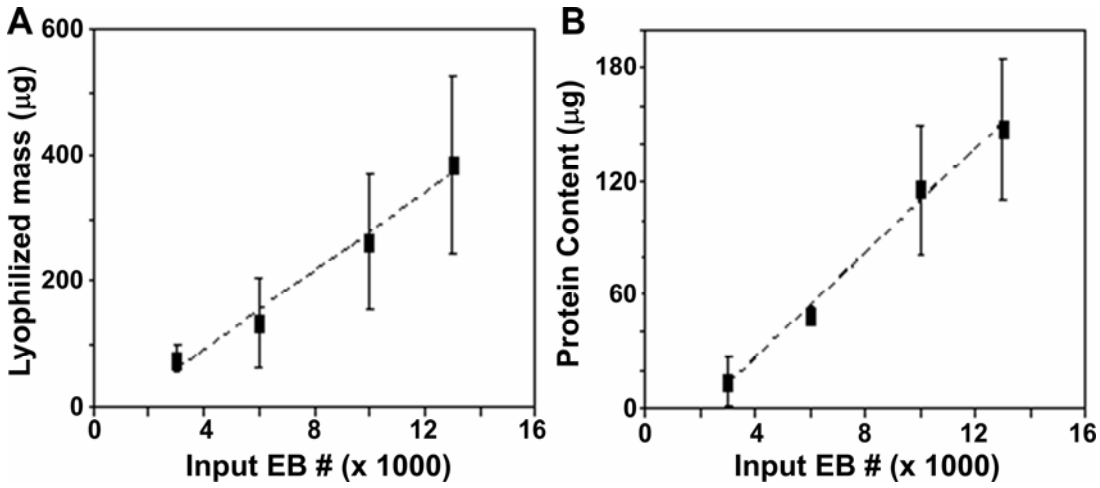

Figure 6.7. Protein and mass scale-up. Lyophilized dry mass (A) and total protein content (B) were analyzed for increasing initial numbers of EBs. The input number of EBs ranged from 3000±640 to 13,006±2800, which corresponded to a mass range of 77±21 to 383±142 μg and a protein range of 14±13 to 148±37 μg. Both parameters scaled linearly with starting EB number, suggesting that derivation of acellular matrices from EBs is amenable to scalable batch processes.

Discussion

These studies indicate that it is possible to successfully decellularize embryoid bodies in a scalable manner at different points of differentiation to yield ESC-derived extracellular matrices. The combination of Triton X-100 and DNase treatment efficiently inhibited cell viability, reduced DNA content, and retained a substantial portion of the initial EB mass and corresponding protein content. Histological and ultrastructural analysis clearly indicated a lack of cellularity within acellular matrices compared to native EBs, and immunostaining results confirmed the retention of extracellular matrix components, such as collagen IV, laminin, fibronectin, and hyaluronan in the EB-derived acellular matrices.

Effective removal of cellular elements was used as the primary criterion to deem EBs "acellular" at the different stages of differentiation. The cell nuclei content of acellular EB-derived matrices (Figures 6.2, 6.3) was comparable to levels previously reported in other acellular tissues [72-75, 91, 188, 216, 217]. The ultrastructure of different acellular tissues often varies drastically depending on the original tissue source and acellular processing methods; some treatments largely preserve the original matrix architecture, while others disrupt native ECM structure [74, 75, 188, 217, 218]. Acellular EB matrices (Figure 6.5) exhibited a vastly different morphology that appeared devoid of cells compared to native EBs, which were comprised of tightly clustered intact individual cells. Complete inhibition of cell viability (>99%) indicated successful decellularization at each of the time points of differentiation examined (Figure 6.4). This metric is commonly used as the minimal decellularization criteria based on current industrial standards. Although the final mass of the acellular matrices increased with

differentiation time, the residual amounts of DNA and protein content in EB-derived acellular matrices remained relatively constant, despite the fact that both parameters increased with time in the native EBs. This trend potentially suggests that acellular matrices from more differentiated EBs may contain an increasing amount of non-protein content, such as glycosaminoglycans (GAGs), while at the same time retaining a small portion of cellular DNA.

A number of different ECM proteins and GAGs present in native EBs at various stages of differentiation were also found in the acellular matrices derived from EBs at the same time points (Figure 6.6). Although the design of the present study only examined a select few ECM molecules commonly synthesized by cells and found in many acellular tissue products, the results indicated that ESCs within EBs are capable of producing ECM that can be retained following decellularization. The relative abundance and spatial distribution of adhesive extracellular matrix proteins, like collagen IV, laminin, and fibronectin, varied as a function of time in the native EBs, and the relative amounts and distribution in the final acellular matrices varied similarly. The production of specific ECM components temporally varies throughout the stages of embryonic development [145-147, 219, 220], and ESCs mimic this phenomenon by dynamically regulating ECM composition during the course of EB differentiation. Therefore, the composition of the acellular matrix may be controlled by varying the stage of differentiation at which EBs are decellularized (Figure 6.8), resulting in a novel method of examining matrix production by cells at varying states of maturation. In addition to adhesive ECM proteins, hyaluronan, a non-sulfated GAG, was present in native EBs and acellular EB-derived matrices. Sulfated GAG content was assayed quantitatively (Wieslab^{TM} sGAG

quantitative kit, Alpco Diagnostics™) and qualitatively (toluidine blue staining), but appeared to be minimally present in native EBs and acellular EB-derived matrices (data not shown). Although sulfated GAGs are commonly present during embryogenesis, hyaluronan has been particularly noted to exert a significant influence on cell morphogenesis during development [145, 221, 222], potentially accounting for its relative abundance in differentiating EB microenvironments relative to sulfated GAGs. This preliminary assessment of ECM molecules indicates the preservation of naturally synthesized molecules after decellularization of EBs, suggesting that this novel approach could be used to separate extracellular matrices from embryonic cells undergoing differentiation in order to study ECM composition and bioactivity.

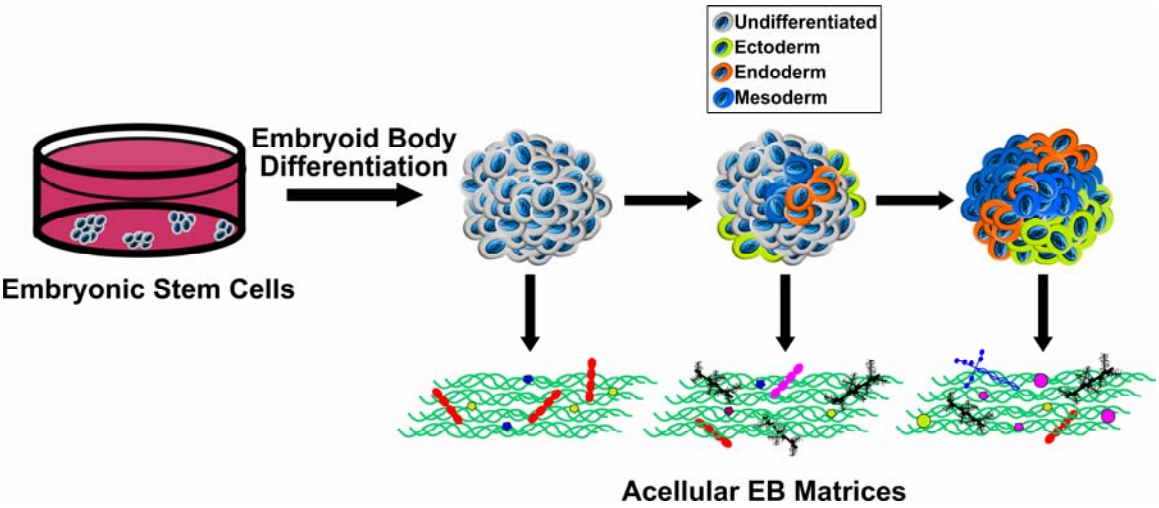

Figure 6.8. Acellular EB matrix modulation. Embryonic stem cells can be induced to differentiate via EB formation. As time progresses over the course of EB differentiation, increasing numbers of cells within the three-dimensional aggregates differentiate into cells of the endoderm, ectoderm, and mesoderm lineages. Decellularizing the EBs at different time points along their differentiation pathway allows for modulation of the acellular matrix, with its composition reflecting the ECM components present in the EB at the time of decellularization.

Despite the fact that individual EBs constitute very small amounts of neo-tissue formation, the summation of larger numbers of EBs could be used to generate larger quantities of acellular matrices. Numerous groups are developing methods to significantly scale-up the production of ESCs and EBs using a variety of different bioreactor systems [223-225]. Since the results of the present study indicate that acellular matrix production is related to the number of EBs (Figure 6.7), increasing the initial number of EBs using bioreactors could serve as a simple means to increase the amounts of acellular EB-derived matrices by orders of magnitude. In addition, the "potency" of EB-derived acellular matrices is likely a more important outcome measure than the actual quantity of material (in terms of mass) that can necessarily be produced. Although the "potency" of acellular EB matrices remains to be determined, it is possible that complex combinations of biomolecules present in the acellular matrix at relatively low independent concentrations could elicit pronounced synergistic biological effects.

Decellularization of EBs serves as a direct route to obtain ECM from embryonic stem cells actively undergoing differentiation and implies that acellular matrices derived from EBs may hold several distinct advantages over those derived from somatic tissue sources. One unique benefit of a matrix isolated from a pluripotent embryonic stem cell source is the potential to alter the final ECM composition by modulating cellular maturation (as discussed above) or by directing differentiation of the cells towards a particular phenotype. The molecular composition of acellular matrices derived from EBs may be tailored towards more specific types of tissues by directing the differentiation of the initial EB population prior to decellularization procedures. Various microenvironmental factors are capable of regulating the differentiation of ESCs into

different cell phenotypes by enhancing lineage-specific cell signaling pathways [40, 62], implying that the presence of particular ECM elements in the EB microenvironment likely change with ESC differentiation. Although current schemes of directed differentiation do not result in completely homogeneous populations, it is entirely possible that improved strategies for directed differentiation could be easily implemented prior to decellularization of EBs. Thus, decellularization of EBs subjected to directed differentiation protocols could theoretically yield acellular matrices composed of biomolecules associated primarily with a specific type of tissue.

The application of stem cells to treat a variety of different injuries and diseases is a central tenet of regenerative medicine therapies; however, the mechanisms whereby stem cells elicit structural and functional improvements in tissue regeneration remain largely unknown. In addition to direct cell replacement via differentiation, stem cell-derived molecules may stimulate endogenous host processes leading to functional tissue restoration. In an initial attempt to examine the composition and bioactivity of biomolecules derived from ESCs undergoing differentiation, we have established methods to decellularize EB microenvironments in order to separate the cells from the ECM they synthesize. If in fact, ECM derived from differentiating ESCs harbors morphogenic factors, acellular matrices derived from EBs could represent a novel manner of extracting molecular elements of embryonic morphogenic environments and could lead to the development of new acellular strategies to stimulate functional tissue regeneration in adult mammalian organisms.

CHAPTER 7

EMBRYONIC STEM CELL-DERIVED MATRICES IMPROVE DERMAL WOUND HEALING IN MICE

Introduction

Investigations into improved regenerative therapies for adult wounds have led to an increasing emphasis on understanding the mechanisms behind regeneration occurring in the embryonic environment. For example, it is well-documented that early gestational dermal wounds can regenerate completely, while adults wounds heal imperfectly, resulting in a visible scar and decreased tensile strength of the healed skin [97, 226, 227]. Researchers are therefore seeking to apply insights from embryonic regeneration mechanisms to improve or develop novel treatments for adult wounds. Studies investigating distinctions between embryonic and adult wound healing environments have highlighted significant differences relating to matrix composition within the wound [100, 228], potentially leading to altered signaling from the endogenous cells. To investigate mechanisms of wound repair, researchers have long used rodent models in which the healing process after full-thickness dermal wounding is analyzed using a variety of quantitative and qualitative metrics [96, 229] that can evaluate the effect of the treatment on wound healing when compared to control groups. In particular, higher rates of wound closure and re-epithelialization as well as increased concentrations of blood vessels, specifically those that extravasate towards the epithelial layer, are commonly associated with improved healing [230].

Embryonic stem cells (ESCs) are derived from the inner cell mass of the pre-implantation blastocyst [1], and their differentiated counterparts may provide an ideal cell source for investigating embryonic mechanisms of wound healing. ESCs can differentiate *in vitro* through the aggregation of cells into three-dimensional aggregates termed embryoid bodies (EBs). EBs recapitulate aspects of early embryonic development, including the dynamic synthesis and remodeling of matrix molecules present in the embryo during early stages of morphogenesis, as discussed previously (Chapters 3, 4). In particular, array data from chapter 3 and more specific analyses presented in chapter 4 demonstrate that EBs are actively synthesizing molecules that have been shown to positively influence wound healing, including hyaluronan [231], transforming growth factor (Tgf)-β3 [232], and vascular endothelial growth factor (Vegf) [233]. The methods developed for isolating the matrix synthesized by differentiating ESCs (Chapters 5, 6) allows for investigations to determine whether an embryonic-derived matrix can improve adult wound healing.

Therefore, in order to examine the effect of ESC-derived ECM on wound healing, acellular EBs were investigated in an acute dermal wound healing model and were compared to fibrin, a commonly used material in dermal injury surgeries. C57Bl/6 mice were subjected to bilateral full thickness 6-mm wounds. Each wound was treated with the ESC-derived matrix alone, matrix along with fibrin that was used as a delivery vehicle (referred to as "matrix-fibrin"), fibrin alone, or the wounds were left untreated. Wounds treated with matrix, either alone or with fibrin, significantly impacted wound closure and blood vessel extravasation towards the epithelial layer. Application of an embryonic-derived matrix to an adult wound can positively affect wound healing,

suggesting that ESCs and their endogenous matrix are critical for improved adult therapies.

Materials and Methods

Cell Culture

Mouse embryonic stem cells (D3) were cultured on 0.1% gelatin-coated 100 mm polystyrene cell culture dishes (Corning) with Dulbecco's modified eagle medium (Mediatech), supplemented with 15% fetal bovine serum (HyClone), 2 mM L-glutamine (Mediatech), 1x MEM non-essential amino acid solution (Mediatech), antibiotic/antimycotics (Mediatech), and 0.1 mM β-mercaptoethanol (MP Biomedicals, LLC). To maintain the cells in their undifferentiated state, 10^3 U/mL leukemia inhibitory factor (LIF) (ESGRO) was added to the culture media upon each re-feeding. Cells were passaged every two to three days before reaching ~70% confluence. For the described studies, cells were used at passage 26. To initiate embryoid body (EB) culture, ESCs were dissociated from the gelatin-coated dishes with 0.05% Trypsin/0.53 mM EDTA (Mediatech). A density of 400,000 cells/mL was used to inoculate 10 mL EB cultures in 100 mm bacteriological grade polystyrene Petri dishes (Corning) using differentiation media (media without LIF). Cultures were placed on rotary orbital shakers (Barnstead Lab-Line, Model 2314) at 40 rpm at 37°C in 5% CO_2 for the entire duration of suspension culture. EBs were cultured in suspension for 10 days and re-fed every other day by collecting EBs via gravity sedimentation in 15 mL conical tubes. Spent media was aspirated and the cultures were replenished with 10 mL of fresh differentiation media before being placed back in the Petri dishes and onto the rotary orbital shakers.

Decellularization

Embryoid bodies were harvested after 10 days of differentiation in rotary orbital suspension culture, and ~5000 EBs were distributed into individual samples in 1.5 mL microcentrifuge tubes. EBs were centrifuged at 18,000 × g (Microfuge® 18 Centrifuge, Beckman-Coulter) for two minutes before addition of 1% Triton X-100 (VWR) under a cell culture hood. Samples were rotated on a LabQuake Rotisserie for 30 minutes, spun down at 18,000 × g for two minutes, rinsed twice with sterile PBS, and rotated in 1 mg/mL DNase (~2,000 Kunitz units/mg, Worthington Biochemical Corp.) for 15 minutes at room temperature. At the end of the Triton X-100/DNase treatments, samples were centrifuged for two minutes at 18,000 × g to obtain the final acellular product and rinsed twice in sterile PBS. To verify that the matrices were decellularized with some retention of total protein, native and acellular EBs were evaluated for total mass, protein content, and DNA. Consistent with previous studies, acellular EBs retained 20.3 ± 2% of the native EB mass and 36.1 ± 4% of the total protein while exhibiting 97.0 ± 0.4% DNA removal compared to untreated EBs.

Dermal Wound Surgeries

Male mice (C57Bl/6, ~10 weeks old; Charles River Laboratories) were used for these studies according to the protocol approved by the Institutional Animal Care and Use Committee (IACUC; approval date July 22, 2009). Mice were briefly anesthetized with isoflurane (5% isoflurane and 1.0 LPM CO_2) prior to intraperitoneal injection of an anesthesia cocktail containing ketamine (50 mg/kg), xylazine (5 mg/kg), and acepromazine (2 mg/kg). A square measuring ~2 cm x 2 cm on the upper back of each

mouse (extending from the base of the skull to approximately the mid-spine) was shaved and then treated with Veet for complete hair removal. The exposed skin was disinfected with three alternate treatments of 2% chlorhexidine (Dermachlor™, Butler Animal Health Supply) and alcohol (70% isopropanol, The Butler Company) prior to actual wounding. With the mouse positioned on its side, the skin was pinched together at the dorsal midline using sterile tweezers and pulled ~1-1.5 cm away from the torso. A 6 mm dermal biopsy punch was then used to create bilateral full thickness dorsal wounds simultaneously. The center of each wound was approximately 1.5 cm from the base of the skull and 0.5 cm on either side of the dorsal midline to prevent the mouse from physically perturbing the wound with their hind legs post-operatively. Wounds were treated with matrices derived from ~$1x10^4$ day 10 decellularized EBs (lyophilized dry weight ~0.32 mg, ~36 μg protein/sample); matrices were applied to wounds alone (n = 8 for each time point) or using fibrin gel yielded by 15 μL of a 75 mg/mL fibrinogen (from bovine plasma, Sigma) and 15 μL of a 25 U/mL thrombin (from bovine plasma, Sigma)) as a delivery vehicle (n = 7 for each time point). Power analysis ($\alpha = 0.05$, $\beta = 0.2$) using preliminary wound closure data determined that a minimum sample size of six animals/group would be sufficient to obtain statistically significant results. However, additional mice were included in each group due to the frequency at which mice perturbed their wounds and compromised the wound site. For matrix-fibrin treatments, the acellular matrices were placed on the wounds immediately prior to the application of fibrinogen and thrombin solutions to fill the remaining wound bed volume. Treated wounds were compared to wounds applied with fibrin alone (n = 7) or those left untreated (n = 8). Treatments were randomly assigned to each wound.

Wound Closure Analysis

Wounds were measured daily for two weeks post-injury. Mice were briefly anesthetized (5% isoflurane and 1.0 LPM CO_2) in order to take images. Pictures were taken using a Sony Cyber-shot camera placed approximately six inches above the mice so that the entire mouse could be imaged. In each image, a circular piece of paper with a reference diameter of 6 mm was placed near the wounds on the back of the mouse. NIH ImageJ was used to quantify the wound area, using the reference length as a scale for each image to obtain the pixels/mm ratio. Each wound was traced with a freehand selections tool and the area quantified. Percent wound closure was calculated as [(area of original wound – area of actual wound)/area of original wound] x 100.

Histology

Mice were euthanized at either 7 or 14 days post-injury according to IACUC approved protocols. Mice were individually placed in a chamber, which was subsequently filled with CO_2. After successful euthanasia was verified, wounds were excised for histological analyses. The skin from the area of the back that had initially been shaved prior to injury was removed, and 10 mm biopsy punches (Acu Punch) were used to specifically excise the wound and surrounding normal tissue. Each biopsy was then sliced in the middle of the wound; one half was fixed in 10% formalin overnight for paraffin embedding, and the other half was soaked overnight in 30% sucrose solution at 4^{o}C for cryo analysis. Formalin-fixed samples were rinsed in PBS and processed for histological sectioning through a series of xylene and alcohol rinses. Wounds were then embedded (wound side down) in paraffin and sectioned at 5 μm. Samples that were

soaked in 30% sucrose were embedded the following day in O.C.T. compound (Tissue Tek) and stored at -80°C until being sectioned at 8 μm each. Formalin-fixed paraffin-embedded samples were stained with hematoxylin and eosin (H&E) using a Leica AutoStainer XL and with Masson's Trichrome. For Masson's staining, slides were incubated in Bouin's solution for 1 hour at 56°C after de-paraffinization and hydration to distilled water. After the samples were cooled to room temperature, they were incubated in Weigert's hematoxylin (2 minutes), Biebrich's scarlet-acid fuchsin (5 minutes), phosphomolybdic-phosphotungstic acid (1 minute), aniline blue (5 minutes), and 1% acetic acid (5 minutes), with intermittent water rinses. Slides were then dehydrated in 95% and 100% alcohol, cleared in xylene, and cover-slipped using Cytoseal™ mounting medium (Richard Allen Scientific).

Immunostaining

For immunofluorescent staining, slides obtained from cryo-sectioning were warmed to room temperature and fixed in acetone (10 minutes, -20°C). Samples were rinsed three times in PBS, then blocked and permeabilized for 45 minutes at room temperature in 2% normal donkey serum (NDS-PBS) in 0.05% Triton X-100-PBS. After three PBS rinses, slides were incubated with polyclonal goat anti-PECAM-1 primary antibody (1:200 in 2% NDS-PBS) overnight at 4°C. Samples were rinsed three times in PBS and incubated with donkey anti-goat Alexa Fluor 488 (1:200 in 2% NDS-PBS) for one hour at room temperature prior to Hoechst (10 μg/mL) counterstaining. Samples were then mounted with coverslips using aqueous mounting medium with anti-fading agents (Electron Microscopy Sciences).

Blood Vessel Quantification

Blood vessels from day 7 and day 14 samples were identified by positive PECAM-1 immunostaining. Individual sections from each sample were imaged ($n \geq 5$ for each group) using a 40x objective. The number of images examined was dependent on the total number of independent fields needed to capture the entire wound bed (2-7 fields, depending on the size of the wound bed). Total area of blood vessels and total number of blood vessels were quantified per area. Each blood vessel was traced with a freehand tool on NIH ImageJ imaging software, and the image scale bar was used to determine pixels/mm so that area of the outlined region could be measured. Total area of the wound was measured by tracing the region between the normal tissue flanking the lateral borders and above the underlying panniculus carnosus muscle layer. Blood vessels that extravasated towards the epithelial layer were also quantified using ImageJ. Prior to analysis of blood vessel extravasation, each image was oriented such that the epithelial layer was positioned horizontally (zero degrees) at the top of the field of view. The angle of each blood vessel relative to the epithelial layer was calculated in ImageJ by tracing a straight line through the center of the vessel, and the number of those with a direction of at least 45^{o} relative to the horizontal axis was quantified per area.

Statistics

For comparisons across multiple groups, analysis of variance (ANOVA) was performed using a 95% confidence interval followed by post-hoc Tukey analysis to determine significant ($p < 0.05$) differences between the different experimental groups.

Results

Wound closure

Dermal wounds were quantified daily and compared to the original area of each starting wound. For all wounds included in the analyses, wounds on each side of the mouse remained separated and undisturbed by the mice. Within the first week of healing, wounds subjected to all treatment conditions exhibited scab formation, and in all groups, the scab was no longer present by day 11. By the end of the two week study, all wounds healed with some evidence of scar formation, or small area of skin that appeared healed, but with no hair re-growth. Overall, the rate of wound closure occurred most rapidly between days 5-9 post-injury and changed nominally between days 10-14. Wounds treated with matrix, either alone or with fibrin, appeared to close at a faster rate than those left untreated (Figure 7.1). Untreated wounds consistently exhibited the lowest percent wound closure over time, while groups treated with fibrin (with or without the addition of matrix) appeared to close especially quickly within the first four days of healing, possibly due to some dehydration and contraction of the fibrin gel itself. However, only the wounds treated with the combination of matrix and fibrin exhibited a significantly higher percent wound closure ($p \leq 0.04$) than untreated wounds at days 1, 2, 4, 5, 6, 11, and 12 post-wounding.

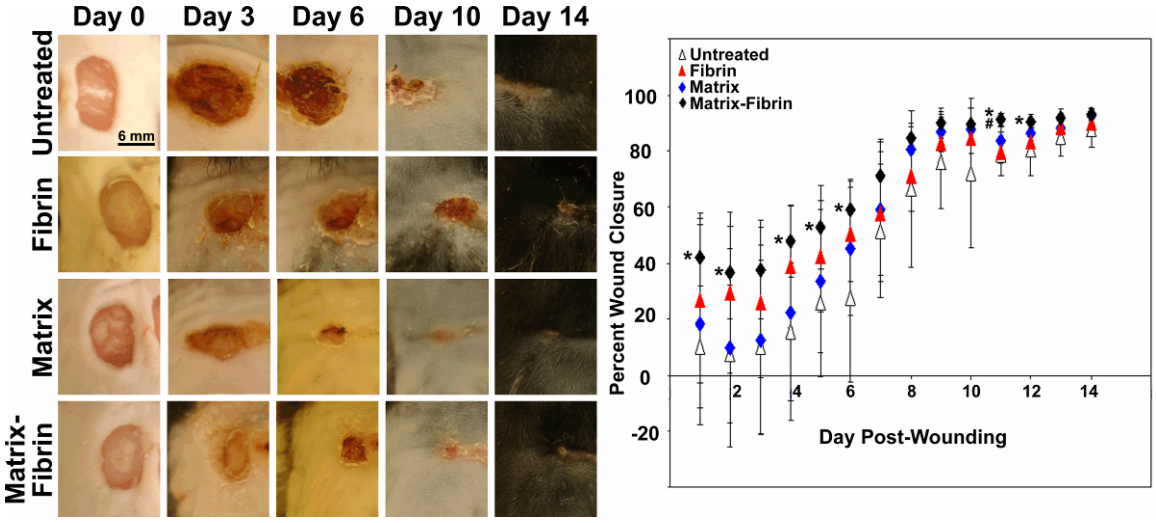

Figure 7.1. Wound closure analysis. Qualitatively, wounds generally closed faster in wounds treated with matrix or a matrix-fibrin combination. When quantified, wounds treated with matrix-fibrin demonstrated exhibited significantly greater percent wound closure than untreated wounds, particularly within the first week of healing. *Significantly different from untreated wounds, $p \leq 0.04$, # significantly different from fibrin-treated wounds, $p = 0.01$ (ANOVA).

Wound Histology

Wounds excised at 7 and 14 days post-wounding were stained with Masson's Trichrome stain (Figure 7.2). Scabs were evident in day 7 wounds, noted in particular by the bright red staining in matrix-fibrin and fibrin samples. At day 7, little collagen (blue stain) was present in the wound bed, but was more abundant by day 14 in all samples. For most treated (fibrin, matrix, matrix-fibrin) wounds, the width of the wound bed (indicated by arrows) was noticeably smaller (at least 30% of the original width) after two weeks compared to the one week time point, indicative of the progressive healing process. In addition, wound bed widths across groups were not significantly different at either days 7 or 14 (data not shown), which corroborates macroscopic would closure rates assessed at those time points. Re-epithelialization was evident in all groups by day 14 post-injury, but there was no indication of gland or hair follicle development.

When viewed at a higher magnification, differences in collagen deposition were noted among treated and control groups (Figure 7.3). Wounds left untreated or those treated with fibrin alone had sparse, thin strands of collagen bundles. In contrast, wounds treated with matrix or matrix-fibrin exhibited more densely packed, thicker bundles of collagen that are typically associated with reduced scar formation. Across all sections examined, wounds treated with matrix (with or without fibrin) appeared to have a higher cellular infiltrate in the wound bed, although the phenotypes across the groups were similar.

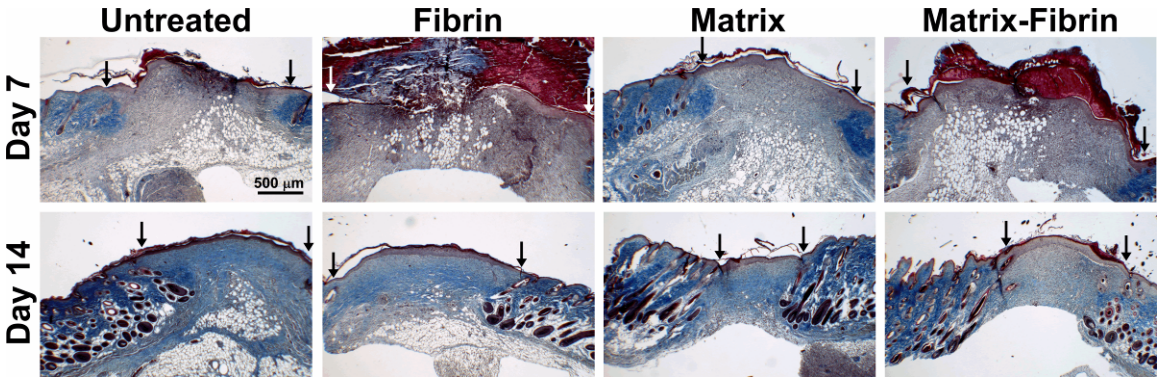

Figure 7.2. Wound histology. Wounds excised at days 7 and 14 post-wounding were stained with Masson's Trichrome. Collagen is stained in blue and has noticeably greater deposition by day 14 compared to day 7 wounds in all groups. Wound edges are indicated by arrows.

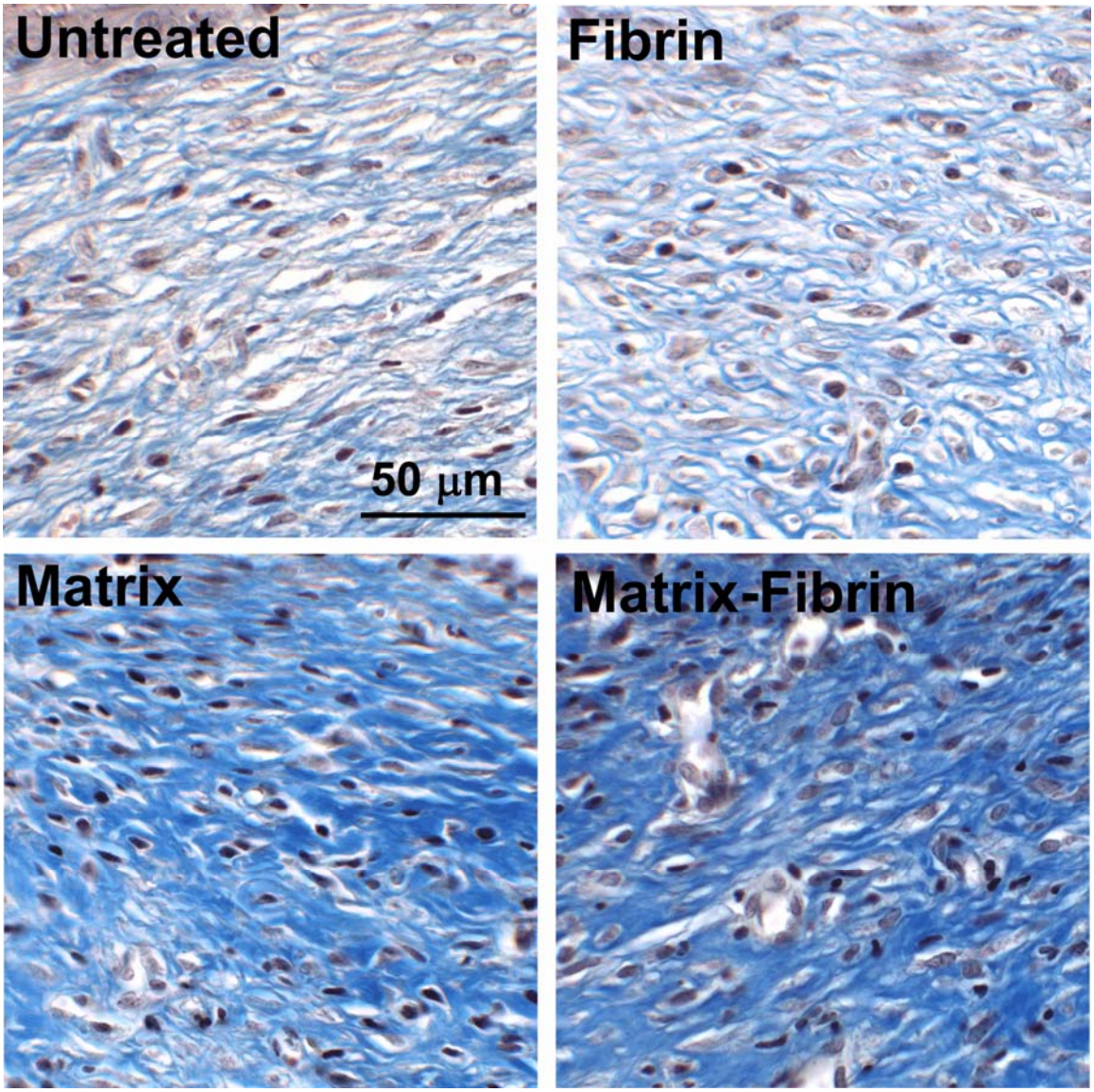

Figure 7.3. Wound bed matrix histological analysis. Magnified images of wound beds stained with Masson's Trichrome show distinct differences in the appearance of collagen (blue) in day 14 wounds. Untreated and fibrin samples exhibit thinner bundles while matrix- and matrix-fibrin-treated samples had thicker, more loosely packed collagen.

Blood vessel quantification

Frozen sections (8 μm) were stained with a PECAM-1 antibody to identify blood vessels. By day 14, there were 118 – 135 total blood vessels/area in all control and experimental groups, while the percent total area occupied by blood vessels ranged from 1.25% – 1.46% (Figure 7.4). This analysis indicated no significant differences across the groups and suggested that angiogenesis was not significantly enhanced or disrupted in treated wounds. Blood vessels that extravasated towards the epithelial layer were quantified at days 7 (Figure 7.5) and 14. By day 7, blood vessels in matrix and matrix-fibrin wounds appeared to extravasate towards the epithelial layer, while blood vessels in fibrin and untreated wounds remained largely parallel to the epithelial layer (Figure 7.3). Blood vessels directed towards the epithelial layer (greater than 45^{o} compared to the horizontal) were quantified per wound area. Matrix-treated wounds had significantly more extravasating blood vessels (30.7 ± 13 vessels/area) than both fibrin (8.6 ± 9; $p = 0.03$) and untreated (13.0 ± 5; $p = 0.01$) wounds, again suggestive of an improved healing response over control groups. By day 14 (data not shown), matrix-treated groups no longer had a significantly different number of extravasating blood vessels and had decreased to 9.8 ± 6 vessels/area, while the other groups remained at ~10-13 vessels/area.

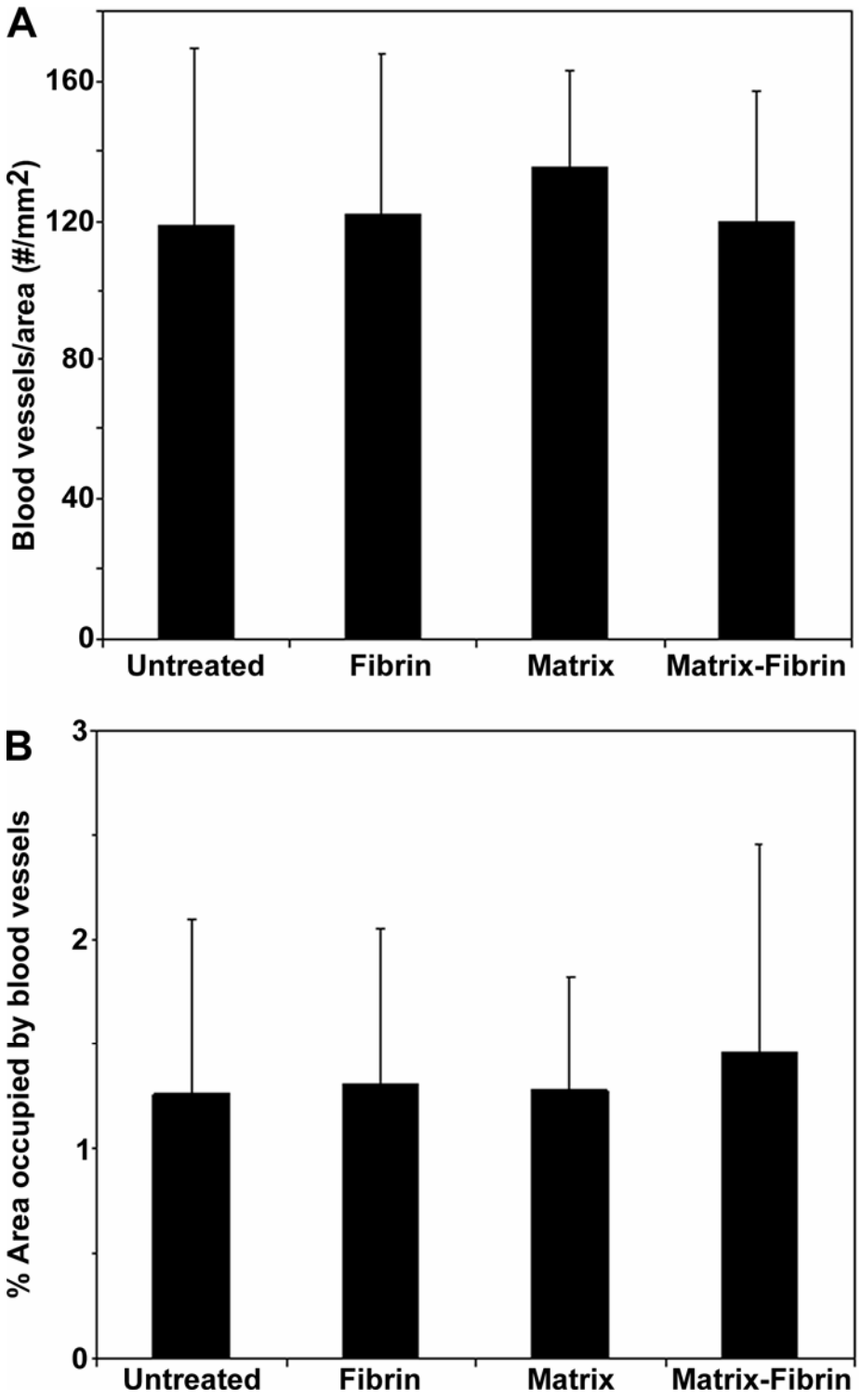

Figure 7.4. Blood vessel quantification. Total number of blood vessels per area (A) and percent of the total area occupied by blood vessels (B) were quantified at 14 days post-wounding. No significant differences were found across the groups (evaluated with ANOVA).

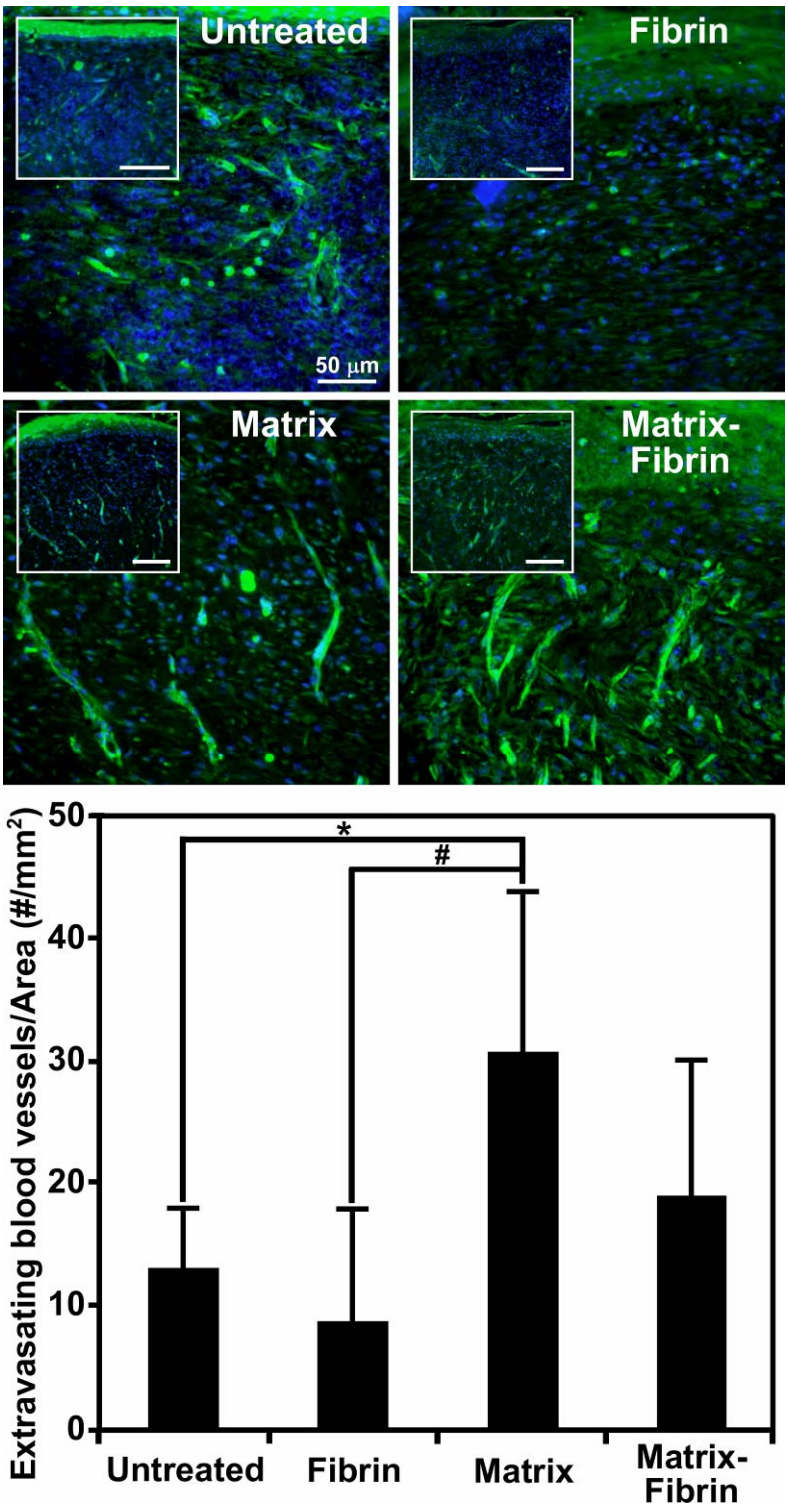

Figure 7.5. Extravasating blood vessel quantification. Blood vessels extravasated towards the epithelial layer in matrix-treated wounds significantly more than those treated with fibrin alone or those left untreated 7 days after wounding. Each image was taken with the epithelial layer horizontal and facing up. Scale bars for inset images are 125 μm. * $p = 0.03$; # $p = 0.01$.

Discussion

The intrinsic machinery that allows for early fetal wound regeneration is not activated in the adult environment, resulting in imperfect repair responses and scar formation. In this study, the ability of an embryonic-derived matrix to elicit an improved healing response in an adult was evaluated by examining acellular EBs applied to a murine excisional dermal wound healing model. Wounds treated with a combination of matrix and fibrin exhibited significantly increased wound closure, primarily within the first week of healing, compared to untreated wounds. In addition, collagen within the wound beds appeared thicker and more loosely packed in matrix-treated wounds, a phenotype typically associated with scarless healing [97], in contrast to the thin, parallel bundles in untreated or fibrin-treated wounds. Although the total number of blood vessels per area were not significantly different across control and experimental groups, the number of vessels extravasating towards the epithelial layer was significantly greater in matrix-treated wounds. Overall these results suggest that EB-derived matrices can improve healing in an adult, possibly due to the wound repair-enhancing factors naturally synthesized by differentiating ESCs and retained within the acellular matrices.

The differences in rates of wound closure observed within the first week of healing may be primarily due to the presence of additional matrix in the wound bed. During the course of wound healing, provisional matrix is typically deposited by the local cell population after several days post-injury [234, 235]. In contrast, wounds treated with acellular EBs (alone or with fibrin) received exogenous matrix molecules that potentially provided stability in the site of injury and offered a substrate for host cell migration and subsequent wound contraction immediately after injury. Applying matrix at such an

early time point likely affected the kinetics of wound healing, resulting not only in differences in percent wound closure, but possibly also affecting the time course of cell infiltration and movement. The addition of fibrin to the matrix resulted in a greater volume that covered the wound bed completely, which, unlike matrix-only treated wounds, provided a substrate for cells that extended between wound edges and could allow for infiltration of host cells residing in the adjacent normal tissue. Therefore, the combination of exogenous matrix along with a physical substrate covering the wound likely resulted directly in significant effects on wound closure.

The differences observed in collagen thickness and density may have been due to differential signaling responses elicited by the presence of the EB-derived matrix. Several *in vitro* and *in vivo* wound healing studies have shown that changes in the local environment from exogenous matrix, cytokine, or growth factors can alter host cell responses, indicating the possibility that factors captured within the acellular EB matrix may elicit similar behaviors [236-238]. This difference in histological collagen observations may be directly related to differences in blood vessel morphology between treated and untreated wounds. Since the total number of blood vessels per area is consistent among all experimental and control groups, angiogenic factors synthesized by differentiating ESCs were perhaps masked in the acellular EBs. However, since differences were noted in the number of blood vessels extravasating towards the epithelial layer, it is possible that the observed differences in collagen deposition and the looser conformation of the collagen allowed for extravasation of the blood vessels, leading to improved nutrient delivery to the upper dermal and epidermal layers and subsequent enhanced wound healing.

In these studies, ECM derived from ~10,000 EBs (~36 μg protein) was applied directly to the wound at the time of injury. For future studies, more potent effects from the matrices may be observed with an increase in dosage. Besides offering a greater quantity of ESC-derived molecules, a dose increase would provide greater coverage for the wound and reduce the air-wound interface, which could further accelerate wound closure [239]. In addition, the application of matrices at multiple time points throughout the healing process could provide a steady supply of ESC-derived molecules that may enhance the quality of wound repair through continuous stimulation of the host cells.

In the studies presented here, significant differences were observed in some of the examined parameters between matrix-treated wounds as compared to control wounds. Subtle differences in healing and wound bed composition may have been masked, however, due to the choice of an acute wound healing animal model. The excisional dermal wound healing model used in these studies provides a good test bed to examine the acute effects of acellular matrices on healing *in vivo*. Within the two week time course evaluated, untreated wounds healed such that hair around the wound had re-grown, no scabs were present, and the scar was the only visible remainder of the wound site. Because of the relatively quick healing response undergone by control wounds, subtle effects elicited by the presence of the acellular matrix may have gone undetected. Therefore, to further parse out differences between groups, future studies could involve examination of the EB matrices in a chronic model, for example in a diabetic mouse [240, 241]. While the wound healing response can be more complex to interpret, subtle differences may be more easily identified, thereby elucidating additional and presently unknown effects of the acellular EBs. But in addition to simply providing a more robust

model for examining the role of acellular matrices in wound healing, chronic models are considered more relevant to injuries (e.g. burns) and diseases (e.g. diabetes mellitus) commonly present within the population of developed countries. There has been some indication that therapy using fetal tissue can contribute to chronic wound repair [242], so examining the EB matrices in a chronic wound healing model could further elucidate mechanisms by which embryonic-derived ECM can alter macroscopic and microscopic features of severe dermal injuries.

The results presented here encourage further investigation into the mechanisms by which extracellular matrix derived from ESCs can alter wound healing. Upon stimulation with exogenous factors, fetal and adult dermal fibroblasts exhibit distinctly different signaling responses *in vitro* that may, in part, translate into differences in wound healing outcomes *in vivo* [237, 243-245]. In addition, differences in wound bed composition between adult and fetal wounds are a result of distinct responses by endogenous fibroblasts [101, 226, 227, 246]. An acellular embryonic-derived matrix may provide morphogenic cues to which host fibroblasts respond in a manner similar to fetal fibroblasts, thereby resulting in enhanced wound healing compared to untreated wounds.

Importantly, the results of these studies encourage examination of other types of injury where healing may benefit from stem cell derived matrices. For such investigations, ESCs that have been differentiated into defined phenotypes could synthesize matrix specific for the injury's environment. Directing the differentiation of ESCs into a specific cell type may induce the synthesis of ECM relevant to that particular tissue, which in turn could be more applicable to treatment of the tissue in its diseased

state. Such embryonic matrices could stimulate endogenous cells to undergo the morphogenic processes typically seen during early development and may therefore provide a robust therapy for a variety of injuries or diseases.

CHAPTER 8

FUTURE CONSIDERATIONS

This work has examined the dynamic nature of ECM synthesized by ESCs and its relevance to differentiation events. Novel techniques were developed to isolate the potent extracellular factors within the EB microenvironment, and the resulting embryonic-derived acellular matrix significantly enhanced wound healing in an adult environment *in vivo*. While other work has highlighted the importance of the extracellular matrix (ECM) and growth factors synthesized by differentiating ESCs, no other studies have derived matrices that harness the potency of these molecules for therapeutic applications.

Gene array analysis provided an initial examination into the range of matrix molecules expressed by differentiating ESCs in EBs. Clustering and pathway analyses emphasized expression trends in subsets of molecules and highlighted specific molecules that were either highly expressed or that served as nodes in differentiation networks. Upon closer examination, expression and localization of the glycosaminoglycan hyaluronan (HA) and the proteoglycan versican were found to be associated with EB differentiation. The results presented here provided evidence that HA and versican have roles in the epithelial-mesenchymal transition in EBs, but future studies should further explore these patterns. For example, while studies where HA and versican are knocked down could directly assess their effects on differentiation, parallel studies where the molecules are delivered exogenously or cells are genetically modified to over-express the ECM components could assess HA and versican's ability to rescue specific phenotypes or

differentiation events. Additional studies with other molecules highlighted in the gene array analysis, such as collagen III, vitronectin, and periostin, could similarly identify key roles in EB development and ESC differentiation.

Other investigations that deconstruct elements of the ECM must also be performed to further identify the molecular regulators of ESC differentiation. In addition to global gene analysis, differential expression in cell populations exhibiting distinct morphological characteristics could be assessed using laser capture microdissection technologies to identify the composition of localized matrix deposition associated with specific cell phenotypes. In addition to gene expression analyses, proteomic analysis of differentiating ESCs should be assessed using mass spectrometry to identify actual protein species present in the complex mixture. Resulting data from global and local gene expression analyses, proteomic assessments, and examination of specific molecules, could not only contribute to the understanding of self-regulated differentiation patterns in ESCs, but would also lend insight into directed differentiation schemes essential for developing robust regenerative medicine therapies. The addition of specific molecules known to be necessary for a particular cell specification event could potentially drive a heterogeneous cell population towards a more defined phenotype. Therefore, identifying which molecules are relevant for the differentiation of specific lineages is critical for the development of such protocols.

The studies presented in this dissertation begin to identify endogenously expressed matrix molecules playing key roles in ESC differentiation. These advances, however, were realized through analysis of one cell line. Therefore, a deeper understanding of the role of ECM within EBs could benefit from the examination and

comparison of gene expression profiles from other ES cell lines, thereby elucidating how genetic differences between cell populations may affect the underlying stem cell biology. Since no directed differentiation schemes were performed prior to the global matrix analysis studies, it is possible that other ES cell lines, possibly tending towards a particular germ lineage when spontaneously differentiated, may exhibit altered matrix molecule and growth factor production. Direct comparisons of such studies with those presented here may elucidate which factors are predominantly expressed by a specific cell line as opposed to those that play more global roles in stem cell biology.

In this work, a novel means of isolating the matrix produced by differentiating ESCs was investigated through comparisons of a variety of reagents capable of disrupting cell membranes and removing cell components. While a portion of the original protein content was found to be maintained after decellularization, these findings warrant more in-depth proteomic analysis of the acellular matrix composition through mass spectrometry. Direct comparisons of protein profiles in EBs and acellular matrices derived from the EBs would provide critical information regarding classes of molecules that are maintained after decellularization treatments. Such information could be useful as additional methods of decellularizing EBs are developed to include more mechanical means of cell disruption that may preserve intact matrix molecules better than chemical treatments. For example, present studies are investigating lyophilized EBs as a purely mechanical means of harboring the potent morphogenic cues synthesized by differentiating ESCs. Along those lines, however, future investigations into any decellularization method should involve analysis of host immune responses to the matrix, as purely mechanical treatments are more likely to retain potentially immunogenic cell

components. The relative level of immunogenicity in ESCs is reduced compared to non-stem cell populations because of the comparatively small amounts of major histocompatibility complex (MHC) class I molecules produced and lack of MHC class II molecules [247]. Class I molecules are up-regulated in EBs [248], however, so the immunogenicity of EB-derived products is an important consideration to evaluate.

One benefit of the protocol developed is the high percentage of DNA removal resulting from the chemical and enzymatic treatments. However, since the "sticky" nuclear material is largely removed, these matrices do not offer high mechanical integrity and are therefore difficult to examine *in vitro* and to apply to wounds *in vivo*. For *in vitro* cell seeding studies, it is extremely challenging to retrieve seeded matrices from culture in tact for subsequent histological analyses. Further, although possible, due to the diminished mechanical integrity of the matrices, they are also difficult to remove from their storage tubes and place on wounds *in vivo*. Ongoing studies are presently evaluating the ability of acellular matrices to be chemically cross-linked and have thus far successfully shown that treatment of the EB matrices with a natural cross-linking agent improves its ease of handling. Subsequently, studies wherein histological analyses and metabolic assays were successfully performed on seeded EB matrices resulted in confirmation that cells could infiltrate and survive in the matrices *in vitro*. Additional formulations, such as an injectable solubilized matrix or a lyophilized powdered matrix, may also facilitate application *in vivo* by providing matrices that are more easily handled. A soluble matrix may be directly injected into the site of injury, while a powdered matrix could be physically interspersed on the surface of the wound. While the studies presented have laid the foundation for examining EB-derived matrices *in vivo*, other

formulations may enhance the ease with which these matrices are handled and possibly lead to improved dosage reproducibility by ensuring that pieces of matrix are not left behind because of mechanical instability.

Furthermore, the promising *in vivo* results presented in this work encourages in-depth analysis of the mechanisms by which host cells respond to acellular EB matrices during wound healing processes. Initially, *in vitro* studies that investigate the signaling pathways activated when dermal fibroblasts are seeded on the acellular EB-derived matrix as compared to an adult fibroblast matrix could begin to elucidate differential responses exhibited by host cells that are critical for the resulting wound healing responses. In addition, examining the potency of the EB matrix *in vivo* compared to an adult fibroblast-derived matrix would more rigorously examine the hypothesis that it is the unique reservoir of embryonic cues harbored in the EB matrix is essential for enhanced wound healing, and not simply the presence of more promiscuous matrix molecules possibly available in a number of tissue matrices. Since the extracellular matrix of fetal wounds is distinctly different from adult wounds, *in vivo* studies comparing embryonic and adult treatments should also involve analysis of the wound bed composition to identify whether application of an embryonic matrix can stimulate host cells to secrete a more embryonic-like provisional matrix.

Motivated by studies suggesting that matrix factors secreted by transplanted ESCs are primarily responsible for observed regenerative events (fraidenraich, chen 2009), the work presented in this thesis analyzed the expression profile of molecules synthesized by ESCs *in vitro* and subsequently evaluated the effect of an extracted portion of these in an *in vivo* model. However, since proteomic or gene expression profiles of factors secreted

in vivo by differentiating ESCs are presently unavailable, it is unknown whether the range of factors synthesized during *in vitro* culture of the cells and captured in the acellular EBs are similar to the matrix secreted by transplanted cells *in vivo*. The presence of central host systems that result in immune and inflammatory responses likely contributes to signaling patterns that are not present in the controlled *in vitro* environment. However, molecules such as collagen III and transforming growth factor (Tgf)-β3 that are present in increasing quantities in EBs differentiating *in vitro* are also known to play key roles in the regenerating fetal wound [97]. The presence of these molecules in ES cell cultures suggests that an isolated EB matrix applied to wounds could induce healing responses similar to those seen in scarless fetal repair.

In addition, the observed regulation of molecules related to EB differentiation lends insight into possible expression patterns necessary for improved *in vivo* healing. For example, the array data presented in chapter 3 showed a decrease in a subset of molecules that appeared to be necessary prior to subsequent differentiation, which raises the possibility that a similar decrease in specific factors during wound healing may allow (or be necessary for) enhanced repair. Specifically, collagen I, which is present in greater amounts in adult scarring tissues compared to embryonic tissues, was found to decrease at early time points of ESC differentiation *in vitro*. Although in the present studies EB matrices were applied only once at the time of wounding, future investigations could involve re-application of the matrix at different time points along the healing time course in order to provide a constant dose of embryonic-derived matrix molecules. Preliminary studies investigating the persistence of the matrices in the wound bed have indicated that by one week post-injury, the acellular EBs are no longer present in the wound site.

Therefore, re-application of the treatment after 5-7 days would provide a prolonged exposure of the host cells to the embryonic matrix. In addition, it may be interesting to apply matrices derived from early EBs at the time of wounding, but to then deliver matrices derived from progressively more mature EBs at subsequent time points during the healing process in order to present a dynamic range of molecules similar to those necessary for the progression of differentiation *in vitro*. As a result, the wound environment would be subjected initially to low doses of collagen I, followed by increasing doses of collagen III and Tgf-β3. This expression pattern is naturally observed during regenerative wound healing [97, 226] and may induce improved responses in the adult.

As discussed previously, one unique feature of ESC-derived matrices is the potential to tailor them for specific applications by directing the differentiation of the cells prior to decellularization. Directed differentiation schemes have remained a significant challenge for stem cell researchers, but analysis of cell-specific matrices in addition to work currently ongoing in our lab that allows for more homogeneous distribution of exogenous factors in EBs may considerably drive the research forward. Matrices derived from a population that is primarily one cell type could subsequently be examined in the corresponding *in vivo* model system to examine tissue-specific effects. In the future, it will be essential to evaluate the translational applicability of the EB-derived acellular matrices. Appropriate formulation and ease of handling are necessary for ultimate clinical use, as is batch culture ESC propagation, which has already been under investigation by numerous researchers. Therefore, an acellular EB matrix could

provide a novel, clinically translatable means of accessing the therapeutic potential of ESCs.

In summary, this research has established the groundwork for investigating the potency of matrices derived from a stem cell source and has shown the significance of such matrices in improving wound healing *in vivo*. The complex mixture of extracellular factors entrapped within the EB microenvironment contribute to the bioactive efficacy of the acellular matrix, and additional understanding and identification of the specific molecules involved could further elucidate the utility of the matrix. Future work that further examines the composition of complex extracellular matrices synthesized by differentiating ESCs and explores the potential of this isolated matrix will undoubtedly uncover unique insights critical to the development of regenerative molecular therapeutics.

REFERENCES

1. Evans MJ, Kaufman MH. Establishment in culture of pluripotential cells from mouse embryos. Nature. 1981;292:154-156.

2. Martin GR. Isolation of a pluripotent cell line from early mouse embryos cultured in medium conditioned by teratocarcinoma stem cells. Proc Natl Acad Sci U S A. 1981;78:7634-7638.

3. Thomson JA, Itskovitz-Eldor J, Shapiro SS, et al. Embryonic stem cell lines derived from human blastocysts. Science. 1998;282:1145-1147.

4. Wobus AM, Holzhausen H, Jakel P, et al. Characterization of a pluripotent stem cell line derived from a mouse embryo. Exp Cell Res. 1984;152:212-219.

5. Desbaillets I, Ziegler U, Groscurth P, et al. Embryoid bodies: an in vitro model of mouse embryogenesis. Exp Physiol. 2000;85:645-651.

6. Dushnik-Levinson M, Benvenisty N. Embryogenesis in vitro: study of differentiation of embryonic stem cells. Biol Neonate. 1995;67:77-83.

7. Keller G. Embryonic stem cell differentiation: emergence of a new era in biology and medicine. Genes Dev. 2005;19:1129-1155.

8. Murashov AK, Pak ES, Hendricks WA, et al. Directed differentiation of embryonic stem cells into dorsal interneurons. FASEB J. 2005;19:252-254.

9. Spence JR, Wells JM. Translational embryology: using embryonic principles to generate pancreatic endocrine cells from embryonic stem cells. Dev Dyn. 2007;236:3218-3227.

10. Rohwedel J, Guan K, Zuschratter W, et al. Loss of beta1 integrin function results in a retardation of myogenic, but an acceleration of neuronal, differentiation of embryonic stem cells in vitro. Dev Biol. 1998;201:167-184.

11. Murray P, Edgar D. Regulation of programmed cell death by basement membranes in embryonic development. J Cell Biol. 2000;150:1215-1221.

12. Smyth N, Vatansever HS, Murray P, et al. Absence of basement membranes after targeting the LAMC1 gene results in embryonic lethality due to failure of endoderm differentiation. J Cell Biol. 1999;144:151-160.

13. Scheele S, Falk M, Franzen A, et al. Laminin alpha1 globular domains 4-5 induce fetal development but are not vital for embryonic basement membrane assembly. Proc Natl Acad Sci U S A. 2005;102:1502-1506.

14. Lohler J, Timpl R, Jaenisch R. Embryonic lethal mutation in mouse collagen I gene causes rupture of blood vessels and is associated with erythropoietic and mesenchymal cell death. Cell. 1984;38:597-607.

15. Hillegass JM, Villano CM, Cooper KR, et al. Matrix metalloproteinase-13 is required for zebra fish (Danio rerio) development and is a target for glucocorticoids. Toxicol Sci. 2007;100:168-179.

16. Gilmour DT, Lyon GJ, Carlton MB, et al. Mice deficient for the secreted glycoprotein SPARC/osteonectin/BM40 develop normally but show severe age-onset cataract formation and disruption of the lens. EMBO J. 1998;17:1860-1870.

17. Xu W, Baribault H, Adamson ED. Vinculin knockout results in heart and brain defects during embryonic development. Development. 1998;125:327-337.

18. Stephens LE, Sutherland AE, Klimanskaya IV, et al. Deletion of beta 1 integrins in mice results in inner cell mass failure and peri-implantation lethality. Genes Dev. 1995;9:1883-1895.

19. Liaw L, Birk DE, Ballas CB, et al. Altered wound healing in mice lacking a functional osteopontin gene (spp1). J Clin Invest. 1998;101:1468-1478.

20. Glukhova MA, Thiery JP. Fibronectin and integrins in development. Semin Cancer Biol. 1993;4:241-249.

21. Singla DK, McDonald DE. Factors released from embryonic stem cells inhibit apoptosis of H9c2 cells. Am J Physiol Heart Circ Physiol. 2007;293:H1590-1595.

22. Singla DK, Singla RD, McDonald DE. Factors released from embryonic stem cells inhibit apoptosis in H9c2 cells through PI3K/Akt but not ERK pathway. Am J Physiol Heart Circ Physiol. 2008;295:H907-913.

23. Crisostomo PR, Abarbanell AM, Wang M, et al. Embryonic stem cells attenuate myocardial dysfunction and inflammation after surgical global ischemia via paracrine actions. Am J Physiol Heart Circ Physiol. 2008;295:H1726-1735.

24. Lu WN, Lu SH, Wang HB, et al. Functional improvement of infarcted heart by co-injection of embryonic stem cells with temperature-responsive chitosan hydrogel. Tissue Eng Part A. 2009;15:1437-1447.

25. Toriumi H, Yoshikawa M, Matsuda R, et al. Treatment of Parkinson's disease model mice with allogeneic embryonic stem cells: necessity of immunosuppressive treatment for sustained improvement. Neurol Res. 2009;31:220-227.

26. Kroon E, Martinson LA, Kadoya K, et al. Pancreatic endoderm derived from human embryonic stem cells generates glucose-responsive insulin-secreting cells in vivo. Nat Biotechnol. 2008;26:443-452.

27. Behr R, Heneweer C, Viebahn C, et al. Epithelial-mesenchymal transition in colonies of rhesus monkey embryonic stem cells: a model for processes involved in gastrulation. Stem Cells. 2005;23:805-816.

28. Rovira M, Delaspre F, Massumi M, et al. Murine embryonic stem cell-derived pancreatic acinar cells recapitulate features of early pancreatic differentiation. Gastroenterology. 2008;135:1301-1310, 1310 e1301-1305.

29. Gerecht-Nir S, Ziskind A, Cohen S, et al. Human embryonic stem cells as an in vitro model for human vascular development and the induction of vascular differentiation. Lab Invest. 2003;83:1811-1820.

30. Moon AM. Mouse models for investigating the developmental basis of human birth defects. Pediatr Res. 2006;59:749-755.

31. Rugg-Gunn PJ, Ferguson-Smith AC, Pedersen RA. Human embryonic stem cells as a model for studying epigenetic regulation during early development. Cell Cycle. 2005;4:1323-1326.

32. Lin S, Tran V, Talbot P. Comparison of toxicity of smoke from traditional and harm-reduction cigarettes using mouse embryonic stem cells as a novel model for preimplantation development. Hum Reprod. 2009;24:386-397.

33. Zdravkovic T, Genbacev O, LaRocque N, et al. Human embryonic stem cells as a model system for studying the effects of smoke exposure on the embryo. Reprod Toxicol. 2008;26:86-93.

34. Bone HK, Welham MJ. Phosphoinositide 3-kinase signalling regulates early development and developmental haemopoiesis. J Cell Sci. 2007;120:1752-1762.

35. Doetschman TC, Eistetter H, Katz M, et al. The in vitro development of blastocyst-derived embryonic stem cell lines: formation of visceral yolk sac, blood islands and myocardium. J Embryol Exp Morphol. 1985;87:27-45.

36. Itskovitz-Eldor J, Schuldiner M, Karsenti D, et al. Differentiation of human embryonic stem cells into embryoid bodies compromising the three embryonic germ layers. Mol Med. 2000;6:88-95.

37. Keller GM. In vitro differentiation of embryonic stem cells. Curr Opin Cell Biol. 1995;7:862-869.

38. Ashcroft GS, Horan MA, Ferguson MW. The effects of ageing on wound healing: immunolocalisation of growth factors and their receptors in a murine incisional model. J Anat. 1997;190 (Pt 3):351-365.

39. Leahy A, Xiong JW, Kuhnert F, et al. Use of developmental marker genes to define temporal and spatial patterns of differentiation during embryoid body formation. J Exp Zool. 1999;284:67-81.

40. Czyz J, Wobus A. Embryonic stem cell differentiation: the role of extracellular factors. Differentiation. 2001;68:167-174.

41. Rodda SJ, Kavanagh SJ, Rathjen J, et al. Embryonic stem cell differentiation and the analysis of mammalian development. Int J Dev Biol. 2002;46:449-458.

42. Beddington R. The origin of foetal tissues during gastrulation in the rodent. Amsterdam: Elsevier; 1983.

43. Lake J, Rathjen J, Remiszewski J, et al. Reversible programming of pluripotent cell differentiation. J Cell Sci. 2000;113 (Pt 3):555-566.

44. Rathjen J, Rathjen PD. Mouse ES cells: experimental exploitation of pluripotent differentiation potential. Curr Opin Genet Dev. 2001;11:587-594.

45. Hogan B, Beddington R, Constantini F, et al. Manipulating the Mouse Embryo: A Laboratory Manual. Cold Spring Harbour: Cold Spring Harbour Laboratory Press; 1994.

46. Coucouvanis E, Martin GR. Signals for death and survival: a two-step mechanism for cavitation in the vertebrate embryo. Cell. 1995;83:279-287.

47. Fraidenraich D, Stillwell E, Romero E, et al. Rescue of cardiac defects in id knockout embryos by injection of embryonic stem cells. Science. 2004;306:247-252.

48. Guttinger M, Fedele D, Koch P, et al. Suppression of kindled seizures by paracrine adenosine release from stem cell-derived brain implants. Epilepsia. 2005;46:1162-1169.

49. Chen X, Song XH, Yin Z, et al. Stepwise differentiation of human embryonic stem cells promotes tendon regeneration by secreting fetal tendon matrix and differentiation factors. Stem Cells. 2009;27:1276-1287.

50. Alberts B, Johnson A, Lewis J, et al. Molecular Biology of the Cell. New York: Garland Science; 2001.

51. Timpl R, Brown JC. The laminins. Matrix Biol. 1994;14:275-281.

52. Schultz GS, Wysocki A. Interactions between extracellular matrix and growth factors in wound healing. Wound Repair Regen. 2009;17:153-162.

53. Flaim CJ, Chien S, Bhatia SN. An extracellular matrix microarray for probing cellular differentiation. Nat Methods. 2005;2:119-125.

54. Flaim CJ, Teng D, Chien S, et al. Combinatorial signaling microenvironments for studying stem cell fate. Stem Cells Dev. 2008;17:29-39.

55. Sakiyama-Elbert SE, Hubbell JA. Development of fibrin derivatives for controlled release of heparin-binding growth factors. J Control Release. 2000;65:389-402.

56. Miller ED, Phillippi JA, Fisher GW, et al. Inkjet printing of growth factor concentration gradients and combinatorial arrays immobilized on biologically-relevant substrates. Comb Chem High Throughput Screen. 2009;12:604-618.

57. Rezania A, Healy KE. Biomimetic peptide surfaces that regulate adhesion, spreading, cytoskeletal organization, and mineralization of the matrix deposited by osteoblast-like cells. Biotechnol Prog. 1999;15:19-32.

58. Reyes CD, Garcia AJ. Alpha2beta1 integrin-specific collagen-mimetic surfaces supporting osteoblastic differentiation. J Biomed Mater Res A. 2004;69:591-600.

59. Weil BR, Markel TA, Herrmann JL, et al. Mesenchymal stem cells enhance the viability and proliferation of human fetal intestinal epithelial cells following hypoxic injury via paracrine mechanisms. Surgery. 2009;146:190-197.

60. Guo Y, Graham-Evans B, Broxmeyer HE. Murine embryonic stem cells secrete cytokines/growth modulators that enhance cell survival/anti-apoptosis and stimulate colony formation of murine hematopoietic progenitor cells. Stem Cells. 2006;24:850-856.

61. Bagutti C, Hutter C, Chiquet-Ehrismann R, et al. Dermal fibroblast-derived growth factors restore the ability of beta(1) integrin-deficient embryonal stem cells to differentiate into keratinocytes. Dev Biol. 2001;231:321-333.

62. Willerth SM, Faxel TE, Gottlieb DI, et al. The effects of soluble growth factors on embryonic stem cell differentiation inside of fibrin scaffolds. Stem Cells. 2007;25:2235-2244.

63. Li L, Arman E, Ekblom P, et al. Distinct GATA6- and laminin-dependent mechanisms regulate endodermal and ectodermal embryonic stem cell fates. Development. 2004;131:5277-5286.

64. Ekblom P, Lonai P, Talts JF. Expression and biological role of laminin-1. Matrix Biol. 2003;22:35-47.

65. Chen SS, Fitzgerald W, Zimmerberg J, et al. Cell-cell and cell-extracellular matrix interactions regulate embryonic stem cell differentiation. Stem Cells. 2007;25:553-561.

66. Dziadek M, Timpl R. Expression of nidogen and laminin in basement membranes during mouse embryogenesis and in teratocarcinoma cells. Dev Biol. 1985;111:372-382.

67. Leivo I, Vaheri A, Timpl R, et al. Appearance and distribution of collagens and laminin in the early mouse embryo. Dev Biol. 1980;76:100-114.

68. Stary M, Pasteiner W, Summer A, et al. Parietal endoderm secreted SPARC promotes early cardiomyogenesis in vitro. Exp Cell Res. 2005;310:331-343.

69. Nairn AV, Kinoshita-Toyoda A, Toyoda H, et al. Glycomics of Proteoglycan Biosynthesis in Murine Embryonic Stem Cell Differentiation. J Proteome Res. 2007;6:4374-4387.

70. Sze SK, de Kleijn DP, Lai RC, et al. Elucidating the secretion proteome of human embryonic stem cell-derived mesenchymal stem cells. Mol Cell Proteomics. 2007;6:1680-1689.

71. Badylak SF, Lantz GC, Coffey A, et al. Small intestinal submucosa as a large diameter vascular graft in the dog. J Surg Res. 1989;47:74-80.

72. Hudson TW, Liu SY, Schmidt CE. Engineering an improved acellular nerve graft via optimized chemical processing. Tissue Eng. 2004;10:1346-1358.

73. Dahl SL, Koh J, Prabhakar V, et al. Decellularized native and engineered arterial scaffolds for transplantation. Cell Transplant. 2003;12:659-666.

74. Mirsadraee S, Wilcox HE, Korossis SA, et al. Development and characterization of an acellular human pericardial matrix for tissue engineering. Tissue Eng. 2006;12:763-773.

75. Chen RN, Ho HO, Tsai YT, et al. Process development of an acellular dermal matrix (ADM) for biomedical applications. Biomaterials. 2004;25:2679-2686.

76. Whitlock PW, Smith TL, Poehling GG, et al. A naturally derived, cytocompatible, and architecturally optimized scaffold for tendon and ligament regeneration. Biomaterials. 2007.

77. Hopper RA, Woodhouse K, Semple JL. Acellularization of human placenta with preservation of the basement membrane: a potential matrix for tissue engineering. Ann Plast Surg. 2003;51:598-602.

78. Brown AL, Brook-Allred TT, Waddell JE, et al. Bladder acellular matrix as a substrate for studying in vitro bladder smooth muscle-urothelial cell interactions. Biomaterials. 2005;26:529-543.

79. Robinson KA, Li J, Mathison M, et al. Extracellular matrix scaffold for cardiac repair. Circulation. 2005;112:I135-143.

80. Badylak SF, Tullius R, Kokini K, et al. The use of xenogeneic small intestinal submucosa as a biomaterial for Achilles tendon repair in a dog model. J Biomed Mater Res. 1995;29:977-985.

81. Prevel CD, Eppley BL, Summerlin DJ, et al. Small intestinal submucosa: utilization as a wound dressing in full-thickness rodent wounds. Ann Plast Surg. 1995;35:381-388.

82. Kim MS, Hong KD, Shin HW, et al. Preparation of porcine small intestinal submucosa sponge and their application as a wound dressing in full-thickness skin defect of rat. Int J Biol Macromol. 2005;36:54-60.

83. Hudson TW, Zawko S, Deister C, et al. Optimized acellular nerve graft is immunologically tolerated and supports regeneration. Tissue Eng. 2004;10:1641-1651.

84. Bhrany AD, Beckstead BL, Lang TC, et al. Development of an esophagus acellular matrix tissue scaffold. Tissue Eng. 2006;12:319-330.

85. Wilson GJ, Courtman DW, Klement P, et al. Acellular matrix: a biomaterials approach for coronary artery bypass and heart valve replacement. Ann Thorac Surg. 1995;60:S353-358.

86. Gilbert TW, Sellaro TL, Badylak SF. Decellularization of tissues and organs. Biomaterials. 2006.

87. Jackson DW, Grood ES, Arnoczky SP, et al. Freeze dried anterior cruciate ligament allografts. Preliminary studies in a goat model. Am J Sports Med. 1987;15:295-303.

88. Jackson DW, Grood ES, Cohn BT, et al. The effects of in situ freezing on the anterior cruciate ligament. An experimental study in goats. J Bone Joint Surg Am. 1991;73:201-213.

89. Pruss A, Kao M, Kiesewetter H, et al. Virus safety of avital bone tissue transplants: evaluation of sterilization steps of spongiosa cuboids using a peracetic acid-methanol mixture. Biologicals. 1999;27:195-201.

90. Hodde JP BS, Brightman AO, Voytik-Harbin SL. Glycosaminoglycan content of small intestinal submucosa: a bioscaffold for tissue replacement. Tissue Eng. 1996;2:209-217.

91. Woods T, Gratzer PF. Effectiveness of three extraction techniques in the development of a decellularized bone-anterior cruciate ligament-bone graft. Biomaterials. 2005;26:7339-7349.

92. Grauss RW, Hazekamp MG, Oppenhuizen F, et al. Histological evaluation of decellularised porcine aortic valves: matrix changes due to different decellularisation methods. Eur J Cardiothorac Surg. 2005;27:566-571.

93. Cartmell JS, Dunn MG. Effect of chemical treatments on tendon cellularity and mechanical properties. J Biomed Mater Res. 2000;49:134-140.

94. Ingber DE, Mow VC, Butler D, et al. Tissue engineering and developmental biology: going biomimetic. Tissue Eng. 2006;12:3265-3283.

95. Gillitzer R, Goebeler M. Chemokines in cutaneous wound healing. J Leukoc Biol. 2001;69:513-521.

96. Birch M, Tomlinson A, Ferguson MW. Animal models for adult dermal wound healing. Methods Mol Med. 2005;117:223-235.

97. Colwell AS, Longaker MT, Lorenz HP. Mammalian fetal organ regeneration. Adv Biochem Eng Biotechnol. 2005;93:83-100.

98. Mast BA, Flood LC, Haynes JH, et al. Hyaluronic acid is a major component of the matrix of fetal rabbit skin and wounds: implications for healing by regeneration. Matrix. 1991;11:63-68.

99. Merkel JR, DiPaolo BR, Hallock GG, et al. Type I and type III collagen content of healing wounds in fetal and adult rats. Proc Soc Exp Biol Med. 1988;187:493-497.

100. Whitby DJ, Ferguson MW. Immunohistochemical localization of growth factors in fetal wound healing. Dev Biol. 1991;147:207-215.

101. Dang CM, Beanes SR, Lee H, et al. Scarless fetal wounds are associated with an increased matrix metalloproteinase-to-tissue-derived inhibitor of metalloproteinase ratio. Plast Reconstr Surg. 2003;111:2273-2285.

102. Soo C, Beanes SR, Hu FY, et al. Ontogenetic transition in fetal wound transforming growth factor-beta regulation correlates with collagen organization. Am J Pathol. 2003;163:2459-2476.

103. Liechty KW, Crombleholme TM, Cass DL, et al. Diminished interleukin-8 (IL-8) production in the fetal wound healing response. J Surg Res. 1998;77:80-84.

104. Liechty KW, Adzick NS, Crombleholme TM. Diminished interleukin 6 (IL-6) production during scarless human fetal wound repair. Cytokine. 2000;12:671-676.

105. Estes JM, Vande Berg JS, Adzick NS, et al. Phenotypic and functional features of myofibroblasts in sheep fetal wounds. Differentiation. 1994;56:173-181.

106. Peranteau WH, Zhang L, Muvarak N, et al. IL-10 overexpression decreases inflammatory mediators and promotes regenerative healing in an adult model of scar formation. J Invest Dermatol. 2008;128:1852-1860.

107. Shah M, Foreman DM, Ferguson MW. Neutralisation of TGF-beta 1 and TGF-beta 2 or exogenous addition of TGF-beta 3 to cutaneous rat wounds reduces scarring. J Cell Sci. 1995;108 (Pt 3):985-1002.

108. King SR, Hickerson WL, Proctor KG. Beneficial actions of exogenous hyaluronic acid on wound healing. Surgery. 1991;109:76-84.

109. Longaker MT, Whitby DJ, Ferguson MW, et al. Adult skin wounds in the fetal environment heal with scar formation. Ann Surg. 1994;219:65-72.

110. Martin P, Parkhurst SM. Parallels between tissue repair and embryo morphogenesis. Development. 2004;131:3021-3034.

111. Grinnell KL, Bickenbach JR. Skin keratinocytes pre-treated with embryonic stem cell-conditioned medium or BMP4 can be directed to an alternative cell lineage. Cell Prolif. 2007;40:685-705.

112. Li Z, Wu JC, Sheikh AY, et al. Differentiation, survival, and function of embryonic stem cell derived endothelial cells for ischemic heart disease. Circulation. 2007;116:I46-54.

113. McCloskey KE, Stice SL, Nerem RM. In vitro derivation and expansion of endothelial cells from embryonic stem cells. Methods Mol Biol. 2006;330:287-301.

114. Baharvand H, Hashemi SM, Shahsavani M. Differentiation of human embryonic stem cells into functional hepatocyte-like cells in a serum-free adherent culture condition. Differentiation. 2008;76:465-477.

115. Abranches E, Silva M, Pradier L, et al. Neural differentiation of embryonic stem cells in vitro: a road map to neurogenesis in the embryo. PLoS One. 2009;4:e6286.

116. Kim M, Habiba A, Doherty JM, et al. Regulation of mouse embryonic stem cell neural differentiation by retinoic acid. Dev Biol. 2009;328:456-471.

117. Boyd NL, Dhara SK, Rekaya R, et al. BMP4 promotes formation of primitive vascular networks in human embryonic stem cell-derived embryoid bodies. Exp Biol Med (Maywood). 2007;232:833-843.

118. Ma W, Tavakoli T, Derby E, et al. Cell-extracellular matrix interactions regulate neural differentiation of human embryonic stem cells. BMC Dev Biol. 2008;8:90.

119. Kelly DL, Rizzino A. DNA microarray analyses of genes regulated during the differentiation of embryonic stem cells. Mol Reprod Dev. 2000;56:113-123.

120. Bhattacharya B, Cai J, Luo Y, et al. Comparison of the gene expression profile of undifferentiated human embryonic stem cell lines and differentiating embryoid bodies. BMC Dev Biol. 2005;5:22.

121. Mansergh FC, Daly CS, Hurley AL, et al. Gene expression profiles during early differentiation of mouse embryonic stem cells. BMC Dev Biol. 2009;9:5.

122. Gunji W, Kai T, Sameshima E, et al. Global analysis of the expression patterns of transcriptional regulatory factors in formation of embryoid bodies using sensitive oligonucleotide microarray systems. Biochem Biophys Res Commun. 2004;325:265-275.

123. Nairn AV, Kinoshita-Toyoda A, Toyoda H, et al. Glycomics of proteoglycan biosynthesis in murine embryonic stem cell differentiation. J Proteome Res. 2007;6:4374-4387.

124. Carpenedo RL, Sargent CY, McDevitt TC. Rotary Suspension Culture Enhances the Efficiency, Yield, and Homogeneity of Embryoid Body Differentiation. Stem Cells. 2007;25:2224-2234.

125. Pfaffl MW. A new mathematical model for relative quantification in real-time RT-PCR. Nucleic Acids Res. 2001;29:e45.

126. Sargent CY, Berguig GY, McDevitt TC. Cardiomyogenic Differentiation of Embryoid Bodies Is Promoted by Rotary Orbital Suspension Culture. Tissue Eng Part A. 2009;15:331-342.

127. Nair R, Shukla S, McDevitt TC. Acellular matrices derived from differentiating embryonic stem cells. J Biomed Mater Res A. 2008.

128. Velcich A, Delli-Bovi P, Mansukhani A, et al. Expression of the K-fgf protooncogene is repressed during differentiation of F9 cells. Oncogene Res. 1989;5:31-37.

129. Dvash T, Mayshar Y, Darr H, et al. Temporal gene expression during differentiation of human embryonic stem cells and embryoid bodies. Hum Reprod. 2004;19:2875-2883.

130. Hailesellasse Sene K, Porter CJ, Palidwor G, et al. Gene function in early mouse embryonic stem cell differentiation. BMC Genomics. 2007;8:85.

131. Lin T, Chao C, Saito S, et al. p53 induces differentiation of mouse embryonic stem cells by suppressing Nanog expression. Nat Cell Biol. 2005;7:165-171.

132. Francis SE, Goh KL, Hodivala-Dilke K, et al. Central roles of alpha5beta1 integrin and fibronectin in vascular development in mouse embryos and embryoid bodies. Arterioscler Thromb Vasc Biol. 2002;22:927-933.

133. Li S, Harrison D, Carbonetto S, et al. Matrix assembly, regulation, and survival functions of laminin and its receptors in embryonic stem cell differentiation. J Cell Biol. 2002;157:1279-1290.

134. Matsuoka Y, Kubota H, Adachi E, et al. Insufficient folding of type IV collagen and formation of abnormal basement membrane-like structure in embryoid bodies derived from Hsp47-null embryonic stem cells. Mol Biol Cell. 2004;15:4467-4475.

135. Michelini M, Franceschini V, Sihui Chen S, et al. Primate embryonic stem cells create their own niche while differentiating in three-dimensional culture systems. Cell Prolif. 2006;39:217-229.

136. Gossler A, Joyner AL, Rossant J, et al. Mouse embryonic stem cells and reporter constructs to detect developmentally regulated genes. Science. 1989;244:463-465.

137. Robbins J, Gulick J, Sanchez A, et al. Mouse embryonic stem cells express the cardiac myosin heavy chain genes during development in vitro. J Biol Chem. 1990;265:11905-11909.

138. D'Amour KA, Bang AG, Eliazer S, et al. Production of pancreatic hormone-expressing endocrine cells from human embryonic stem cells. Nat Biotechnol. 2006;24:1392-1401.

139. Bain G, Kitchens D, Yao M, et al. Embryonic stem cells express neuronal properties in vitro. Dev Biol. 1995;168:342-357.

140. Spencer HL, Eastham AM, Merry CL, et al. E-cadherin inhibits cell surface localization of the pro-migratory 5T4 oncofetal antigen in mouse embryonic stem cells. Mol Biol Cell. 2007;18:2838-2851.

141. Denker HW, Behr R, Heneweer C, et al. Epithelial-mesenchymal transition in Rhesus monkey embryonic stem cell colonies: a model for processes involved in gastrulation? Cells Tissues Organs. 2007;185:48-50.

142. Ullmann U, In't Veld P, Gilles C, et al. Epithelial-mesenchymal transition process in human embryonic stem cells cultured in feeder-free conditions. Mol Hum Reprod. 2007;13:21-32.

143. D'Amour KA, Agulnick AD, Eliazer S, et al. Efficient differentiation of human embryonic stem cells to definitive endoderm. Nat Biotechnol. 2005;23:1534-1541.

144. Eastham AM, Spencer H, Soncin F, et al. Epithelial-mesenchymal transition events during human embryonic stem cell differentiation. Cancer Res. 2007;67:11254-11262.

145. Fenderson BA, Stamenkovic I, Aruffo A. Localization of hyaluronan in mouse embryos during implantation, gastrulation and organogenesis. Differentiation. 1993;54:85-98.

146. Ffrench-Constant C, Hynes RO. Alternative splicing of fibronectin is temporally and spatially regulated in the chicken embryo. Development. 1989;106:375-388.

147. Wan YJ, Wu TC, Chung AE, et al. Monoclonal antibodies to laminin reveal the heterogeneity of basement membranes in the developing and adult mouse tissues. J Cell Biol. 1984;98:971-979.

148. Kern CB, Twal WO, Mjaatvedt CH, et al. Proteolytic cleavage of versican during cardiac cushion morphogenesis. Dev Dyn. 2006;235:2238-2247.

149. Toole BP, Zoltan-Jones A, Misra S, et al. Hyaluronan: a critical component of epithelial-mesenchymal and epithelial-carcinoma transitions. Cells Tissues Organs. 2005;179:66-72.

150. Zoltan-Jones A, Huang L, Ghatak S, et al. Elevated hyaluronan production induces mesenchymal and transformed properties in epithelial cells. J Biol Chem. 2003;278:45801-45810.

151. Henderson DJ, Copp AJ. Versican expression is associated with chamber specification, septation, and valvulogenesis in the developing mouse heart. Circ Res. 1998;83:523-532.

152. Mjaatvedt CH, Yamamura H, Capehart AA, et al. The Cspg2 gene, disrupted in the hdf mutant, is required for right cardiac chamber and endocardial cushion formation. Dev Biol. 1998;202:56-66.

153. Camenisch TD, Spicer AP, Brehm-Gibson T, et al. Disruption of hyaluronan synthase-2 abrogates normal cardiac morphogenesis and hyaluronan-mediated transformation of epithelium to mesenchyme. J Clin Invest. 2000;106:349-360.

154. Toole BP. Hyaluronan: from extracellular glue to pericellular cue. Nat Rev Cancer. 2004;4:528-539.

155. Allison DD, Grande-Allen KJ. Review. Hyaluronan: a powerful tissue engineering tool. Tissue Eng. 2006;12:2131-2140.

156. Schoenfelder M, Einspanier R. Expression of hyaluronan synthases and corresponding hyaluronan receptors is differentially regulated during oocyte maturation in cattle. Biol Reprod. 2003;69:269-277.

157. Trabucchi E, Pallotta S, Morini M, et al. Low molecular weight hyaluronic acid prevents oxygen free radical damage to granulation tissue during wound healing. Int J Tissue React. 2002;24:65-71.

158. Foschi D, Castoldi L, Radaelli E, et al. Hyaluronic acid prevents oxygen free-radical damage to granulation tissue: a study in rats. Int J Tissue React. 1990;12:333-339.

159. West DC, Hampson IN, Arnold F, et al. Angiogenesis induced by degradation products of hyaluronic acid. Science. 1985;228:1324-1326.

160. Wight TN. Versican: a versatile extracellular matrix proteoglycan in cell biology. Curr Opin Cell Biol. 2002;14:617-623.

161. Murphy CL, Polak JM. Differentiating embryonic stem cells: GAPDH, but neither HPRT nor beta-tubulin is suitable as an internal standard for measuring RNA levels. Tissue Eng. 2002;8:551-559.

162. Kenagy RD, Plaas AH, Wight TN. Versican degradation and vascular disease. Trends Cardiovasc Med. 2006;16:209-215.

163. Sandy JD, Westling J, Kenagy RD, et al. Versican V1 proteolysis in human aorta in vivo occurs at the Glu441-Ala442 bond, a site that is cleaved by recombinant ADAMTS-1 and ADAMTS-4. J Biol Chem. 2001;276:13372-13378.

164. Seidelmann SB, Kuo C, Pleskac N, et al. Athsq1 is an atherosclerosis modifier locus with dramatic effects on lesion area and prominent accumulation of versican. Arterioscler Thromb Vasc Biol. 2008;28:2180-2186.

165. Longpre JM, McCulloch DR, Koo BH, et al. Characterization of proADAMTS5 processing by proprotein convertases. Int J Biochem Cell Biol. 2009;41:1116-1126.

166. Wight TN, Merrilees MJ. Proteoglycans in atherosclerosis and restenosis: key roles for versican. Circ Res. 2004;94:1158-1167.

167. Ricciardelli C, Russell DL, Ween MP, et al. Formation of hyaluronan- and versican-rich pericellular matrix by prostate cancer cells promotes cell motility. J Biol Chem. 2007;282:10814-10825.

168. Kishimoto J, Ehama R, Wu L, et al. Selective activation of the versican promoter by epithelial- mesenchymal interactions during hair follicle development. Proc Natl Acad Sci U S A. 1999;96:7336-7341.

169. Spicer AP, Tien JL, Joo A, et al. Investigation of hyaluronan function in the mouse through targeted mutagenesis. Glycoconj J. 2002;19:341-345.

170. Choudhary M, Zhang X, Stojkovic P, et al. Putative role of hyaluronan and its related genes, HAS2 and RHAMM, in human early preimplantation embryogenesis and embryonic stem cell characterization. Stem Cells. 2007;25:3045-3057.

171. Tesar PJ, Chenoweth JG, Brook FA, et al. New cell lines from mouse epiblast share defining features with human embryonic stem cells. Nature. 2007;448:196-199.

172. Dutt S, Kleber M, Matasci M, et al. Versican V0 and V1 guide migratory neural crest cells. J Biol Chem. 2006;281:12123-12131.

173. Kamiya N, Watanabe H, Habuchi H, et al. Versican/PG-M regulates chondrogenesis as an extracellular matrix molecule crucial for mesenchymal condensation. J Biol Chem. 2006;281:2390-2400.

174. Landolt RM, Vaughan L, Winterhalter KH, et al. Versican is selectively expressed in embryonic tissues that act as barriers to neural crest cell migration and axon outgrowth. Development. 1995;121:2303-2312.

175. Perissinotto D, Iacopetti P, Bellina I, et al. Avian neural crest cell migration is diversely regulated by the two major hyaluronan-binding proteoglycans PG-M/versican and aggrecan. Development. 2000;127:2823-2842.

176. Nakamura M, Sone S, Takahashi I, et al. Expression of versican and ADAMTS1, 4, and 5 during bone development in the rat mandible and hind limb. J Histochem Cytochem. 2005;53:1553-1562.

177. Sone S, Nakamura M, Maruya Y, et al. Expression of versican and ADAMTS during rat tooth eruption. J Mol Histol. 2005;36:281-288.

178. McCulloch DR, Goff CL, Bhatt S, et al. Adamts5, the gene encoding a proteoglycan-degrading metalloprotease, is expressed by specific cell lineages during mouse embryonic development and in adult tissues. Gene Expr Patterns. 2009;9:314-323.

179. Kolossov E, Bostani T, Roell W, et al. Engraftment of engineered ES cell-derived cardiomyocytes but not BM cells restores contractile function to the infarcted myocardium. J Exp Med. 2006;203:2315-2327.

180. von Unge M, Dirckx JJ, Olivius NP. Embryonic stem cells enhance the healing of tympanic membrane perforations. Int J Pediatr Otorhinolaryngol. 2003;67:215-219.

181. Kimura H, Yoshikawa M, Matsuda R, et al. Transplantation of embryonic stem cell-derived neural stem cells for spinal cord injury in adult mice. Neurol Res. 2005;27:812-819.

182. Hodgson DM, Behfar A, Zingman LV, et al. Stable benefit of embryonic stem cell therapy in myocardial infarction. Am J Physiol Heart Circ Physiol. 2004;287:H471-479.

183. Chen F, Yoo JJ, Atala A. Acellular collagen matrix as a possible "off the shelf" biomaterial for urethral repair. Urology. 1999;54:407-410.

184. Gilbert TW, Stolz DB, Biancaniello F, et al. Production and characterization of ECM powder: implications for tissue engineering applications. Biomaterials. 2005;26:1431-1435.

185. Kim BS, Yoo JJ, Atala A. Peripheral nerve regeneration using acellular nerve grafts. J Biomed Mater Res A. 2004;68:201-209.

186. O'Brien MF, Goldstein S, Walsh S, et al. The SynerGraft valve: a new acellular (nonglutaraldehyde-fixed) tissue heart valve for autologous recellularization first experimental studies before clinical implantation. Semin Thorac Cardiovasc Surg. 1999;11:194-200.

187. Booth C, Korossis SA, Wilcox HE, et al. Tissue engineering of cardiac valve prostheses I: development and histological characterization of an acellular porcine scaffold. J Heart Valve Dis. 2002;11:457-462.

188. Kasimir MT, Rieder E, Seebacher G, et al. Comparison of different decellularization procedures of porcine heart valves. Int J Artif Organs. 2003;26:421-427.

189. Voytik-Harbin SL, Brightman AO, Kraine MR, et al. Identification of extractable growth factors from small intestinal submucosa. J Cell Biochem. 1997;67:478-491.

190. Kropp BP, Ludlow JK, Spicer D, et al. Rabbit urethral regeneration using small intestinal submucosa onlay grafts. Urology. 1998;52:138-142.

191. Abraham GA, Murray J, Billiar K, et al. Evaluation of the porcine intestinal collagen layer as a biomaterial. J Biomed Mater Res. 2000;51:442-452.

192. Xu CC, Chan RW, Tirunagari N. A Biodegradable, Acellular Xenogeneic Scaffold for Regeneration of the Vocal Fold Lamina Propria. Tissue Eng. 2006.

193. Chang Y, Chen SC, Wei HJ, et al. Tissue regeneration observed in a porous acellular bovine pericardium used to repair a myocardial defect in the right ventricle of a rat model. J Thorac Cardiovasc Surg. 2005;130:705-711.

194. Lantz GC, Badylak SF, Coffey AC, et al. Small intestinal submucosa as a small-diameter arterial graft in the dog. J Invest Surg. 1990;3:217-227.

195. Franklin ME, Jr., Gonzalez JJ, Jr., Michaelson RP, et al. Preliminary experience with new bioactive prosthetic material for repair of hernias in infected fields. Hernia. 2002;6:171-174.

196. Buinewicz B, Rosen B. Acellular cadaveric dermis (AlloDerm): a new alternative for abdominal hernia repair. Ann Plast Surg. 2004;52:188-194.

197. Hodde J, Badylak S, Brightman A, et al. Glycosaminoglycan content of small intestinal submucosa: a bioscaffold for tissue replacement. Tissue Eng. 1996;2:209-217.

198. Hodde J, Record R, Tullius R, et al. Fibronectin peptides mediate HMEC adhesion to porcine-derived extracellular matrix. Biomaterials. 2002;23:1841-1848.

199. Carpenedo RL, Sargent CY, McDevitt TC. Rotary Suspension Culture Enhances the Efficiency, Yield and Homogeneity of Embryoid Body Differentiation. Stem Cells. 2007.

200. Huang Q, Dawson RA, Pegg DE, et al. Use of peracetic acid to sterilize human donor skin for production of acellular dermal matrices for clinical use. Wound Repair Regen. 2004;12:276-287.

201. Brown B, Lindberg K, Reing J, et al. The basement membrane component of biologic scaffolds derived from extracellular matrix. Tissue Eng. 2006;12:519-526.

202. Rieder E, Kasimir MT, Silberhumer G, et al. Decellularization protocols of porcine heart valves differ importantly in efficiency of cell removal and susceptibility of the matrix to recellularization with human vascular cells. J Thorac Cardiovasc Surg. 2004;127:399-405.

203. Gratzer PF, Harrison RD, Woods T. Matrix Alteration and Not Residual Sodium Dodecyl Sulfate Cytotoxicity Affects the Cellular Repopulation of a Decellularized Matrix. Tissue Eng. 2006.

204. Zhou L, Higginbotham EJ, Yue BY. Effects of ascorbic acid on levels of fibronectin, laminin and collagen type 1 in bovine trabecular meshwork in organ culture. Curr Eye Res. 1998;17:211-217.

205. Sawaguchi S, Yue BY, Chang IL, et al. Ascorbic acid modulates collagen type I gene expression by cells from an eye tissue--trabecular meshwork. Cell Mol Biol. 1992;38:587-604.

206. Aberdam D. Derivation of keratinocyte progenitor cells and skin formation from embryonic stem cells. Int J Dev Biol. 2004;48:203-206.

207. Bagutti C, Wobus AM, Fassler R, et al. Differentiation of embryonal stem cells into keratinocytes: comparison of wild-type and beta 1 integrin-deficient cells. Dev Biol. 1996;179:184-196.

208. Coraux C, Hilmi C, Rouleau M, et al. Reconstituted skin from murine embryonic stem cells. Curr Biol. 2003;13:849-853.

209. Kofidis T, de Bruin JL, Hoyt G, et al. Myocardial restoration with embryonic stem cell bioartificial tissue transplantation. J Heart Lung Transplant. 2005;24:737-744.

210. Kofidis T, Lebl DR, Martinez EC, et al. Novel injectable bioartificial tissue facilitates targeted, less invasive, large-scale tissue restoration on the beating heart after myocardial injury. Circulation. 2005;112:I173-177.

211. McCloskey KE, Gilroy ME, Nerem RM. Use of embryonic stem cell-derived endothelial cells as a cell source to generate vessel structures in vitro. Tissue Eng. 2005;11:497-505.

212. Aoki H, Hara A, Nakagawa S, et al. Embryonic stem cells that differentiate into RPE cell precursors in vitro develop into RPE cell monolayers in vivo. Exp Eye Res. 2006;82:265-274.

213. Coburn JC, Brody S, Billiar KL, et al. Biaxial mechanical evaluation of cholecyst-derived extracellular matrix: a weakly anisotropic potential tissue engineered biomaterial. J Biomed Mater Res A. 2007;81:250-256.

214. Whitlock PW, Smith TL, Poehling GG, et al. A naturally derived, cytocompatible, and architecturally optimized scaffold for tendon and ligament regeneration. Biomaterials. 2007;28:4321-4329.

215. Nair R, Ngangan AV, McDevitt TC. Efficacy of solvent extraction methods for acellularization of embryoid bodies. J. Biomater. Sci. Polymer Edn. 2007.

216. Uchimura E, Sawa Y, Taketani S, et al. Novel method of preparing acellular cardiovascular grafts by decellularization with poly(ethylene glycol). J Biomed Mater Res A. 2003;67:834-837.

217. Xu CC, Chan RW, Tirunagari N. A biodegradable, acellular xenogeneic scaffold for regeneration of the vocal fold lamina propria. Tissue Eng. 2007;13:551-566.

218. Flynn L, Semple JL, Woodhouse KA. Decellularized placental matrices for adipose tissue engineering. J Biomed Mater Res A. 2006;79:359-369.

219. Melnick M, Jaskoll T, Brownell AG, et al. Spatiotemporal patterns of fibronectin distribution during embryonic development. I. Chick limbs. J Embryol Exp Morphol. 1981;63:193-206.

220. Funderburgh JL, Caterson B, Conrad GW. Keratan sulfate proteoglycan during embryonic development of the chicken cornea. Dev Biol. 1986;116:267-277.

221. Oohira A, Matsui F, Matsuda M, et al. Developmental change in the glycosaminoglycan composition of the rat brain. J Neurochem. 1986;47:588-593.

222. Burkart T, Wiesmann UN. Sulfated glycosaminoglycans (GAG) in the developing mouse brain. Quantitative aspects on the metabolism of total and individual sulfated GAG in vivo. Dev Biol. 1987;120:447-456.

223. Cormier JT, zur Nieden NI, Rancourt DE, et al. Expansion of undifferentiated murine embryonic stem cells as aggregates in suspension culture bioreactors. Tissue Eng. 2006;12:3233-3245.

224. Dang SM, Gerecht-Nir S, Chen J, et al. Controlled, scalable embryonic stem cell differentiation culture. Stem Cells. 2004;22:275-282.

225. Gerecht-Nir S, Cohen S, Itskovitz-Eldor J. Bioreactor cultivation enhances the efficiency of human embryoid body (hEB) formation and differentiation. Biotechnol Bioeng. 2004;86:493-502.

226. Adzick NS, Lorenz HP. Cells, matrix, growth factors, and the surgeon. The biology of scarless fetal wound repair. Ann Surg. 1994;220:10-18.

227. Ferguson MW, O'Kane S. Scar-free healing: from embryonic mechanisms to adult therapeutic intervention. Philos Trans R Soc Lond B Biol Sci. 2004;359:839-850.

228. Whitby DJ, Ferguson MW. The extracellular matrix of lip wounds in fetal, neonatal and adult mice. Development. 1991;112:651-668.

229. Adzick NS, Longaker MT. Animal models for the study of fetal tissue repair. J Surg Res. 1991;51:216-222.

230. Supp DM, Boyce ST. Overexpression of vascular endothelial growth factor accelerates early vascularization and improves healing of genetically modified cultured skin substitutes. J Burn Care Rehabil. 2002;23:10-20.

231. Iocono JA, Ehrlich HP, Keefer KA, et al. Hyaluronan induces scarless repair in mouse limb organ culture. J Pediatr Surg. 1998;33:564-567.

232. Kohama K, Nonaka K, Hosokawa R, et al. TGF-beta-3 promotes scarless repair of cleft lip in mouse fetuses. J Dent Res. 2002;81:688-694.

233. Colwell AS, Beanes SR, Soo C, et al. Increased angiogenesis and expression of vascular endothelial growth factor during scarless repair. Plast Reconstr Surg. 2005;115:204-212.

234. Gurtner GC, Werner S, Barrandon Y, et al. Wound repair and regeneration. Nature. 2008;453:314-321.

235. Martin P. Wound healing--aiming for perfect skin regeneration. Science. 1997;276:75-81.

236. Malinda KM, Wysocki AB, Koblinski JE, et al. Angiogenic laminin-derived peptides stimulate wound healing. Int J Biochem Cell Biol. 2008;40:2771-2780.

237. Rolfe KJ, Cambrey AD, Richardson J, et al. Dermal fibroblasts derived from fetal and postnatal humans exhibit distinct responses to insulin like growth factors. BMC Dev Biol. 2007;7:124.

238. Sewall GK, Robertson KM, Connor NP, et al. Effect of topical mitomycin on skin wound contraction. Arch Facial Plast Surg. 2003;5:59-62.

239. Barnett A, Dave B, Ksander GA, et al. A concentration gradient of bacteria within wound tissues and scab. J Surg Res. 1986;41:326-332.

240. Lindblad WJ. Considerations for selecting the correct animal model for dermal wound-healing studies. J Biomater Sci Polym Ed. 2008;19:1087-1096.

241. Wall SJ, Bevan D, Thomas DW, et al. Differential expression of matrix metalloproteinases during impaired wound healing of the diabetes mouse. J Invest Dermatol. 2002;119:91-98.

242. Ramelet AA, Hirt-Burri N, Raffoul W, et al. Chronic wound healing by fetal cell therapy may be explained by differential gene profiling observed in fetal versus old skin cells. Exp Gerontol. 2009;44:208-218.

243. Broker BJ, Chakrabarti R, Blynman T, et al. Comparison of growth factor expression in fetal and adult fibroblasts: a preliminary report. Arch Otolaryngol Head Neck Surg. 1999;125:676-680.

244. Chin GS, Kim WJ, Lee TY, et al. Differential expression of receptor tyrosine kinases and Shc in fetal and adult rat fibroblasts: toward defining scarless versus scarring fibroblast phenotypes. Plast Reconstr Surg. 2000;105:972-979.

245. Rolfe KJ, Richardson J, Vigor C, et al. A Role for TGF-beta1-Induced Cellular Responses during Wound Healing of the Non-Scarring Early Human Fetus? J Invest Dermatol. 2007.

246. Dang C, Beanes SR, Soo C, et al. A high ratio of TGFβ3 to TGFβ1 expression in wounds is associated with scarless repair. Wound Repair Regen. 2001;9:153.

247. Chidgey AP, Layton D, Trounson A, et al. Tolerance strategies for stem-cell-based therapies. Nature. 2008;453:330-337.

248. Drukker M, Katz G, Urbach A, et al. Characterization of the expression of MHC proteins in human embryonic stem cells. Proc Natl Acad Sci U S A. 2002;99:9864-9869.